Jagiellonian University

**THE FACULTY OF PHYSICS, ASTRONOMY,
AND APPLIED COMPUTER SCIENCE
MARIAN SMOLUCHOWSKI INSTITUTE OF PHYSICS**

Model Description of Proton Induced Fragmentation of Atomic Nuclei

Małgorzata Fidelus

PhD dissertation performed
in the Nuclear Physics Department
Thesis supervisor: Prof. dr hab. Bogusław Kamys

Cracow, 2010

Contents

Chapter 1

Introduction

The knowledge of the production cross sections for various residual nuclei by medium- and high-energy protons interacting with atomic nuclei is essential for a large number of applications in science and technology. They concern such different subjects like the design and operation of neutron spallation sources, the optimization of isotope production, the accelerator-driven subcritical reactor systems considered for the transmutation of nuclear waste, the interpretation of reaction products of cosmic ray interaction with terrestrial and extraterrestrial matter, etc. Various and abundant applications demand the knowledge of cross-sections for numerous target - ejectile combinations and for a broad range of proton beam energies. In spite of the fact that a large number of experiments were performed in the past to determine production cross-sections, the experimental knowledge of them is still not satisfactory. Therefore the only practical method to predict the production cross sections for all important target-ejectile combinations in a broad range of proton energies is to rely on realistic models of proton-nucleus interactions. Thus, the task to investigate a mechanism of the reactions induced by medium- and high-energy protons on atomic nuclei is not only interesting by itself, but it is also very important from practical reasons. Unfortunately, many aspects of the reaction mechanism are still not well understood what causes that even most essential and simple observables, i.e. total production cross sections, cannot be properly reproduced by existing models (cf. e.g. ref. [1]).

It was shown by the PISA (**P**roton **I**nduced **S**p**A**llation) collaboration in recent studies of proton interaction with Ni and Au targets at proton beam energies 1.2-2.5 GeV [2–5], that the double differential cross sections $\frac{d\sigma}{d\Omega dE}$ obtained in inclusive measurements for light charged particles (LCP), i.e. Hydrogen and Helium isotopes, as well as for intermediate mass fragments (IMF), i.e., particles with atomic number Z larger than 2 but smaller than fission fragments, revealed specific angular and energy dependencies, which could not be reproduced by the traditional two-step model of the reaction mechanism. It turned out that for all ejectiles two components of the energy spectra are present. The isotropic, low-energy part can be attributed to evaporation of ejectiles from excited remnants of the intranuclear cascade of nucleon-nucleon collisions induced by the proton impinging on to the nucleus. The origin of the anisotropic,

high–energy part, which was observed for all ejectiles, is not clear. Whereas for LCPs such a high energy contribution could be, at least partially, traced to emission from the first step of the reaction, i.e., from the cascade stage of the proton - nucleus collision, the origin of the high energy tail in IMF spectra was not explained.

It was claimed by authors of refs [2–5] that phenomenological introduction of emission of particles from sources moving along the beam direction is necessary to achieve a good description of the angular and energy dependence of double differential cross sections. The interpretation of the origin of moving sources proposed in these references is based on the assumption that the proton impinging on to the target may interact *simultaneously* with a group of nucleons lying on its straight way through the nucleus. This interaction, which is neglected in the model of intranuclear cascade, results in the emission of a small, fast and hot group of nucleons moving in the forward direction, i.e., along the beam. Such a group of nucleons, called "*fireball*" decays isotropically in its centre of mass reference frame emitting nucleons and composite light charged particles (LCPs). In the laboratory reference frame this emission gives a strongly anisotropic, high-energy contribution to the LCP spectra. The intermediate mass fragment (IMF) spectra are, however, not influenced by the presence of the fireball because its mass is smaller than the mass of most IMFs.

It is worth to emphasize, that the hypothesis of the fireball is compatible with the presence and properties of two moving sources emitting intermediate mass fragments as postulated in refs [2–5]. The following reasoning leads to the above statement: It is natural to conjecture that the remnant of the target nucleus, which remains after emission of the fireball, is excited and deformed. Thus it may break-up into two prefragments which are still excited and act as moving sources of ejectiles. This process is called "*fast break-up*" because it appears in the first, fast stage of the reaction. Since the probability distribution of the impact parameter of the beam protons favours peripheral collisions, the two prefragments have usually quite different masses. It seems reasonable to expect that the energy as well as the momentum transfers from the fireball to both prefragments are approximately the same. In such a case the velocity and the excitation energy per nucleon of the lighter prefragment have to be larger than the velocity and the excitation energy per nucleon of the heavier prefragment. These facts agree well with experimental observations of refs [2–5].

The question arises, whether the above described picture of the reaction mechanism remains valid for very light targets, like ^{12}C, where the fireball would exhaust large part of the mass of the target nucleus and therefore the eventual break-up of the rest of the target nucleus cannot cause an emission of two intermediate mass fragments. Furthermore, it was reported in refs [2–5] that the lighter of two moving sources observed in p-Ni and p-Au collisions is built of 20-25 nucleons. It is impossible in p+^{12}C and highly improbable in p+^{27}Al collisions to obtain such a prefragment as a result of the break-up of the excited target remnant after emission of several nucleons, both in the form of a fireball or as nucleons from the nucleon-nucleon intranuclear

cascade. Thus, an eventual observation of two different contributions to the spectra of IMFs in proton-Carbon and/or proton-Aluminium collisions should find another explanation than the two-body break-up of an excited remnant nucleus. On the other hand, emission of a fireball consisted of $\sim$ 3-5 nucleons from these collisions is not excluded, thus it may be expected that spectra of light charged particles should contain the contribution, which for heavier targets was attributed to the emission from a fireball.

The aim of the present work is to study the mechanism of interaction of protons with energy 1.2 - 2.5 GeV impinging on to ^{12}C and ^{27}Al targets. The goal of this investigation is twofold:

(i) to examine experimentally whether the effects which have been attributed to the fast break-up of the target nucleus in proton-Ni and proton-Au collisions [2–5] are present in proton induced reactions on very light targets, and

(ii) to check whether another reaction mechanism is able to reproduce experimental data obtained for these light targets.

This thesis is organized as follows: A short review of most important experimental facts concerning mechanism of the proton induced reactions at GeV energies is presented in the section 2. The emphasis is put on two general properties of the reactions at such high energies: on the limiting fragmentation hypothesis (subsection 2.1) and on the multifragmentation of atomic nuclei (subsection 2.2).

The theoretical models used most commonly for description of such reactions are discussed in the section 3. All of them assume two stage mechanism of the reactions. First four subsections of the section 3 describe models of the first stage of the reaction whereas next four subsections deal with the models of the second stage.

The experiment PISA, in which reactions induced by protons on Aluminium and Carbon targets were studied, is described in the section 4 putting emphasis on the experimental setup and experimental procedure (subsection 4.1), on the absolute normalization of the cross sections (subsection 4.2), and on the comparison with the data from the literature (subsection 4.3).

Qualitative properties of the obtained data are presented in the section 5, separately for p+Al collisions (in the subsection 5.1), and for p+C collisions (in the subsection 5.2).

Application of various models of the reaction to the experimental data is presented in the section 6. Three versions of the analysis are discussed in the following subsections:
6.1 – The traditional two-step model consisted of the intranuclear cascade for description of the first stage of the reaction followed by the evaporation of particles in the second stage,
6.2 – The two step model, in which the first stage of the reaction is described by the intranuclear

cascade, whereas the second stage is modeled by the evaporation (for slightly excited remnants of the cascade) or by the multifragmentation (for highly excited remnants),
6.3 – The two step model, analogous to that used in the preceding subsection, but with the inclusion of the fireball emission besides the intranuclear cascade in the first step of the reaction.

Discussion of the obtained results is presented in the section 7 and the summary of the performed investigations forms the content of the section 8.

List of the experiments dealing with reactions in p+Al and p+C systems at proton GeV energies is given in the Appendix A, whereas details of the phenomenological model of moving sources are presented in the Appendix B.

The literature references are collected in the Bibliography.

Chapter 2

Earlier results

Intense experimental and theoretical investigations have been performed in last tens of years with the aim to get knowledge on reactions induced by energetic protons interacting with atomic nuclei. Most of the experiments were devoted to inclusive measurements of total production cross sections, see e.g., [6,7]. Measurements of differential cross sections were less abundant even for inclusive experiments and were almost not present for coincidence studies [8–11]. Results of these investigations lead to the following conclusions:

1. Total cross sections for production of light charged particles and intermediate mass fragments vary smoothly with the mass of target nuclei as well as with proton beam energy. Moreover, the value of the total cross sections seems to level at high beam energies for all reaction products. The threshold energy at which the leveling starts increases with the mass of the target [6, 7, 12, 13].

   This behaviour is illustrated by fig. 2.1 where the energy dependence of production cross sections of ^{7}Be in proton induced reactions is presented for six targets: ^{12}C, ^{16}O, ^{27}Al, ^{58}Ni, ^{107}Ag, and ^{197}Au. The lines shown on fig. 2.1 depict results of parameterization of the experimental data made by Bubak et al. [13]. All excitation functions level at high energies but the threshold energy for this effect depends on the mass of the target. A maximum of the cross section is visible for the lightest targets in the neighbourhood of 100 MeV, what is not the case for targets heavier than Al. At higher energies all excitation functions behave in the same manner, i.e. they approach a plateau of different height for different particles.

   The energy dependence of total production cross sections of other particles exhibits the same general trend as that for ^{7}Be (see e.g. [14]).

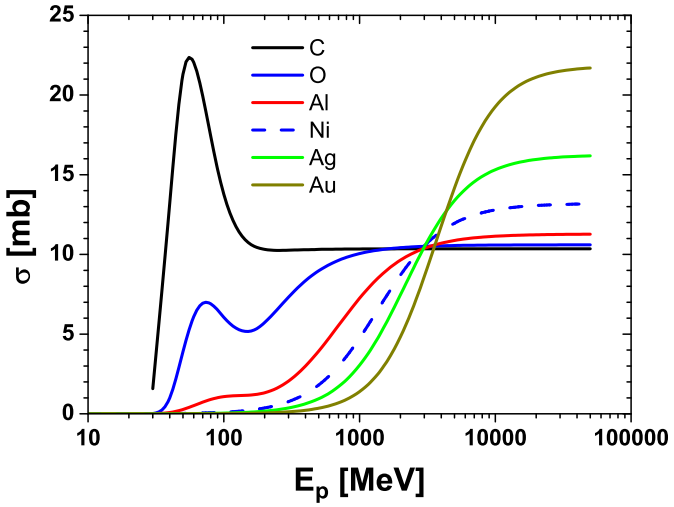

Figure 2.1: Energy dependence of the total production cross section of ^{7}Be in proton induced reactions on various targets [13].

2. Angular distributions and energy spectra of differential cross sections indicate the presence of ***at least two components*** for all ejectiles and targets.

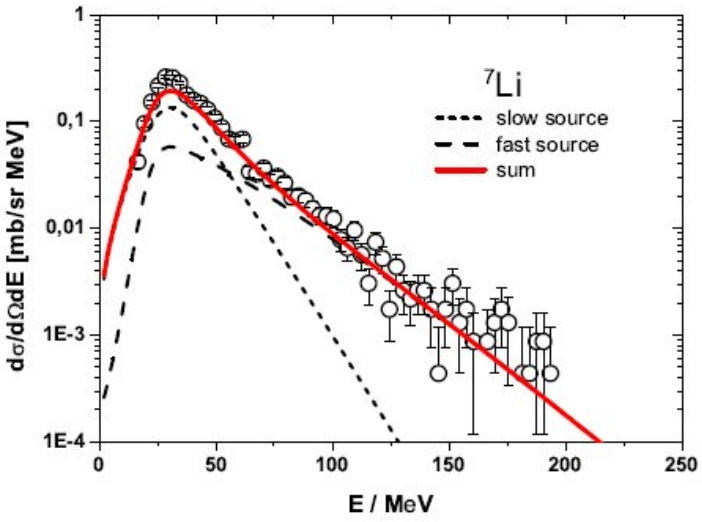

Figure 2.2: Energy spectrum of ^{7}Li at 35° from p+Au collisions at 2.5 GeV proton beam energy [2]

First component, which contributes mainly to the low energy part of the spectra is isotropic and has a Maxwellian energy dependence typical for the evaporation from equilibrated source. ***The second one*** participates predominantly in the high-energy, exponential part of the spectra and decreases with detection angle. These properties indicate that such a component corresponds to processes in which an equilibrium of full nucleus is not achieved [11].

There was observed that for the lightest products, i.e. protons, deuterons, tritons, ^{3}He and ^{4}He ***the additional high energy components*** of the spectra are present [3, 4]. These components may partially originate as result of emission from the cascade stage of the reaction and may also appear due to emission from a hot, fast moving source called "fireball". The angular distributions of these both processes are strongly anisotropic, peaked in forward (parallel to the beam) direction [3, 4, 9, 15, 16]. The apparent temperature of the fireball is significantly higher than the temperatures of the two emitting sources discussed above.

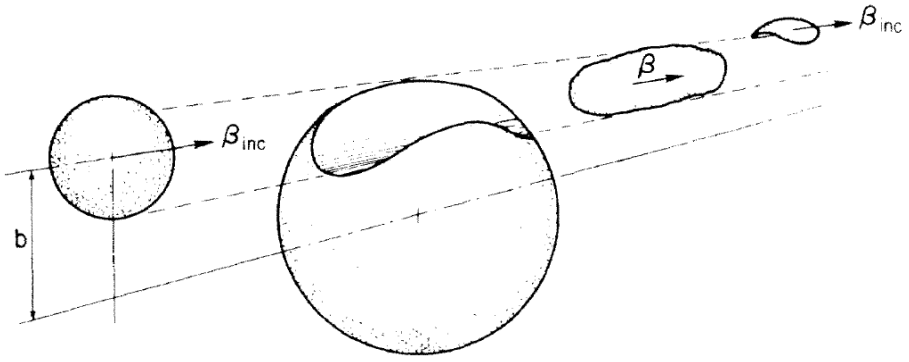

Figure 2.3: A model of fireball emission. The nucleons, which are mutually swept out from the nucleus by the projectile impinging on to the target from the left side of the figure, form a hot and fast group of nucleons called "fireball". The picture was taken from [15].

The contribution of such reaction mechanism is shown in fig. 2.4 for deuteron spectra from p+Au collisions [3]. The dash-dotted line presents the fireball contribution, the dashed line depicts the sum of two components; emission of deuterons from the coalescence process and evaporation from the excited remnant of the target after intranuclear cascade. The first component contributes mainly to the high energy tail of the spectra whereas the second one to the low energy part of spectra. The solid line depicts the sum of all reaction mechanisms. As can be seen the fireball contribution is significant for smallest scattering angle and quickly decreases for larger angles.

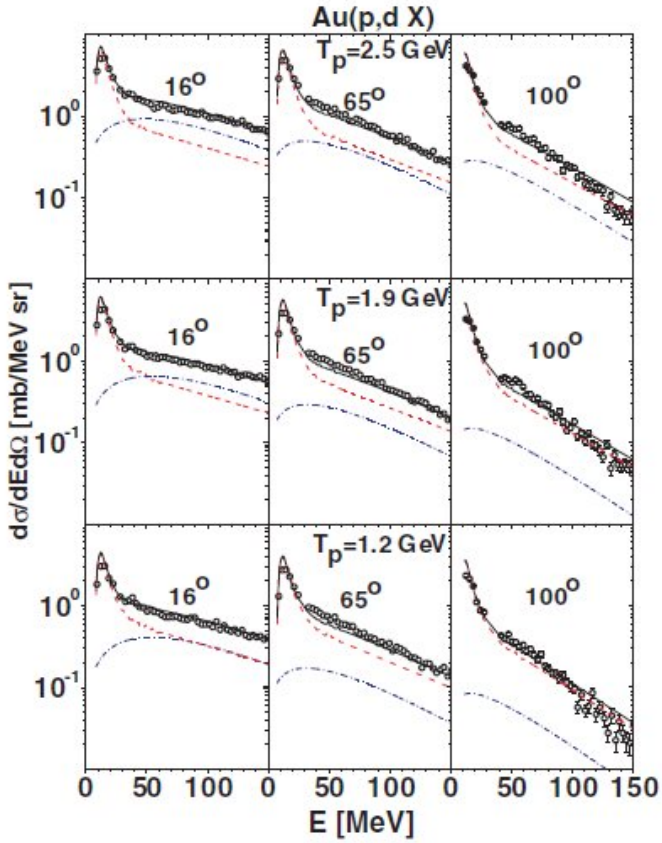

Figure 2.4: Experimental deuteron spectra (circles) from p+Au collisions measured at three proton beam energies. The upper, middle and lower panels correspond to beam energy 2.5, 1.9, and 1.2 GeV, respectively. The left, middle and right panels represent spectra at 16° , 65° , and 100° , respectively. The lines depict model predictions of different reaction mechanisms (see text) [3].

3. It was reported [6,7,13,14], that significant changes in reaction mechanism occur at beam energies below the region where the leveling of the excitation functions appears. These changes were interpreted as transition from binary breakup to multifragmentation of the target nuclei. The energy deposited by the projectile in the target nucleus increases to such values at which a phase transition appears – from the nuclear liquid to gas consisted of free nucleons and intermediate mass fragments. Further increase of the beam energy does not influence the values of the total cross sections as well as the shape of energy spectra. This fact, known as limiting fragmentation hypothesis, might indicate the lack of possibility to absorb more energy by target nuclei. Then the products of the reaction which originate due to the emission from excited remnants of the target nuclei should be

characterized by the energy independent cross sections.

2.1 Limiting fragmentation hypothesis

The limiting fragmentation hypothesis, originally proposed by Benecke et al. [17] for collisions of hadrons, suggests that at sufficiently high bombarding energies fragmentation cross sections of the target investigated in its rest system should reach their asymptotic values. Such a limiting behaviour is conjectured for both, differential and total production cross sections. Thus constancy of the total production cross sections for high beam energies shown for ^{7}Be on fig. 2.1 as well as constancy of production cross sections for other ejectiles reported, e.g., by Porile et al. [14] and Cumming et al. [18–20] is a straightforward consequence of validity of the limiting fragmentation hypothesis. It is important to emphasize that the momentum distributions of fragments should also reach their asymptotic forms. Figure 2.5 shows energy dependence of spectra for selected products of p+Ni and p+Au collisions measured by PISA collaboration [5] and [3].

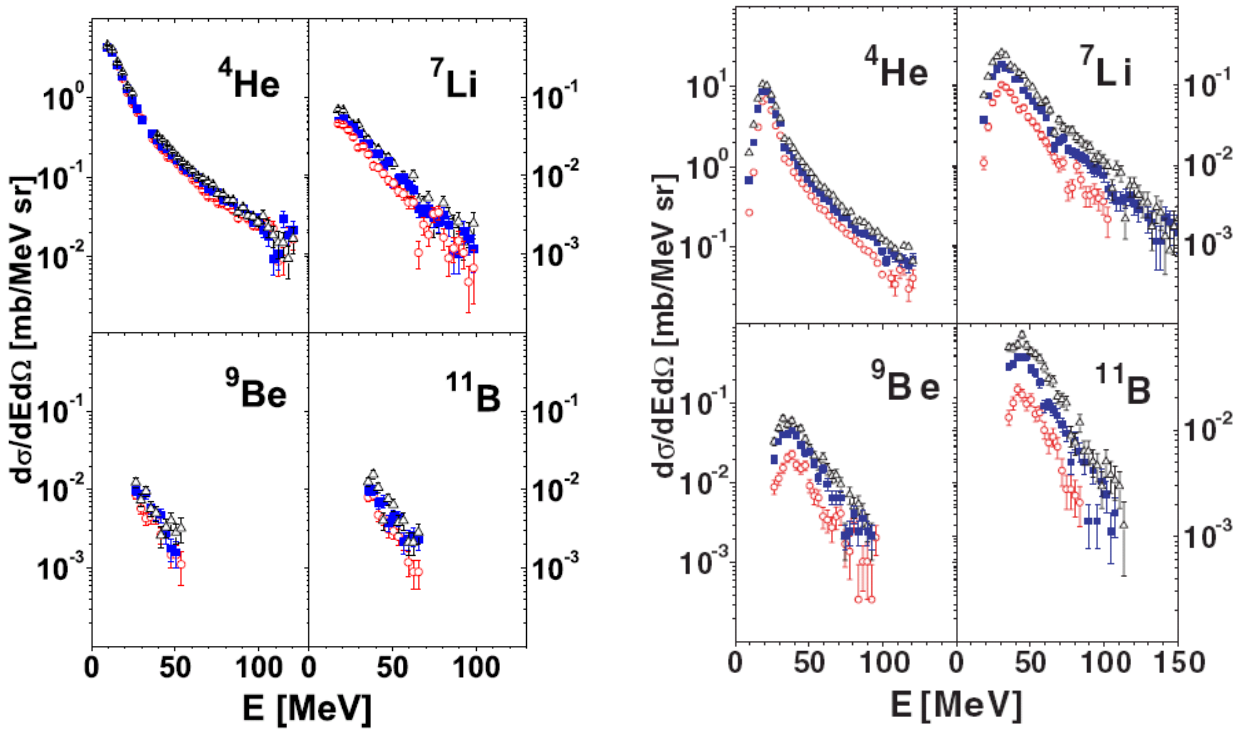

Figure 2.5: Spectra of ^{4}He, ^{7}Li, ^{9}Be, and ^{11}B produced in p+Ni (left figure) and p+Au (right figure) collisions at three proton beam energies; 1.2, 1.9, and 2.5 GeV (open circles, full squares, and open triangles, respectively), measured at 35° . Figures were taken from [5] and [3].

It is evident that the shape of the spectra does not change in the proton energy range 1.2 - 2.5 GeV for all particles and both targets, however, the absolute value of the cross sections increases by factor $\sim$ 3 - 4 for Au target whereas this increase is much smaller for Ni target (by factor $\sim$ 1.5 - 2). This is in line with dependence of the total cross sections for ^{7}Be production depicted in fig. 2.1, where the stabilization of the cross sections starts at lower energy for light targets than for heavier targets.

This can be understood as an effect caused by difference between threshold energies for fragmentation of both targets. Indeed, the inspection of excitation functions for ^{7}Be production presented on Fig. 2.1 shows that fragmentation starts for Ni target at lower energies than for Au target. Therefore the beam energy range (1.2 - 2.5 GeV) studied by PISA collaboration corresponds to the region where the production cross section starts to saturate for Ni target, whereas for Au target this is the region where the production cross section starts to rise quickly.

The effects of limiting fragmentation should also be visible in the excitation functions of total production cross sections studied in literature for Al and C targets, which are the subjects of investigations performed in the present work. Furthermore, it may be expected that leveling of the excitation functions for C target should appear at lower energy than that for Al target.

Representative examples of excitation functions of total production cross sections for light charged particles (^{3}H and ^{4}He) and heavier fragments (^{7}Be, ^{11}C, ^{18}F, and ^{24}Na) produced in proton collisions with ***Aluminium target*** are presented in fig. 2.6. All excitation functions increase with the energy for proton energies smaller than $\sim$ 100 MeV, where the maxima appear for heavy reaction products (^{18}F, and ^{24}Na). These maxima are not visible for lighter particles. The excitation functions rise for higher energies (up to $\sim$ 1 GeV), where they start to level for ^{4}He, ^{11}C, ^{18}F, and ^{24}Na but they still slightly increase for ^{7}Be and ^{3}H. The asymptotic value of the cross section is depicted in fig. 2.6 by the horizontal line determined as arithmetic average of the cross sections measured for beam energies in the range of 1 GeV – 8 GeV. A large spread of the experimental production cross sections of tritons and ^{7}Be observed for energies in the neighbourhood of 1 GeV does not allow to extract precisely the asymptotic value of the cross sections for these particles. Thus the limiting fragmentation hypothesis, claiming that the cross sections level at asymptotically high beam energies seems to be fulfilled at energies above $\sim$ 1 GeV for former products while this is not evident for the latter ejectiles. Moreover, increasing of the total cross sections for tritons and ^{7}Be is quite prominent for energies smaller than 1 GeV, therefore, the limiting fragmentation certainly does not occur for these particles at energies lower than 1 GeV.

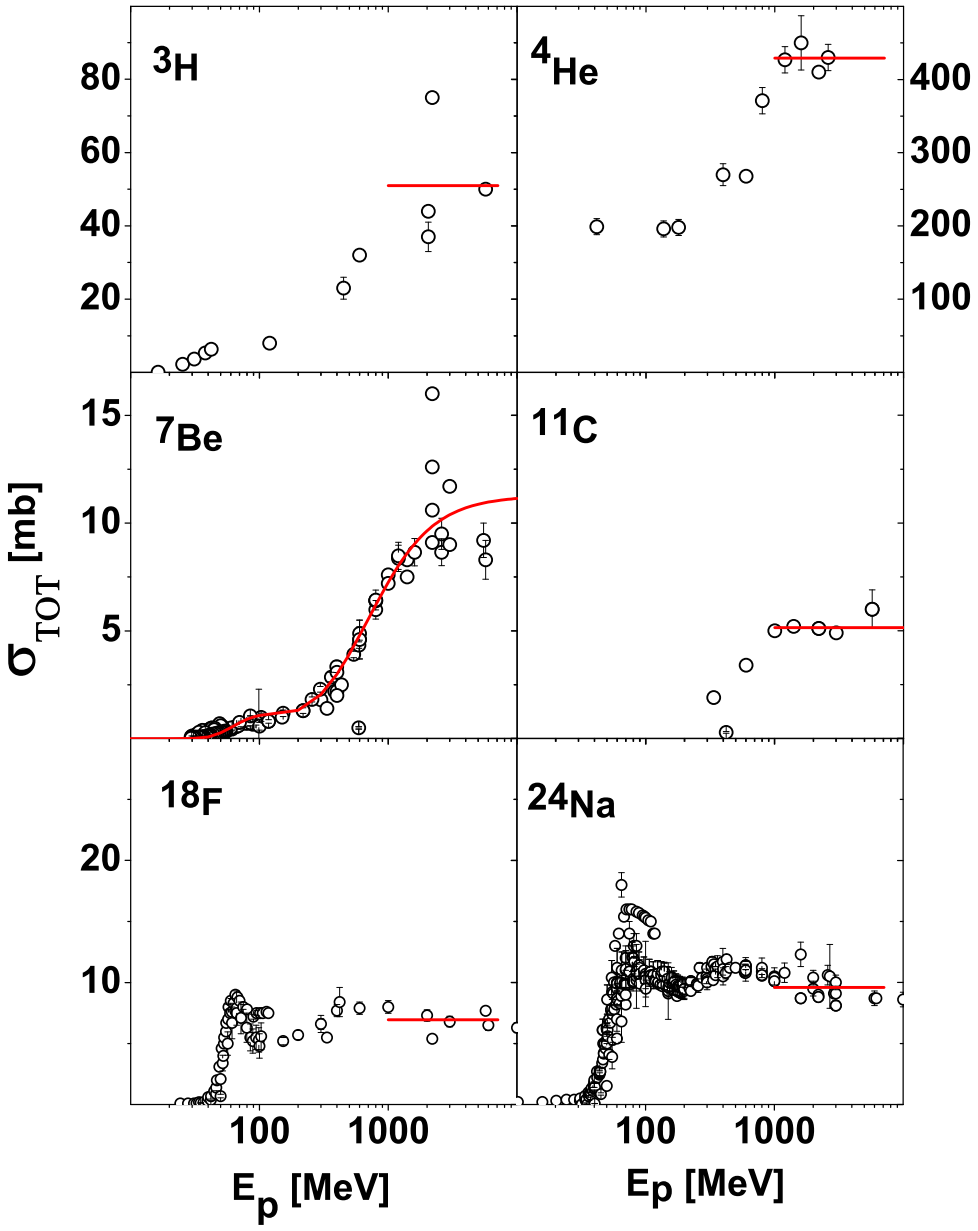

Figure 2.6: Excitation functions for production of ^{3}H, ^{4}He, ^{7}Be, ^{11}C, ^{18}F, and ^{24}Na in proton induced reactions on Aluminium target. The points represent experimental results published in literature by several collaborations listed in table A.1. The horizontal lines show the asymptotic cross section values, which are discussed in the text. The smooth line interpolating the ^{7}Be excitation curve presents results of parameterization of ^{7}Be data by Bubak et al. [13].

Table 2.1: Total production cross sections of ejectiles emerging from p+^{27}Al collisions in the energy region $E_p > 1$ GeV, which can be treated as limiting fragmentation region for ejectiles heavier than ^{10}Be. The right column presents compilation of the cross sections from literature averaged over 1 GeV - 8 GeV proton energy range. The quoted error corresponds to the standard deviation of the average value of data obtained in various publications, estimated from the spread of the data.

particle	σ_{tot} / mb
^{3}H	51.0(5.2)
^{3}He	61.4(4.7)
^{4}He	435.7(7.2)
^{6}He	1.20(10)
^{7}Be	9.73(65)
^{9}Li	0.185(55)
^{10}Be	2.96(10)
^{11}C	5.33(18)
^{13}N	1.633(67)
^{16}C	0.60(10)
^{17}N	0.690(30)
^{18}F	6.95(38)
^{20}Ne	22.4(2.0)
^{21}Ne	22.9(2.2)
^{22}Ne	18.8(3.2)
^{22}Na	13.52(57)
^{24}Na	9.59(21)
^{26}Al	20.60(72)

Following publications serve as a source of the data listed in table 2.1: ^{3}H [21–25], ^{3}He [6, 24], ^{4}He [6, 24], ^{6}He [26], ^{9}Li [27], ^{7}Be [6, 23, 25, 28–31], ^{10}Be [6, 25, 32, 33], ^{11}C [23, 28, 31, 34–37] ^{16}C [27], ^{13}N [23, 28, 31] ^{17}N [27], ^{18}F [23, 31, 36–39], ^{20}Ne [6, 24], ^{21}Ne [6, 24], ^{22}Ne [6, 24], ^{22}Na [6, 23, 25, 28, 30, 31, 36, 39, 40], ^{24}Na [6, 28, 31, 41–44], ^{26}Al [6, 25].

It should be pointed out that the production cross sections of ejectiles lighter than $\sim^{11}$C still vary in the studied energy range and therefore the quoted values of the data cannot be treated as asymptotic values of the cross sections for p+ ^{27}Al collisions.

In fig.2.7 excitation functions for production of ^{3}H, ^{4}He, ^{7}Li, ^{7}Be, ^{10}B, and ^{11}C on ***carbon target*** are presented. The pronounced maxima of the cross section are visible in excitation

functions for ^{4}He, ^{7}Be, and ^{11}C products below 100 MeV proton beam energy. Maxima of the cross sections are not present in excitation functions for ^{3}H, ^{7}Li, and ^{10}B. All excitation functions level at high proton beam energies. Leveling appears at energies smaller than 1 GeV, with exception of ^{3}H data where a large spread of experimental cross sections does not allow to derive ultimate conclusions.

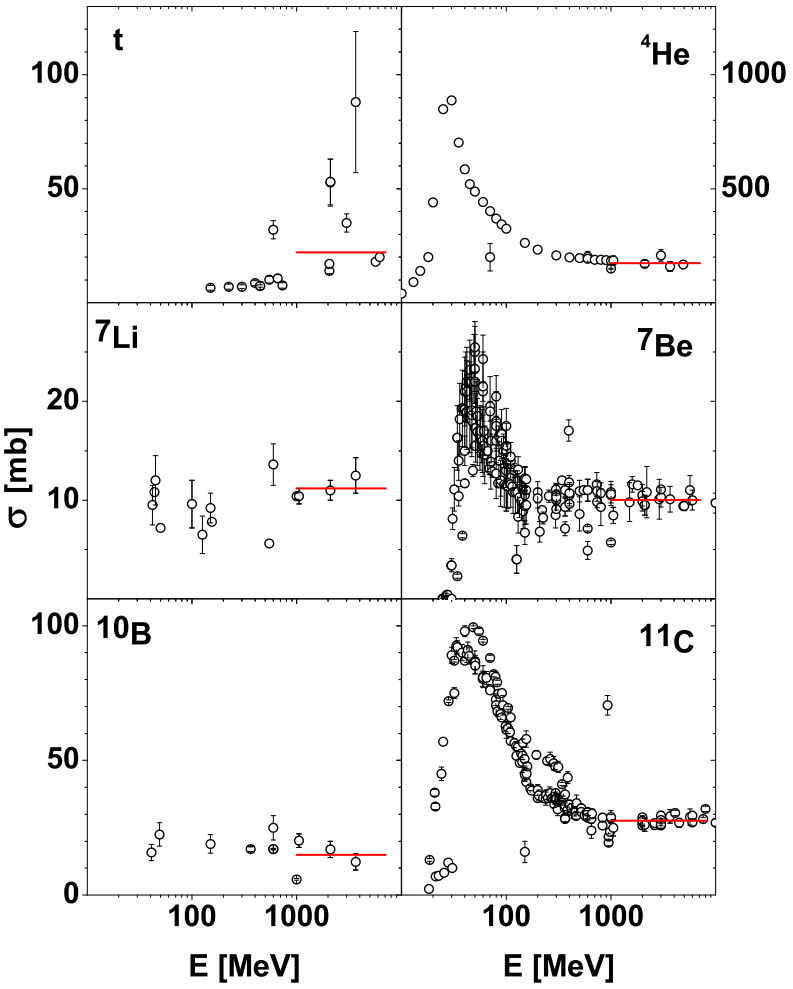

Figure 2.7: Excitation functions for production of tritons, ^{4}He, ^{7}Li, ^{7}Be, ^{10}B, and ^{11}C in proton induced reactions on Carbon target. The points represent experimental results published in the literature by several collaborations listed in the table A.2. The horizontal lines show the asymptotic cross section values, which are discussed in the text.

The asymptotic values of the total production cross sections, obtained as arithmetic mean

of values measured for proton beam energy larger than 1 GeV and smaller than 8 GeV, are listed in table 2.2 for all ejectiles observed in experiments described in the literature.

Table 2.2: Total production cross sections of ejectiles emerging from p+^{12}C collisions in the limiting fragmentation energy region ($E_p > 1$ GeV). The left column presents compilation of the cross sections from literature averaged over 1 GeV - 8 GeV proton energy range. The quoted error corresponds to the standard deviation of the average value of data obtained in various publications, estimated from the spread of the data. Two next columns present literature data from compilation prepared by Olson et al. [45], where interaction of carbon beam with hydrogen target was studied.

	present compilation	Olson et al [45]	
	$E_p \geq 1.0$ GeV	$E_C = 1.05$ GeV/nucleon	$E_C = 2.1$ GeV/nucleon
Ejectile	σ_{tot} / mb	σ_{tot}/ mb	σ_{tot} / mb
^{2}H	127.6(4.6)	125(16)	105(15)
^{3}H	33.7(5.8)		53(10)
^{3}He	42.3(2.3)	46.4(5.1)	51.5(4.5)
^{4}He	168.5(4.2)	185(19)	171(15)
^{6}He	0.821(46)	0.94(19)	0.91(21)
^{6}Li	10.09(92)	11.5(2.2)	13.9(1.5)
^{7}Li	9.53(78)	10.40(80)	11.0(1.0)
^{7}Be	10.00(24)	8.45(81)	9.5(1.0)
^{8}Li	1.12(20)	0.77(14)	1.13(16)
^{8}B	0.503(49)	0.600(90)	0.47(11)
^{9}Li	0.304(42)	0.400(90)	0.410(80)
^{9}Be	4.99(98)	5.13(54)	5.92(54)
^{9}C		0.280(60)	0.380(70)
^{10}Be	3.29(58)	3.41(54)	3.42(35)
^{10}B	15.0(2.7)	20.2(2.5)	16.9(3.0)
^{10}C	2.65(33)	2.52(28)	2.38(24)
^{11}B	22.6(6.8)	29.3(2.7)	30.9(3.4)
^{11}C	27.63(31)	25.0(3.0)	26.1(2.4)
^{12}B		0.050(10)	0.060(10)
^{12}N	0.040(10)	0.05	0.030(10)

The lists of experiments on spallation reactions induced by protons on Al and C targets are presented in tables A.1 and A.2, respectively (Appendix A). The largest amount of experiments was devoted to measurements of total production cross sections and only several papers dealt with determination of differential cross sections.

2.2 Multifragmentation and nuclear phase transition

The energy dependence of total production cross sections shown for p+C collisions in Fig. 2.7 indicates that multiplicity of ejectiles stabilizes at high proton beam energies starting from energies lower than those used in the present experiment (1.2 - 2.5 GeV) and remains constant in this energy range. This is true for all observed ejectiles with exception of the lightest (deuterons and tritons) for which experimental values of the cross sections are strongly scattered.

In the case of p+Al collisions the cross sections of light ejectiles (up to ^{7}Be) still slightly increase within the studied proton energy range but for heavier ejectiles, e.g., for ^{11}C the cross sections are constant in this energy range.

The knowledge of the asymptotic values of the production cross sections collected in Tables 2.1 (for p+Al collisions) and 2.2 (for p+C collisions) as well as the absorption cross section from parameterization of Tripathi et al. [46] allows for estimation of average multiplicity of ejectiles from these collisions. For example, summing the total cross sections of d, t, ^{3}He, and ^{4}He from table 2.2 and dividing them by absorption cross section, which for p+C system is equal $\sim$ 250 mb in the studied beam energy range, leads to average multiplicity:

$$\langle M \rangle \equiv \sigma_{inclusive}/\sigma_{absorption} \approx 1.5$$

Since cross sections for emission of nucleons is always bigger than the largest among d, t, ^{3}He, and ^{4}He production cross sections, it may be conjectured that the average multiplicity of ejectiles (including nucleons) is larger than 3 - 4. Process with such number of products is called ***multifragmentation*** [47] and requires large energy deposition in the target nucleus. Exactly speaking, the term multifragmentation was introduced for processes in which more than two fragments heavier than ^{4}He are emitted, however, in the case of ^{12}C target all the fragments must have small mass number.

The mechanism of multifragmentation has attracted the attention of physicists since over the last two decades and led to different theoretical models which were aimed to describe such reactions. One of the most interesting interpretation of multifragmentation corresponds to treating the multifragmentation ***as a phase transition*** from a quantum liquid (nuclei in the ground state) to a quantum gas (mixture of free nucleons and light fragments) [48].

A specific behaviour of caloric curve (a dependence of the temperature of atomic nucleus on its excitation energy per nucleon) is expected for such a phase transition. According to Natovitz et al. such specific signs for the existence of the phase transition are indeed observed in many experiments [49]. A compilation of caloric curves obtained in various experiments is presented in fig. 2.8. For all caloric curves a range of excitation energies can be found for which the temperature is constant, what corresponds to the phase transition in analogy to boiling of water.

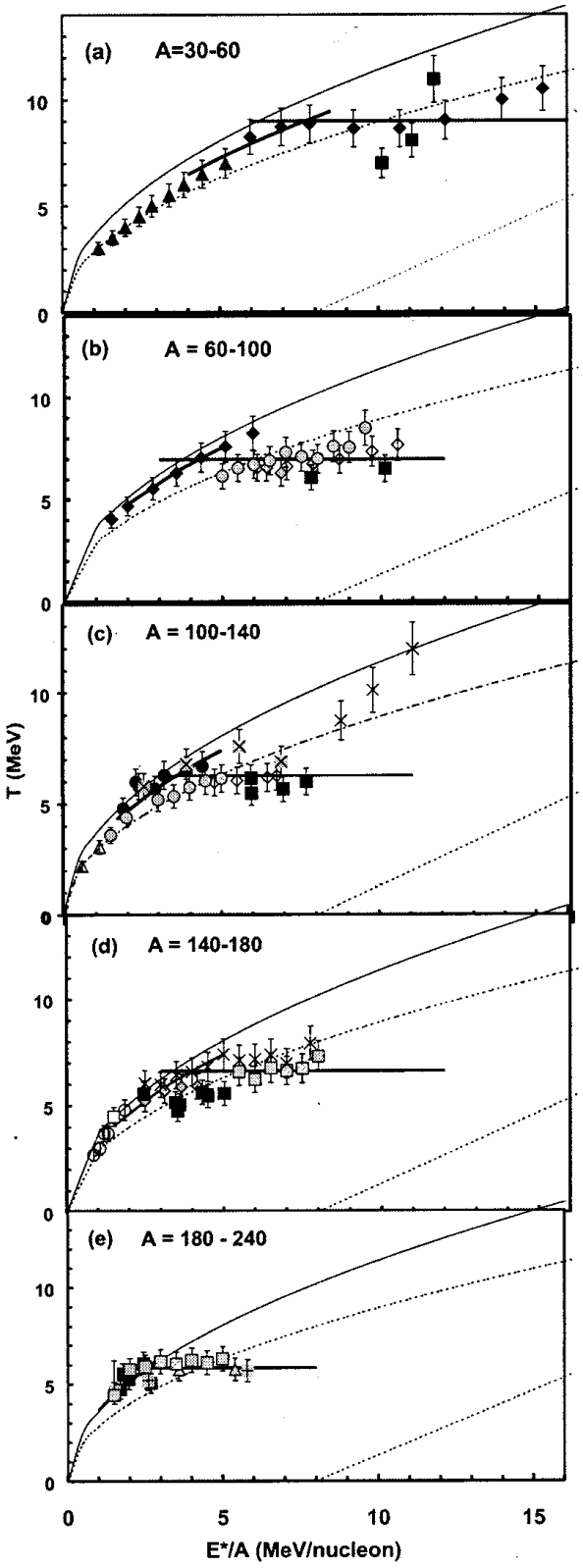

Figure 2.8: Caloric curves for various nuclei as studied by Natowitz et al. [49]

Information on caloric curves has been obtained in exclusive experiments as performed by INDRA, ALADIN, ISiS collaborations in which 4π detectors were used to detect all charged products. This method of measurements allowed to put gates on the collisions with an appropriate reaction mechanism.

The excitation energy per nucleon at which the "boiling" starts is different for different atomic nuclei - decreasing with increase of the mass number of nucleus. This dependence of critical value of the excitation energy per nucleon on the mass number of the nucleus is shown on fig. 2.9. Points with errors were taken from the reference [49] whereas the straight line represents the regression curve fitted to the data by the least squares method. There are also shown confidence intervals corresponding to one (dashed line) and two standard deviations (solid line) of the regression curve.

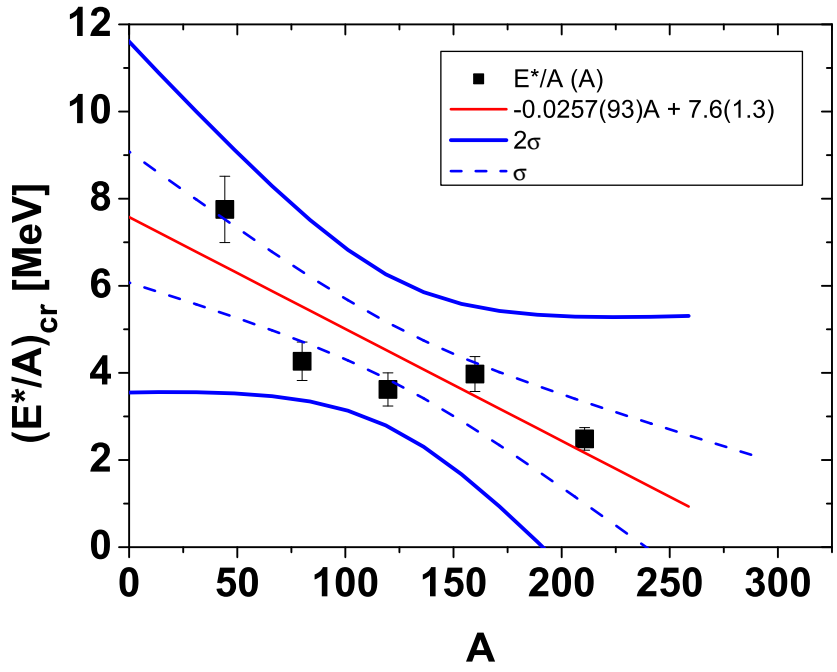

Figure 2.9: Dependence of the critical value of the excitation energy per nucleon on the mass of the excited nucleus which is subject to the phase transition. Data are taken from Natovitz et al. [49]. The straight line was fitted by means of the least squares method. The dashed and solid hyperbolas represent boarders of the confidence intervals for the regression line corresponding to its one and two standard deviations.

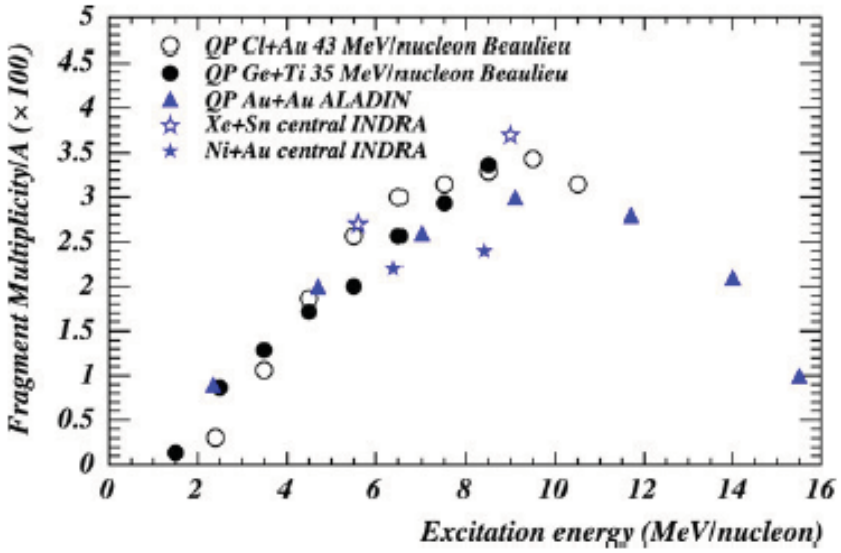

Figure 2.10: Average fragment multiplicity (normalized to the number of incident nucleons) as a function of the excitation energy per nucleon. Figure was taken from [50].

A compilation of average fragment multiplicities observed in various reactions for different nuclear excitation energies per nucleon is presented on fig. 2.10. Since the data were collected for various interacting systems the multiplicity is normalized to number of incident nucleons. Very regular behaviour of the dependence of fragment multiplicity on the excitation energy per nucleon indicates following facts:

(i) Multifragmentation is a general phenomenon, common for all interacting nuclear systems.

(ii) The excitation energy per nucleon of the nuclear system is a reliable parameter which decides about a fate of excited nucleus.

(iii) The onset of multifragmentation is visible for excitation energies around 3 MeV/nucleon and the maximum for fragment production is present around 9 MeV/nucleon, i.e. close to the binding energy per nucleon of nuclei. This last conclusion agrees well with results of Natowitz et al. [49] presented in fig. 2.9 above. At higher excitation energy, the fragment production decreases because fragments decay into nucleons and thus a vaporization of the nucleus appears [50].

The concept of phase transition is well grounded in thermodynamic description of macroscopic systems. Nuclei are large enough to be described by a thermodynamic formalism, however, they exhibit also such properties which do not allow for simple extrapolation of the standard theory. The competition of the surface tension and the long-range Coulomb force, which is larger than the size of atomic nuclei causes, that the approximation of infinitely large, macroscopic system cannot be automatically applied to the nuclei.

Moreover, it is evident that a deposition of energy in proton-nucleus collision depends not only on the energy of projectile but also on the impact parameter. It was proved in exclusive experiments that ***a strong correlation between deposition of energy and multiplicity of ejectiles exists*** [11] (cf. fig. 2.11).

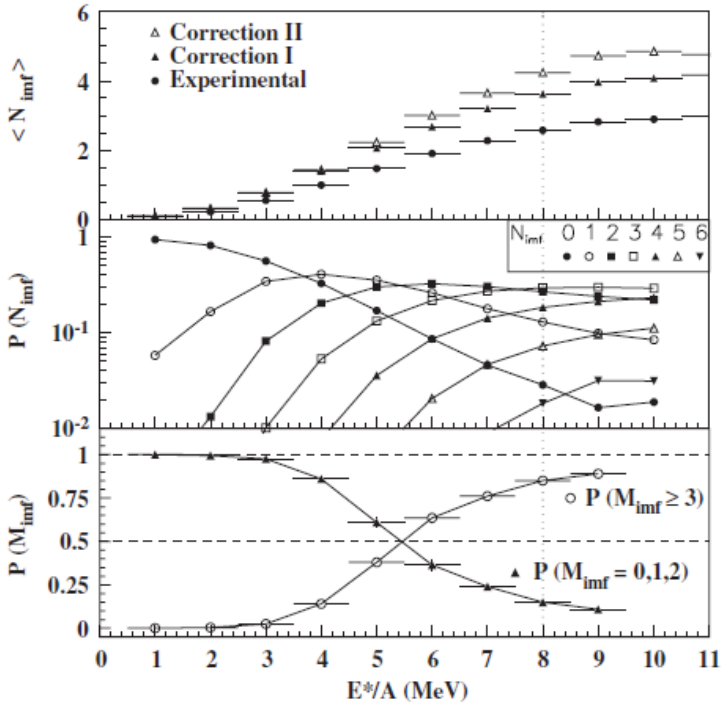

Figure 2.11: Experimentally determined dependence of the average multiplicity of intermediate mass fragments (upper panel), of the probability for different multiplicities (middle panel), and of the probability for (N=0)+(N=1)+(N=2) multiplicities and (N $\geq$ 3) multiplicities (lower panel) on the reduced excitation energy of decaying nucleus. The figure was taken from ref. [11] and corresponds to 8 GeV/c π^- induced fragmentation of ^{197}Au nuclei.

This figure (called frequently *Arrhenius plot*) illustrates the effect of temperature, which is in the first approximation proportional to the excitation energy per nucleon E^*/A, on the rates of nuclear reactions. It is obvious intuitively that the small impact parameters, where the projectile meets many nucleons on its way through the nucleus, should correspond in average to larger energy transfer to the nucleus and thus to higher excitation energy per nucleon than the peripheral collisions. This intuitive picture is confirmed by calculations performed in the frame of Quantum Molecular Dynamics, which simulate microscopically a time development of nucleus-nucleus collisions, showing that ***peripheral collisions produce predominantly smaller number of ejectiles than central collisions.*** (cf. fig. 2.12). This, in turn, proves that ***the peripheral collisions deposit in average smaller energy in the nuclei than***

the central collisions.

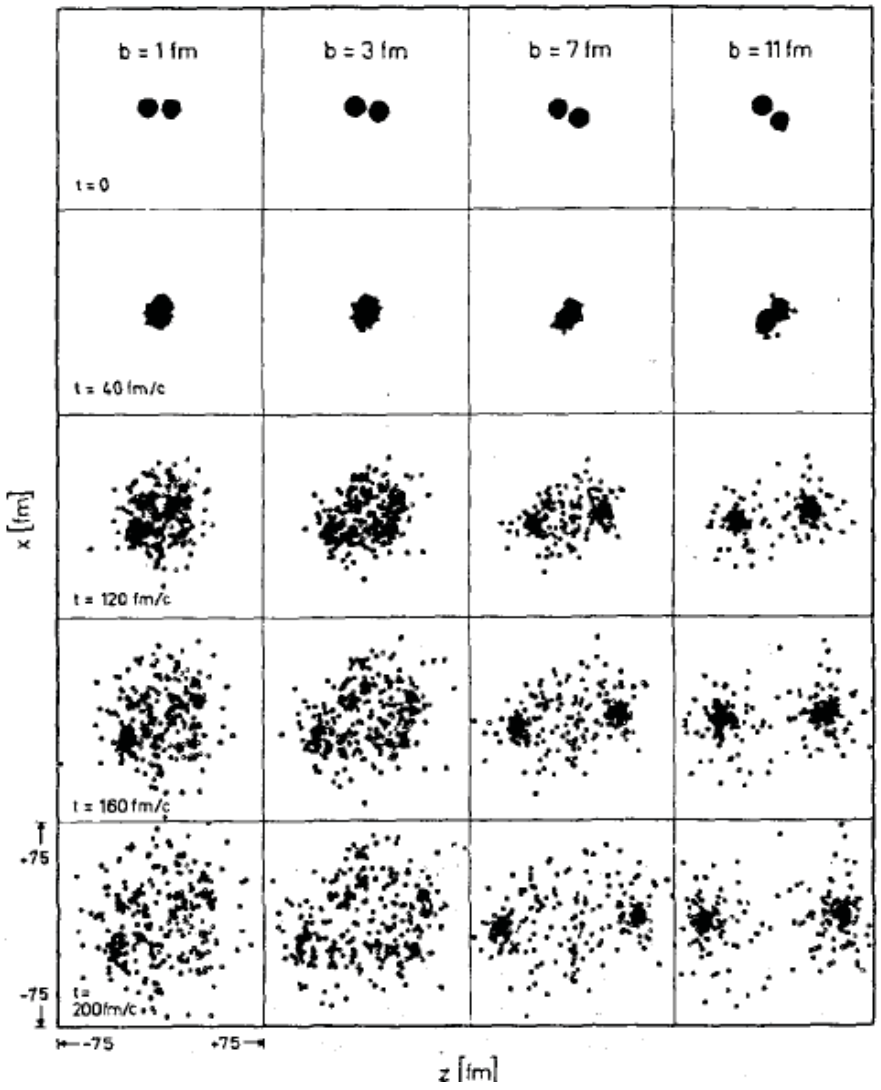

Figure 2.12: Time development of Au+Au collisions evaluated in the frame of QMD (Quantum Molecular Dynamics) model [51]. The nucleons are presented in the reaction plane. The consecutive columns from left to right correspond to impact parameter values b=1, 3, 7, and 11 fm, respectively. The consecutive rows (starting from the top) represent situation achieved after different periods of time t from beginning of the collision: t=0, 40, 120, 160, and 200 fm/c, respectively. The figure was taken from ref. [51].

Therefore, it is important to know that at given beam energy not all collisions of proton with target nucleus are able to deposit energy, which is large enough to initiate a multifragmentation of the nucleus. Since inclusive experiments are not able to trigger events which correspond to

such high excitation energy, the contributions of various reaction mechanisms cannot be easily disentangled. For this purpose exclusive experiments are necessary.

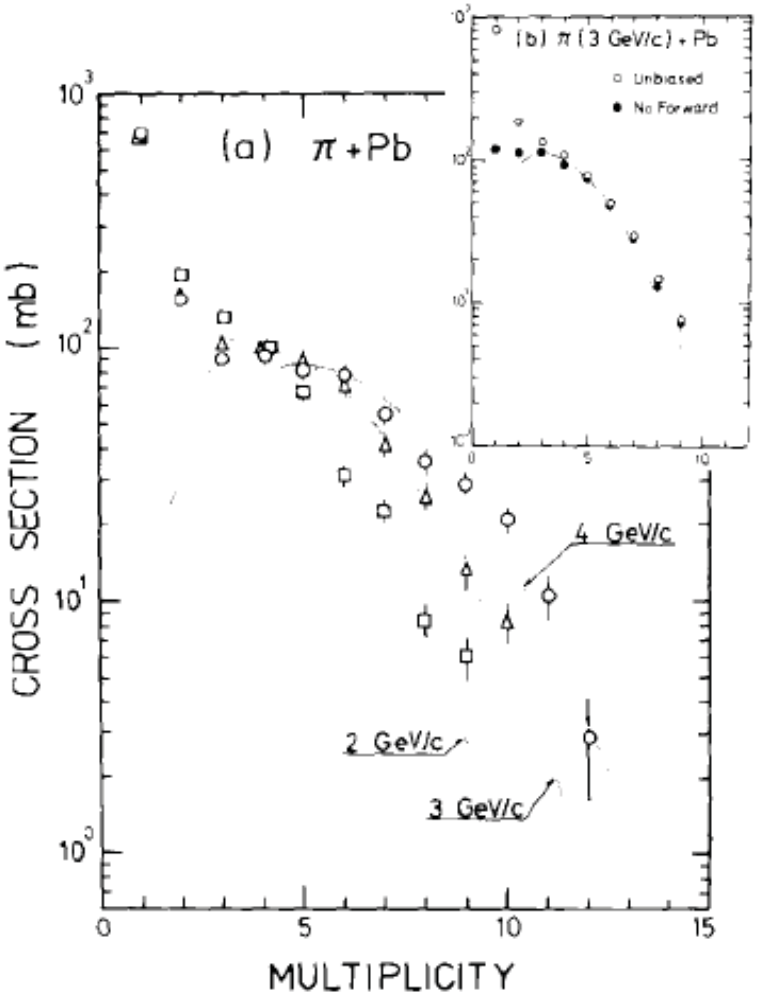

Figure 2.13: Multiplicity distributions of ejectiles from π+Pb collisions at several pion beam momenta (left, lower panel), and multiplicity distributions gated by coincidence with forward emitted particles (empty circles) and without gating condition (full dots) from the same reaction at beam momentum 3 GeV/c. Figure was taken from ref. [52].

An example of such exclusive - coincidence measurements which enable to achieve this goal are the coincidence studies of proton and pion induced reactions on Pb target, performed with the aid of 4π spectrometer at energies of several GeV [9, 52]. These investigations showed, that the low multiplicity events appear in most cases together with emission of fast particles at very small angles (smaller than $\approx 10^{\circ}$ in respect to the beam direction) . This is illustrated

by fig. 2.13. The above presented results indicate that ***the emission of fast particles in the forward direction is accompanied by a small energy deposition in the target nucleus.***

Chapter 3

Theoretical models

Theoretical models of the reaction mechanism induced by protons on atomic nuclei will be discussed in the present chapter. It is usually assumed that the proton impinging on the atomic nucleus initiates a series of nucleon-nucleon collisions which leads to emission of several nucleons and to equilibration of the remnant nucleus. There exist many theoretical models which describe both stages of nuclear reaction. All the models are equivalent to solving of many body Schroedinger equation. Since at present this task cannot be done accurately all the models introduce various simplifying assumptions which allow for practical calculations.

3.1 First stage of the reaction

In this section three microscopic models of the first stage of the proton-nucleus collisions are presented. They are chosen as to represent typical assumptions made to allow for practical calculations. In the subsection 3.1.1 *the intranuclear cascade* is discussed as realized in the Liége Intranuclear Cascade INCL model, in the subsection 3.1.2 *the Boltzmann-Uehling-Uhlenbeck model* is outlined and in the 3.1.3 subsection *the Quantum Molecular Dynamics model* is presented. As can be seen big part of assumptions is the same for all the models, as e.g., treatment of the Pauli principle. They differ, however, in several important aspects, as e.g., in treatment of the medium field, which is experienced by nucleons. The fourth subsection 3.1.4 is devoted to the ideas of a straight line interaction between projectile and nucleons, which are on its way through the nuclai.

3.1.1 Intranuclear cascade - INC

The models which assume, that the interactions of high-energy particles with the nucleus can be represented by free particle-particle collisions inside the nucleus are called intranuclear cascade models. They are realized in many different versions and use various refinements in comparison to such simple picture as mentioned above. Here, the INCL (*Liège Intranuclear Cascade*) model

will be discussed. The INCL model was for the first time presented in ref. [53] in version devoted to heavy ion collisions in the GeV range. Specific version of the model built in order to describe reactions induced by nucleons is published in ref. [54]. Its improved version, called INCL4.2, was presented in ref. [55] and was implemented in GEANT4 9.2. This version, generalized to allow for emission of clusters [56] is called INCL4.3. In the present work INCL4.3 was applied for description of the first stage of the proton-nucleus collisions.

The main assumptions and features of this version of the Intranuclear Cascade Model are following:

- The *spatial distribution* of nucleons inside the target nucleus is prepared according to a Saxon-Woods formula $\varrho(r)$ of radius R_0 and diffuseness parameter a, cut at $R_{max} = R_0 + 8a$:

$$\varrho(r) = \begin{cases} \varrho_0 / \left[1 + \exp\left(\frac{r - R_0}{a}\right)\right] & \text{for } r < R_{max} \\ 0 & \text{for } r \geqslant R_{max} \end{cases}$$

  where $R_0 = (2.745 \times 10^{-4} A_T + 1.063) A_T^{1/3}$ fm, $a = 0.510 + 1.63 \times 10^{-4} A_T$ fm and ϱ_0 is such that the distribution is normalized to A_T , the target mass number. The random *momentum distribution* of target nucleons was chosen inside a sphere with the radius equal to the Fermi momentum p_F.

- Target nucleons are placed in static (time independent), attractive potential of the square well shape with the radius R(p) and the depth V_0. The radius $R(p)$ is defined by formula:

$$\left(\frac{p}{p_F}\right)^3 = -\frac{4\pi}{3A_T} \int_0^{R(p)} \frac{d\rho(r)}{dr}\, r^3\, dr$$

  Nucleons with momentum larger than p_F, appearing in the case when the nucleus is excited, are moving in the potential well with radius R_{max}.

- Nucleons move inside the nucleus along straight trajectories until two of them collide or until one nucleon reaches the nucleus surface, where it can be transmitted or reflected. The collisions are allowed only between the nucleon from the beam and nucleons of the target (first collision) or between nucleons which took part in previous collisions and other nucleons (sequential collisions). It means that the collisions between spectators are forbidden.

- The collision takes place when the distance between two nucleons is smaller than

$$d_{min} \leqslant \sqrt{\sigma_{tot}/\pi}$$

where σ_{tot} is the total nucleon-nucleon cross section. The two particles scatter elastically or inelastically (with Δ emission and its sequential decay into pion and nucleon) in agreement with energy and momentum conservation laws.
The following possible reactions are considered:

$$NN \to NN, \;\; NN \to N\Delta, \;\; N\Delta \to N\Delta, \;\; \Delta\Delta \to \Delta\Delta, \;\; \pi N \to \Delta$$

- Whereas the motion of nucleons in the nucleus is treated classically, the quantum effects are not totally neglected, i.e. *the Pauli blocking* is introduced for occupation of the final states which might be populated due to the collision. This is realized in the following way: The collisions appears with probability $P = (1 - f_i)(1 - f_j)$, where f_i and f_j are phase space (r and p-spaces) occupations for i and j-particles. The phase-space occupation probabilities f_i are evaluated by counting nearby nucleons in a small phase-space volume

$$f_i = \frac{1}{2} \frac{(2\pi\hbar)^3}{\frac{4\pi}{3} r_{PB}^3 \frac{4\pi}{3} p_{PB}^3} \sum_{k \neq i} \theta\left(r_{PB} - |\vec{r}_k - \vec{r}_i|\right) \times \theta\left(p_{PB} - |\vec{p}_k - \vec{p}_i|\right)$$

  where $r_{PB} = 3.18$ fm and $p_{PB} = 200$ MeV/c. The sum over k is limited to particles with the same isospin component as particle i and factor $1/2$ appears because of two spin components which are not treated explicitly.

- The light charged particles (LCP) can be emitted besides the nucleons, Δ's, and pions. Emission of LCPs is treated as the coalescence process: The nucleon, which would be able to leave the target is allowed to attach one, two or even more nucleons, which are lying on its path through the nucleus if momenta of these nucleons are close to its momentum. Then a group of nucleons forming the complex particle is emitted instead the single nucleon. Coalescence criterion is determined by the following condition of a close position (in r- and p-space) of the nucleons forming the complex ejectile:

$$r_{i,[i-1]} p_{i,[i-1]} \leqslant h_0$$

  where h_0 was chosen to be equal 387 MeV fm/c and indices i and $i-1$ enumerate the Jacobi coordinates of the i-th nucleon of the ejectile in respect to a group of i-1 nucleons of this particle. The biggest particle, which can leave the target during the coalescence process is ^{4}He, because of decreasing probability to find more than 4 nucleons close enough in a phase space.

Further details of the model, as e.g., the parametrization of total elastic and inelastic cross sections, stopping criteria of the calculations, details of the hierarchy between clusters formed by coalescence, etc., can be found in refs [55, 56] and references cited therein.

3.1.2 Boltzmann-Uehling-Uhlenbeck model - BUU

The BUU *(Boltzmann-Uehling-Uhlenbeck)* model is based on the transport equation [57–60]

$$\begin{aligned} \frac{\partial f}{\partial t} + \vec{v} \bullet \nabla_r f - \nabla_r U \bullet \nabla_p f &= -\frac{4}{(2\pi)^6} \int d^3p_2 \; d^3p_{2'} \; d\Omega \; \frac{d\sigma}{d\Omega} \; v_{12} \\ &\times \; \{[f f_2 (1-f_{1'})(1-f_{2'}) - f_{1'} f_{2'} (1-f)(1-f_2)] \\ &\times \; (2\pi)^3 \delta^3(\vec{p} + \vec{p}_2 - \vec{p}_{1'} - \vec{p}_{2'})\} \end{aligned} \tag{3.1}$$

which allows to find single particle phase space distribution ($f_1(\vec{r}, \vec{p}, t) \equiv f$) of nucleons.

The left hand side of the equation determines a motion of the nucleon "1" in the mean field U produced by other nucleons taking part in the reaction. The right hand side of the equation is responsible for two-body collisions among the nucleons. The index "2" denotes the nucleon which collides with nucleon "1" – before their collision, whereas the indices "$1'$", "$2'$" represent the nucleons "1" and "2" – after collision. The symbols "f" and "p" should be read as "f_1" and "p_1", respectively. The differential nucleon-nucleon cross section is denoted by $\frac{d\sigma}{d\Omega}$ and the modulus of the relative velocity of colliding nucleons by v_{12}. The formula closed into square parentheses contains factors responsible for obeying the Fermi-Dirac statistics by the nucleons (see below). The conservation of the momentum is granted by presence of the Dirac's delta function $\delta^3(\vec{p} + \vec{p}_2 - \vec{p}_{1'} - \vec{p}_{2'})$.

In the original Boltzmann transport equation the phase space distribution $f(\vec{r}, \vec{p}, t)$ is normalized in such a way that number of particles N, placed in the moment t in the phase space element $d^3r \; d^3p$ around the phase space point $(\vec{r}, \vec{p})$, is equal to:

$$N = f(\vec{r}, \vec{p}, t) \; d^3r \; d^3p.$$

In the case of the BUU equation it is more favourable to change the normalization of f in order to take into account the quantum effect caused by the fact that nucleons are fermions and they must respect the Pauli principle. It means, that the number N must be smaller or equal to number of allowed quantum states for the nucleons placed in the phase space element $d^3r \; d^3p$:

$$N \leqslant 4 \; d^3r \; d^3p/h$$

where h is the Planck constant and the factor 4 appears due to the spin and isospin degeneracy of nucleon states.

The usual choice of normalization of the function f is to put $f = 1$ for the case when all quantum states are occupied and $f = 0$ when all quantum states are empty. This choice allows to interpret the $f(\vec{r}, \vec{p}, t)$ function as the *occupation probability* of the $d^3r \; d^3p$ phase space element in the moment t and to interpret the factor $1 - f(\vec{r}, \vec{p}, t)$ as the probability that the phase

space element is empty. Therefore the collision $1+2 \rightarrow 1^{'}+2^{'}$ is possible when the probability ff_2 to find nucleons 1 and 2 in the same point of the phase space as well as the probability $(1-f_{1'})(1-f_{2'})$ to find empty states for scattered nucleons $1^{'}$ and $2^{'}$ are both different from zero. The analogous reasoning is true for the reaction $1^{'}+2^{'} \rightarrow 1+2$, which also contributes to the r.h.s. of the BUU equation. The presence of the above factors has so called "*Pauli blocking*" effect on solution of the BUU equation.

The BUU transport equation (3.1) for unknown function $f(\vec{r},\vec{p},t)$ can be solved when the nucleon-nucleon cross sections $\frac{d\sigma}{d\Omega}$ are known as well as the mean field $U(\vec{r},\vec{p},t=0)$ and the distribution function $f(\vec{r},\vec{p},t=0)$ in the initial moment of time. It should be, however pointed out that the evolution of the mean field in time is not determined by the BUU equation itself, thus the introducing of additional assumptions concerning relationship of the mean field and the f-function is necessary. Usually the specific form of this dependence, called *the Skyrme parametrization*, is postulated:

$$U(\varrho) = A(\varrho/\varrho_0) + B(\varrho/\varrho_0)^{\sigma}$$

where ϱ is a spatial density distribution of the nucleons which depends implicitly on the f function and ϱ_0 is a ground state density of the nuclei ($\varrho_0 \approx 0.17$ fm^{-3}). Coefficients A and B represent the attractive and repulsive force respectively and $\sigma >1$ is a parameter. Values of the constants A and B are determined from requirement to reproduce the known position and depth of the minimum of the energy in the nuclear matter, i.e., the minimum is obtained at $\varrho = \varrho_0 \approx 0.17\ fm^{-3}$ with energy value E/A$= -16$ MeV. Value of the σ constant is fixed when the incompressibility coefficient K of the nuclear matter is known. This coefficient is directly related to the second derivative of the equation of state (EOS) of symmetric nuclear matter:

$$E[\varrho] \approx E[\varrho_0] + \frac{K}{18}\left(\frac{\varrho-\varrho_0}{\varrho_0}\right)^2$$

A value of K $\approx$ 200 MeV is commonly used for *a soft EOS*, while K $\approx$ 380 MeV corresponds to *a stiff EOS*.

These two values of incompressibility parameter together with known values of $\varrho_0 \approx 0.17$ fm^{-3} and $(E/A)|_{\varrho_0} \approx -16$ MeV allow to determine all three constants in the Skyrme parametrization by the formula:

$$K = 9 \times \left(A + B\sigma + \frac{p_F^2}{3m}\right)$$

where p_F is the Fermi momentum and m denotes mass of the nucleon:

- for a soft EOS: A$= -356$ MeV, B$=$303 MeV, $\sigma = 7/6$, whereas
- for a stiff EOS: A$= -124$ MeV, B$=$70.5 MeV, $\sigma = 2$ (cf. ref. [59]).

Of course, these choices of the prescription for the mean field are not unique. In the Giessen BUU model [61], which we used for comparison with INCL model, the mean field was constructed adding the Yukawa term to the Skyrme force, and (for protons) the Coulomb potential:

$$U(\vec{r}) = A\left(\frac{\varrho\left(\vec{r}\right)}{\varrho_0}\right) + B\left(\frac{\varrho\left(\vec{r}\right)}{\varrho_0}\right)^{4/3} + V_0 \int d^3\vec{r}' \frac{\exp\left(-\mu\left|\vec{r}-\vec{r}'\right|\right)}{\mu\left|\vec{r}-\vec{r}'\right|}\varrho\left(\vec{r}'\right) + V_{Coul}$$

where A= -141.62 MeV, B= 165.23 MeV, V_0=-378 MeV, $\mu = 2.175$ fm^{-1}, ϱ_0= 0.168 fm^{-3}.

The BUU equation (3.1) is an integro - differential equation in seven-dimensional space $(\vec{r}, \vec{p}, t)$, which cannot be solved analytically. It was shown (see e.g. the ref. [58]) that the efficient method of solution of BUU equation consists in Monte Carlo simulation of motion of so called "test particles" in dynamically varying mean field U with inclusion of two-particle collisions. Each nucleon is represented by a group of "n" test particles.

The main assumptions and methods of searching for the solution of BUU equation in the Giessen BUU model are listed below:

- The initial *spatial* distribution of nucleons in the nucleus of mass number A follows the Woods-Saxon distribution:

  $$\varrho(r) = \varrho_0 / \left[1 + \exp\left(\frac{r - R_0}{a}\right)\right]$$

  with $\varrho_0 = 0.168$ nucleon/fm^3, R=1.124 A$^{1/3}$ fm, a= 0.025 A$^{1/3}$ + 0.29 fm.

  The initial *momentum* distribution of nucleons in the nucleus is homogenous in the Fermi sphere with the radius $p_F(r)$ dependent on the local spatial density of nucleons:

  $$p_F(r) = \left(\frac{3\pi^2\varrho(r)}{2}\right)^{1/3}$$

  The test particles representing the proton impinging on to the target nucleus are randomly distributed in the cylinder which axis is parallel to the proton beam momentum and goes through the center of the target nucleus, the radius is equal to the maximal expected impact parameter, and the height is very small. Such choice of the spatial distribution of the test particles assures averaging over all impact parameters. Of course, all test particles move with the same momentum – equal to momentum of the proton from the beam.

- Target nucleons move in the dynamically varying in time the mean field U described above. The density $\varrho(\vec{r})$ entering the formula for the mean field is calculated on the grid

points $\vec{r}_g$, summing over all (n · A(t)) test particles and weighting the contribution of the i-th test particle to the density by the Gauss function:

$$\varrho(\vec{r}_g) = \frac{1}{n}\sum_{i=1}^{nA(t)} \frac{1}{(2\pi\Delta^2)^{3/2}} \exp\left(-\frac{(\vec{r}_g - \vec{r}_i)^2}{2\Delta^2}\right)$$

where $A(t)$ represents number of nucleons present in the nucleus at moment t. The Δ parameter denotes standard deviation of the Gauss distribution and it is usually assumed to be equal 1 fm.

- The test particles move along straight lines between collisions according to classical Hamilton equations:

$$\begin{aligned} \dot{\vec{p}}_i &= -\frac{\partial U\left(\vec{r}_i, \vec{p}_i, t\right)}{\partial \vec{r}_i} \\ \dot{\vec{r}}_i &= \frac{\vec{p}_i}{\sqrt{m^2 + p_i^2}} + \frac{\partial U\left(\vec{r}_i, \vec{p}_i, t\right)}{\partial \vec{p}_i} \end{aligned}$$

Collisions are allowed only for test particles representing different nucleons. It should be pointed out, that position and momentum of each test particle is checked in constant time steps (not only at moments of collisions as in the INCL model) because such knowledge is necessary to determine time dependence of the f function. This function is calculated for given t - moment according to the formula:

$$f(\vec{r}, \vec{p}, t) = \frac{1}{n}\sum_{i=1}^{n\cdot A(t)} \delta^3(\vec{r} - \vec{r}_i(t))\delta^3(\vec{p} - \vec{p}_i(t))$$

where the sum is done over all test particles.

- The same condition for the collision is used as that in the INCL model, i.e., the collision occurs when the impact parameter value d_{min} (equal to the smallest distance between two test particles) is smaller than $\sqrt{\sigma_{tot}/\pi}$. It is assumed that only two-body final channels are realized in the collisions with the explicite energy and momentum conservation. The present version of Giessen BUU model allows for production of various nucleonic resonances besides the Δ resonance. Of course, unstable resonances decay later emitting nucleons and mesons.

- The *Pauli blocking* is implemented in the BUU model by the requirement that only such collisions are allowed which lead to empty or partially occupied final states. This is done in analogous way as in the INCL model.

- The BUU model allows to obtain yields of nucleons, mesons and remnants of the target nucleus after the fast stage of the reaction, however, the emission of light complex fragments like deuterons, tritons, etc., is not considered.

In summary, the Monte Carlo method of solution of BUU equation is very similar to that used in the INCL model. There are three main differences besides the possibility of the INCL4.3 model to calculate coalescence of nucleons into light charged particles:

(1.) The static potential in which move nucleons according to INCL model is replaced by dynamically varying mean field in BUU model.

(2.) Tracing of the fate of all nucleons participating in the reaction, present in the INCL, is replaced in the BUU model by observation of motion of n test particles per each nucleon.

(3.) In the INCL the information on position and momentum of nucleons is gathered only at the moments of collisions whereas in the BUU model full information is obtained for all test particles in constant time intervals.

The first of the above differences is of physical origin, i.e. the BUU model allows to study collective effects governed by modification of the mean field during the reaction whereas it is impossible for intranuclear cascade model. Typical example of such effects is excitation and decay of monopole giant resonances. Two other differences are more of technical nature caused by different numerical methods of solution, appropriate for both models. This differences lead to more complicated calculations in the frame of BUU than the respective calculations made by INCL model.

3.1.3 Quantum Molecular Dynamics - QMD

Derivation of the QMD (*Quantum Molecular Dynamics*) model, the introduced assumptions and simplifications are described in detail in review article of Aichelin [51]. The specific model realization - JQMD (Jaeri Quantum Molecular Dynamics) by Niita et al. [62] is discussed below.

Nucleons participating in the reaction are represented by product of Gaussian shape wave functions:

$$\phi(\vec{r},\vec{p},t) = \prod_i \phi_i(\vec{r},\vec{p},t) = \prod_i \frac{1}{(2\pi L)^{3/4}} \exp\left[-\frac{\left(\vec{r} - \vec{R}_i(t)\right)^2}{4L} \; + \; \frac{i}{\hbar}\vec{p}\cdot\vec{r} \right]$$

where L is a width of a Gauss function (in JQMD $L = 2$ fm^2) and $\vec{R}_i(t)$ denotes position of the centre of the i-th nucleon. The wave function is then transformed to so called *Wigner density* (cf., e.g., [59]):

$$\begin{aligned} f(\vec{r},\vec{p},t) &\equiv \prod_i f_i\left(\vec{r},\vec{p},t\right) \\ &= \prod_i 8\,\exp\left[-\frac{\left(\vec{r}-\vec{R}_i(t)\right)^2}{4L} - \frac{2L\left(\vec{p}-\vec{P}_i(t)\right)^2}{\hbar^2}\right] \end{aligned}$$

where P_i is coordinate of the center of the packet representing i-th nucleon in the momentum space.

Time evolution of $R_i(t)$ and $P_i(t)$ is found in similar way as in the transport equation. Namely:

- Initial spatial positions $\vec{R}_i(t=0)$ of nucleon wave packet centers in the ground state of target nucleus are randomly chosen according to Woods-Saxon distribution with radius $R = 1.124A^{1/3} - 0.5$ fm and diffuseness $a = 0.2$ fm. The tail of the distribution is cut at $R_{max} = 1.124A^{1/3}$. During the sampling of nucleon positions the relative distance between nucleons of the same kind is limited to values larger than 1.5 fm and distance between neutrons and protons to values larger than 1.0 fm. This assures that spatial density fluctuations are not too large.

  Knowledge of positions of all nucleons allows to find the density of nucleus in each point and then to calculate the potential energy (see below). This also allows to determine local Fermi momentum $p_F(\vec{R}_i)$. The center of wave packet in the momentum space $\vec{P}_i(t=0)$ is randomly sampled in the sphere of the radius equal to the local Fermi momentum.

  Further constraints are used to assure that the set of nucleon packets represents well the ground state of the nucleus. First, it is checked whether the sum of kinetic and potential energy of the sampled nucleon is positive. Such unbound nucleons are rejected from the sampling. Next condition requires that the obtained phase space factor $f(\vec{r},\vec{p})$ must obey Pauli exclusion principle. Otherwise the sampled nucleon is also rejected. The last condition to accept the constructed "nucleus" as the real nucleus in its ground state is to obtain in the sampling the proper total binding energy. This is checked by comparison of evaluated binding energy with the simple drop model formula:

  $$E_{bind} = -16.56\,A + 17.23\,A^{2/3} + 46.57\frac{(N-Z)^2}{2A} + \frac{3}{5}\frac{Z^2e^2}{1.24A^{1/3}}$$

  If the evaluated binding energy per nucleon deviates from the drop model value less than 0.5 MeV the set of sampled nucleons is accepted as a good approximation of the target

nucleus in its ground state. Thus it is granted, that the "ground state" obtained by this procedure has an appropriate binding energy. However, it is not the energy minimum state of fermions, therefore only $\sim 70\%$ of the collisions are blocked by the final state Pauli blocking. To avoid spontaneous emission of nucleons from the ground state of the nucleus due to collisions of nucleons of the same nucleus, the nucleons of the target nucleus may collide only with the proton from the beam or with those nucleons of the target which previously experienced a collision.

It should be pointed out that the above conditions are quite restrictive and reject most of the sets of nucleons obtained in the sampling procedure which gives reasonable spatial and momentum distributions.

- The time evolution of the $R_i(t)$ and $P_i(t)$ is governed by Newtonian equations of motion:

$$\begin{aligned} \frac{d\vec{R}_i(t)}{dt} &= \frac{\partial H}{\partial \vec{P}_i} \\ \frac{d\vec{P}_i(t)}{dt} &= -\frac{\partial H}{\partial \vec{R}_i} \end{aligned}$$

where the hamiltonian H contains both, single particle energy and energy of two-body interactions:

$$\begin{aligned} H &= \sum_i \sqrt{m_i^2 + P_i^2} + \frac{1}{2}\frac{A}{\rho_0}\sum_i \langle \rho_i \rangle + \frac{1}{1+\sigma}\frac{B}{\rho_0^\sigma}\sum_i \langle \rho_i \rangle^\sigma + \\ &+ \frac{1}{2}\sum_{i,j\neq i} c_i c_j \frac{e^2}{\left|\vec{R}_i - \vec{R}_j\right|} erf\left(\left|\vec{R}_i - \vec{R}_j\right| / \sqrt{4L}\right) + \\ &+ \frac{C_S}{2\rho_0}\sum_{i,j\neq i}\left(1 - 2\left|c_i - c_j\right|\right)\rho_{ij} \end{aligned}$$

where "erf" denotes error function. The first sum represents the mass term, the next two sums – the effective Skyrme interaction, the fourth sum gives the Coulomb, and the last sum – the symmetry term.

The constants used in this formula have following values:

$$c_i = \begin{cases} 1 & \text{for protons} \\ 0 & \text{for neutrons} \end{cases}$$

the symmetry energy parameter:

$$C_S = 25 \text{ MeV}$$

and Skyrme parametrization parameters:

$$A = -219.4 \text{ MeV}, \;\; \text{B} = 165.3 \text{ MeV}, \; \sigma = 4/3$$

The symbol $< \varrho_i >$ represents an overlap of i-th nucleon density with density of other nucleons defined as

$$\begin{aligned} \langle \varrho_i \rangle &\equiv \sum_{j \neq i} \varrho_{ij} \equiv \sum_{j \neq i} \int d\vec{r}\, \varrho_i(\vec{r})\, \varrho_j(\vec{r}) = \\ &= \sum_{j \neq i} \frac{\exp\left[-\left(\vec{R}_i - \vec{R}_j \right)^2 / 4L \right]}{(4\pi L)^{3/2}} \end{aligned}$$

where

$$\begin{aligned} \rho_i(\vec{r}) &\equiv \int \frac{d\vec{p}}{(2\pi\hbar)^3}\, f_i(\vec{r}, \vec{p}) = \\ &= \frac{\exp\left[-\left(\vec{r} - \vec{R}_i \right)^2 / 2L \right]}{(2\pi L)^{3/2}} \end{aligned}$$

The L parameters equals to 2 fm as it was stated earlier.

- The condition for collisions of the nucleons is the same as in the INCL and BUU models, i.e., the collision occurs when the minimal distance between two nucleons is smaller than $d_{min} = \sqrt{\sigma/\pi}$. The elastic as well as inelastic collisions with creation of deltas ($\Delta(1232)$) and N* (N*(1440)) are considered. The Δ's and $N^{*'}$s are propagated in the same interactions as the nucleons except for the symmetry term. These resonances are allowed to decay with emission of pions. The pion propagation is determined only by the Coulomb interaction. Detailed description of the elementary cross sections used in JQMD can be found in ref. [62].

- The Pauli exclusion principle is also taken into account in the same method as in the Giessen BUU model described above.

- JQMD allows to study not only emission of nucleons, barionic resonanses and pions but, what is specific for this model, to study emission of clusters of nucleons. Different criteria can be used for treatment of a group of nucleons as an excited cluster.

Further details of the JQMD, as ,e.g., approximate treatment of the relativistic effects may be found in the work of Niita et al. [62].

The QMD model is considered as the most realistic simulation of the nucleus - nucleus interaction among the three discussed above models. Its drawback is, however, quite cumbersome calculations leading to very time consuming analysis of the data.

3.1.4 Interaction of the projectile with a group of nucleons

The models described above, i.e., INCL, BUU, and QMD assume that the projectile interacts with individual nucleons only. This means that the interaction of the projectile with a group of nucleons is completely neglected. There are, however, indications that protons of high energy collide also with several nucleons in a single act of interaction what can lead to quite pronounced effects. For example such a process was crucial for understanding of the momentum transfer in deep spallation reactions induced by protons on gold target as found by Cumming [63]. Similar observations has been made by Meng Ta-chung [64] for multiparticle production. It was claimed that "the nucleons along the path of the incident hadron inside the target nucleus can be viewed as acting collectively, and in the first-order approximation can be considered as a single object - an *effective target*". Dimension of the "effective target" was estimated by Meng Ta-Chung to be approximately equal to $A^{1/3}$ nucleons, where A is mass number of the target nucleus. Similar results for the size of the "effective target", i.e. 3.1 ± 0.4 nucleons for proton - gold collisions, was obtained by Cumming [63]. Such observations indicate that a specific effects may appear in first stage of proton-nucleus collisions, which cannot be reproduced by a set of nucleon-nucleon interactions. Several models which try to exploit idea of the "effective target" have been proposed. The most popular are the "**fireball model**" of Westfall et al. [15,65] and the "**firestreak model**" of Myers [66], and of Gosset et al. [67].

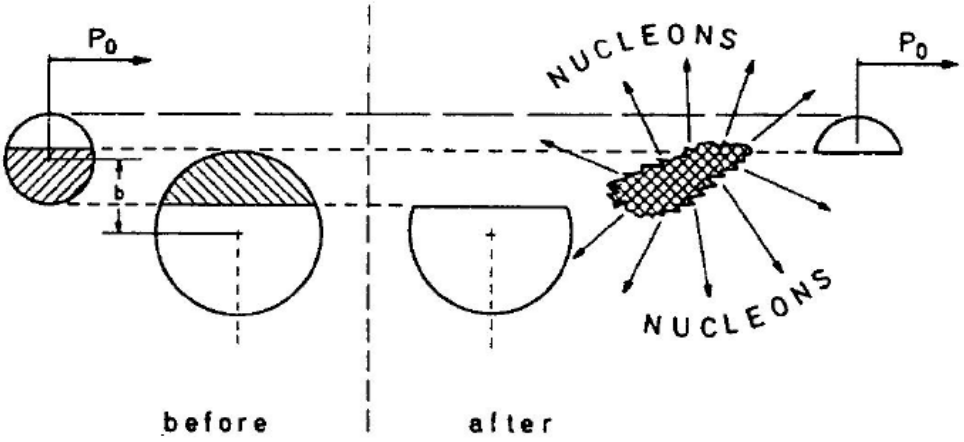

Figure 3.1: Formation of the fireball in collision of two heavy nuclei. The shaded area in the overlap zone represents nucleons, which take part in the collision and are named participants. These nucleons build the fireball. The figure comes from [68].

The **fireball model** assumes a straight line trajectory of the projectile, which cut a cylindrical shape through the target. The nucleons which are present inside volume of the cylinder fly together out of the nucleus forming a fast and hot group of nucleons called "the fireball". It

is worth to point out that the nucleons which belong to the fireball are not correlated dynamically to form the cluster. They are only spatially correlated due to their close position inside the nucleus. The scheme of the process of the fireball production in collision of two heavy nuclei is presented in Fig. 3.1.

The size of the fireball depends on the size of the projectile and the target as well as on the impact parameter. The total cross section for the fireball production is given by:

$$\sigma_t = \pi(A_1 R_2^2 + A_2 R_1^2) \tag{3.2}$$

where A_i and R_i are the number of participant nucleons in the nucleus "i" and the radius of the cylindrical cut in this nucleus, respectively. This cross section is larger than the geometrical cross section $\pi(R_1 + R_2)^2$ because it counts all individual emerging participant particles.

The fireball is treated as an ideal gas characterized by the temperature τ. Thus in the original fireball model all nucleons are independent and can be emitted separately. The temperature τ of the fireball is determined by available energy per nucleon ϵ through the relation: $\epsilon = (3/2)\tau$. The energy distribution has a Maxwell-Boltzmann shape characteristic for given temperature τ. Emission of nucleons (and emission of other particles in more involved version of the model) from the fireball is isotropic in its rest frame. Due to the fact that the fireball moves along the beam direction with the velocity which has an intermediate value between velocity of the projectile and the velocity of the target, the emission of particles is forward peaked in the laboratory system.

This model can predict the mean multiplicity and inclusive spectra for nucleons and pions [15]. The generalized version of the model allows also for emission of complex particles, however then the model is lacking a predictive power, i.e., it is rather treated as a method of parametrization of the inclusive energy and angular distributions of the cross sections [69].

The **firestreak model** Myers [66], Gosset et al. [67] assumes interactions of collinear rows of nucleons belonging to the projectile and the target in the overlapping volume. Thus the minifireballs are produced from each collinear row. The collisions are completely inelastic and the nuclear matter is treated as a thermodynamic system in the chemical equilibrium. The latter assumption gives a possibility to calculate relative concentrations and inclusive spectra of pions, nucleons and light nuclei.

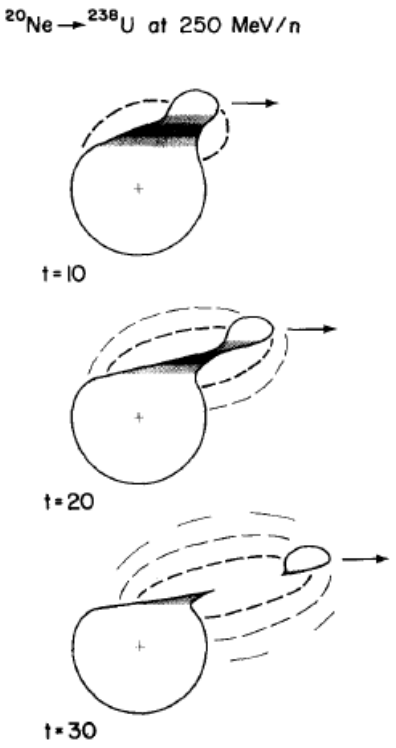

Figure 3.2: The scheme of the collision of 250-MeV ^{20}Ne with ^{238}U at impact parameter b=8 fm in the firestreak model. Three pictures represent time evolution of the collision showing the situation for 10, 20 and 30 fm/c, respectively. The figure comes from [66].

In the present work the fireball model is used in the form appropriated for parametrization of the experimental double differential cross sections $\frac{d\sigma}{d\Omega dE}$ from inclusive measurements of proton nucleus collisions. Details of the applied parametrization are described in the Appendix B.

3.2 Second stage of the reaction

Deexcitation of the target remnant after the first, fast stage of the reaction may lead to different processes. It is generally assumed that the most important mechanism of deexcitation is the evaporation of low energy particles (typically 1 – 10 MeV). Emission of nucleons, especially of neutrons, is more probable than the emission of complex LCPs or heavier particles. The evaporation may compete with the so-called high-energy fission in the case of heavy target nuclei. For light nuclei, as those considered in the present work, this process is not observed.

The sequential emission of particles by evaporation is expected to be an appropriate picture of the deexcitation process when the relaxation time of the excited nucleus is shorter than the time interval between successive emissions of the particles. It may be expected, that at excitation energies comparable with the binding energy of nucleons, i.e., 5 - 8 MeV/nucleon the existence of compound nucleus, in which all degrees of freedom are equilibrated, becomes unlikely. Therefore another mechanism should compete with the sequential emission, namely the simultaneous emission of several particles. In this case the excitation energy of the nucleus may be shared between many particles without limitations imposed by binary decays, thus the resulting spectra and angular distributions may be qualitatively different.

In the following several reaction models of the second stage of the reaction will be outlined, using their specific realizations as examples. First, *the GEM model* of Furihata [70, 71] dealing with *evaporation of particles* from the equilibrated, excited nucleus will be presented. In the next subsection *the GEMINI model* of Charity et al. [72], which treats the deexcitation of equilibrated nucleus as a *sequence of two-body decays*, will be described. The simultaneous decay of the excited nucleus into several particles, i.e. *multifragmentation* will be discussed in two next subsections using as examples *the Fermi break-up model (FBM)* [73] and *the Statistical Multifragmentation Model (SMM)* of Bondorf et al. [74].

3.2.1 Generalized Evaporation Model - GEM

Generalized Evaporation Model (GEM) of Furihata [70, 71] follows the Weisskopf-Ewing formalizm [75], according to which the probability of emission of particle j with CM kinetic energy in the interval $[\varepsilon, \varepsilon + d\varepsilon]$, by the nucleus i excited to the energy E_i^*, is equal to:

$$P_j(\varepsilon)\, d\varepsilon = g_j\, \sigma_{inv}(\varepsilon)\, \frac{\varrho_d(E_i^* - Q - \varepsilon)}{\varrho_i(E_i^*)}\, \varepsilon\, d\varepsilon \tag{3.3}$$

where index d depicts the daughter nucleus produced after emission of particle j, Q denotes the Q-value for this emission, and ϱ_i, ϱ_d are the density of states for parent and daughter nuclei,

respectively. Other symbols present in this formula have the following meaning: $\sigma_{inv}(\varepsilon)$ is the cross section for inverse reaction and g_j is determined by the formula:

$$g_j = (2\,S_j + 1)\;m_j/\pi^2\hbar^2 \tag{3.4}$$

where S_j and m_j denote spin and mass of the particle j.

Equation (3.3) determines completely the probability distribution of kinetic energy ε of the particle j providing that the appropriate densities of nuclear states ϱ_d and ϱ_i as well as the cross section for inverse reaction σ_{inv} are known. In the computer program GEM2 of Furihata [70,71] the Gilbert-Cameron formula [76] for density of states was applied with modifications proposed by Cook and Ignatyuk (cf. LAHET code [77]) and the cross section for inverse reaction was parametrized by a simple formula (for details see refs. [70] and [71]).

Knowledge of the probability distribution (3.3) allows to determine kinetic energy of given particle j by Monte Carlo sampling. Another Monte Carlo sampling is earlier necessary to find the kind (j) of emitted particle. This sampling is done using the probability distribution p_j:

$$p_j = \frac{\Gamma_j}{\sum_j \Gamma_j}, \tag{3.5}$$

where Γ_j is the probability of emission of particle j with kinetic energy ε in the range between the Coulomb barrier V (of the particle j and the daughter nucleus d) and the maximal available energy $E_i^* - Q$. This probability is calculated by integrating the equation (3.3) over kinetic energy ε of the emitted particle:

$$\Gamma_j = \frac{g_j}{\varrho_i(E_i^*)} \int_V^{E_i^*-Q} \sigma_{inv}(\varepsilon)\,\varrho_d(E_i^* - Q - \varepsilon)\;\varepsilon\,d\varepsilon \tag{3.6}$$

In the GEM2 program 66 stable and long lived ejectiles j are taken into account. They fulfill the following conditions:

- $Z_j \leqslant 12$
- naturally existing isotopes or isotopes near stability line
- isotopes with the half-life longer than 1 ms

These ejectiles are listed in the table below.

It was found necessary to take into account also the excited ejectiles because it greatly increases emission of heavy particles. These excited particles j^* were included, which have the lifetime $T_{1/2}/ln\,2$ longer than the average time $\hbar/\Gamma_j^*$ of their emission by the nucleus:

$$\frac{T_{1/2}}{ln\,2} > \frac{\hbar}{\Gamma_j^*} \tag{3.7}$$

Table 3.1: Isotopes taken explicitly into consideration as ejectiles in the GEM2 program

Z_j	Ejectiles						
0	n						
1	p	d	t				
2	^{3}He	^{4}He	^{6}He	^{8}He			
3	^{6}Li	^{7}Li	^{8}Li	^{9}Li			
4	^{7}Be	^{9}Be	^{10}Be	^{11}Be	^{12}Be		
5	^{8}B	^{10}B	^{11}B	^{12}B	^{13}B		
6	^{10}C	^{11}C	^{12}C	^{13}C	^{14}C	^{15}C	^{16}C
7	^{12}N	^{13}N	^{14}N	^{15}N	^{16}N	^{17}N	
8	^{14}O	^{15}O	^{16}O	^{17}O	^{18}O	^{19}O	^{20}O
9	^{17}F	^{18}F	^{19}F	^{20}F	^{21}F		
10	^{18}Ne	^{19}Ne	^{20}Ne	^{21}Ne	^{22}Ne	^{23}Ne	^{24}Ne
11	^{21}Na	^{22}Na	^{23}Na	^{24}Na	^{24}Na	^{25}Na	
12	^{22}Mg	^{23}Mg	^{24}Mg	^{25}Mg	^{26}Mg	^{27}Mg	^{28}Mg

This was done implicitly by increasing the Γ_j for stable or long living ejectiles listed in the table 3.1 by adding to their width for emission in the ground state $\Gamma_j^{g.s.}$ the width corresponding to emission in the above excited states Γ_j^*:

$$\Gamma_j \equiv \Gamma_j^{g.s.} + \sum_n (\Gamma_j^*)_n \tag{3.8}$$

If the daughter nucleus appears to be excited, the GEM2 program checks the possibility to evaporate next particles and eventually the Monte Carlo sampling is repeated.

The differential cross sections $\frac{d\sigma}{d\Omega dE}$ can be calculated by Monte Carlo sampling the kind j of evaporated particle (using eq. (3.5)), kinetic energy ε of the particle (using eq. (3.3)), and direction ϑ, φ of its motion (assuming isotropic emission in the CM system of the excited nucleus).

Further details of the Generalized Evaporation Model and its GEM2 computer program realization may be found in refs. [70, 71].

3.2.2 Sequential decay - GEMINI

Another realization of the sequential emission of particles from the excited nucleus is proposed by the GEMINI model [72]. This model takes into consideration all binary decay channels. The produced fragments undergo subsequent decays until the next decay is energetically impossible. This is quite analogous to the method applied by GEM but another formulae are used for evaluation of the probability of particle emission.

The decay width for evaporation of **particles with $Z_1 \leqslant 2$** from the compound nucleus with spin J_0, density of states ϱ_0, and excitation energy E^* is evaluated according to the Hauser-Feshbach formalism [78]

$$\Gamma_{J_2}(Z_1, A_1, Z_2, A_2) = \frac{2J_1+1}{2\pi\rho_0} \sum_{l=|J_0-J_2|}^{J_0+J_2} \int_0^{E^*-B-E_{rot}(J_2)} T_l(\varepsilon)\, \rho_2(U_2, J_2)\, d\varepsilon \tag{3.9}$$

where Z_1, A_1, J_1, l, and ε are charge, mass, spin, orbital angular momentum, and kinetic energy of the evaporated light particle whereas Z_2, A_2 and J_2 are the charge, mass, and spin quantum numbers for the daughter nucleus appearing with thermal excitation energy U_2 and level density $\rho_2(U_2, J_2)$.

The quantity U_2 is obtained by subtraction of kinetic energy ε of the evaporated particle, its binding energy B in the parent nucleus, and the rotation plus deformation energy $E_{rot}(J_2)$ of the daughter nucleus from the excitation energy E^* of the decaying parent nucleus:

$$U_2 = E^* - B - E_{rot}(J_2) - \varepsilon \tag{3.10}$$

The transmission coefficient $T_l(\varepsilon)$ is parametrized by the formula:

$$T_l = \begin{cases} 0 & \text{for } \varepsilon < E_{coul} + \frac{\hbar^2 l(l+1)}{2\mu R^2} \\ 1 & \text{for } \varepsilon \geqslant E_{coul} + \frac{\hbar^2 l(l+1)}{2\mu R^2} \end{cases} \tag{3.11}$$

where μ is a reduced mass and R is the absorptive radius given by the expressions:

$$R = \begin{cases} 1.16\, A_2^{1/3} + 2.6 \text{ fm} & \text{for p, n emission} \\ 1.16\, A_2^{1/3} + 3.7 \text{ fm} & \text{for } \alpha \text{ emission} \end{cases} \tag{3.12}$$

The Coulomb barrier E_{coul} is calculated using empirical prescription given by Vaz and Alexander [79] and rotation plus deformation energy $E_{rot}(J_2)$ is determined according to formulae of Sierk [80].

Probability for emission of **heavy fragments ($Z_1 >$2)** is described by the decay width, which is evaluated in the frame of the Moretto's transition state formalism [81]

$$\Gamma(Z_1, A_1, Z_2, A_2) = \frac{1}{2\pi\varrho_0} \int_0^{E^*-E_{sad}(J_0)} \varrho_{sad}(U_{sad}, J_0)\, d\varepsilon \tag{3.13}$$

where: U_{sad} and ϱ_{sad} - thermal excitation energy and level density of the decaying nucleus at the saddle point configuration,

$$U_{sad} = E^* - E_{sad}(J_0) - \varepsilon \tag{3.14}$$

$E_{sad}(J_0)$ is rotation plus deformation energy for saddle point configuration and it is taken from Rotating Finite Range Model (RFRM) by Sierk [80], J_0, ϱ_0 and ε have the same meaning as for emission of light particles.

All level densities were taken in the form derived from the Fermi gas model of nuclei:

$$\varrho(U,J) = (2J+1)\left[\frac{\hbar^2}{2\Im}\right]^{3/2} \frac{\sqrt{a}}{12} \frac{exp(2\sqrt{aU}}{U^2} \tag{3.15}$$

where $\Im$ is the moment of inertia of the residual nucleus or the saddle point configuration and a is the level density parameter, which was taken as A/8.5 MeV^{-1} for residual nucleus and for decaying nucleus at the saddle point configuration.

The integrals present in the equations (3.9) and (3.13) for decay widths can be simplified by expanding the integrands around the lower limit of integration. This procedure leads to the following formulae for total decay width **in the case of light ejectiles ($Z_1 \leqslant 2$)**:

$$\Gamma(Z_1,A_1,Z_2,A_2) = \sum_{J_2=0}^{\infty} \Gamma_{J_2}(Z_1,A_1,Z_2,Z_2) = \sum_{J_2=0}^{\infty} \left[\frac{(2J_1+1)}{2\pi\varrho_0} \sum_{l=|J_0-J_2|}^{J_0+J_2} t_2 \; \varrho_2(U_2,J_2) \right] \tag{3.16}$$

where thermal excitation energy U_2 is evaluated from the expression

$$U_2 = E^* - B - E_{rot}(J_2) - E_{coul} - \frac{\hbar^2 l(l+1)}{2\pi R^2}$$

and nuclear temperature t_2 is approximated by

$$t_2 = \sqrt{U_2/a}$$

In the case of heavy ejectiles ($Z_1 > 2$) the corresponding expressions have the following form:

$$\Gamma(Z_1,A_1,Z_2,A_2) = \frac{1}{2\pi\varrho_0} t_{sad} \; \varrho_{sad}(U_{sad},J_0) \tag{3.17}$$

where the thermal excitation energy U_{sad} and the temperature t_{sad} at the saddle point configuration are evaluated from the formulae:

$$U_{sad} = E^* - E_{sad}(J_0)$$

$$t_{sad} = \sqrt{U_{sad}/a}$$

The excited products (A_1, Z_1) and (A_2, Z_2) of the binary decay may also undergo the sequential decay, therefore spin and excitation energy of them have to be determined.

For evaporation of particles with Z $\leqslant$ 2 the spin of residuum (A_2, Z_2) is sampled by Monte Carlo method from partial decay widths $\Gamma_{J_2}(A_1, Z_1, A_2, Z_2)$ (cf. eqs.(3.9) and (3.16)) and the excitation energy is calculated from the following expression:

$$E_2^* = U_2 - 2t_2 + E_{rot}(J_2) \tag{3.18}$$

For emission of heavier particles (Z > 2) the spin J_i of the excited fragment i is calculated from the formula:

$$J_i = (\Im_i/\Im)J_0 \tag{3.19}$$

where $\Im_i$ and $\Im$ denote the moment of inertia of the fragment and the moment of inertia of whole system, respectively, and the excitation energy E_i^* of the fragment is determined by the expression:

$$E_i^* = \frac{A_i}{A_0}[U_{sad} - t_{sad}] + E_{rot}(J_i) \tag{3.20}$$

assuming equal temperatures of both fragments.

In summary, GEMINI is a Monte Carlo code which follows the decay of a compound nucleus by a series of sequential binary decays until such decays are impossible due to energy conservation or improbable due to gamma-ray competition. It explicitly uses angular momentum degrees of freedom, both in the Hauser-Feshbach and Moretto formalism, because it is better suited for treating emission of particles at high angular momentum than the Weisskopf-Ewing formalism, usually applied in the statistical codes. The cost of this better treatment of angular momentum is increased time necessary to perform the calculations.

3.2.3 Simultaneous multifragmentation - Fermi break-up model

The Fermi break-up model (FBM) has been proposed by Fermi [73] to explain large multiplicity of products observed in nucleon-nucleon and nucleon-pion collisions at high energies. When

applied to excited nuclei (cf., e.g., [82]) it describes emission of particles as an explosive decay of the nucleus into several clusters and nucleons.

The model assumes that the excited nucleus decays simultaneously into cold or slightly excited fragments, which have lifetimes longer than the decay time – crudely estimated to be about 100 fm/c. The break-up configuration is characterized by some freeze-out volume V, where the produced fragments are placed. This volume is larger than the volume of the nucleus in the ground state, i.e., at the normal density $\varrho \approx 0.17$ nucleon/fm^{-3}, to allow for the translational motion of the fragments.

The probability of an individual break-up channel containing n particles with masses m_i ($\sum_{i+1}^{n} m_i = M$ -total mass of the fragments) is proportional to its phase-space volume $M_n(E)$:

$$M_n(E) = \int_{-\infty}^{\infty} \delta\left(\sum_{i=1}^{n} \vec{p}_i\right) \cdot \delta\left(E - \sum_{i=1}^{n} \sqrt{p_i^2 + m_i^2}\right) \cdot \prod_{i=1}^{n} d^3 p_i \tag{3.21}$$

where the above integral over momenta of all particles can be evaluated analytically in the nonrelativistic case. Using this approximation and taking into consideration spins s_i of the particles as well as identity of some among n particles the probability can be written as follows:

$$P(E_{kin}, n) \;\propto\; S_n \cdot G_n \cdot \left(\frac{V}{h^3}\right)^{n-1} \cdot \left(\frac{\prod_{i=1}^{n} m_i}{M}\right)^{3/2} \cdot \frac{(2\pi)^{\frac{3}{2}(n-1)}}{\Gamma\left(\frac{3}{2}(n-1)\right)} \cdot \left(E_{kin} - U_C\right)^{\frac{3n}{2}-\frac{5}{2}} \tag{3.22}$$

where S_n is the spin degeneracy factor

$$S_n = \prod_{i=1}^{n} (2s_i + 1) \tag{3.23}$$

and G_n is the permutation factor which takes into account identity of n_j particles of kind j ($\sum_{j=1}^{k} n_j = n$)

$$G_n = \prod_{j=1}^{k} \frac{1}{n_1!}. \tag{3.24}$$

E_{kin} is equal to kinetic energy of all n particles at infinity, related to the decaying nucleus excitation energy E^* by the formula:

$$E_{kin} = E^* + M_0 c^2 - \sum_{i=1}^{n} m_i c^2 \tag{3.25}$$

where M_0 is the mass of the nucleus.
The last two quantities (h and U_C) are the Planck constant and the Coulomb energy of the decaying nucleus at the freeze-out configuration, respectively. The Coulomb energy is usually calculated in the Wigner-Seitz approximation:

$$U_C = \frac{3e^2}{5r_0}\left[\frac{Z_0^2}{A_0^{1/3}} - \sum_{i=1}^{n}\frac{Z_i^2}{A_i^{1/3}}\right] \tag{3.26}$$

where the r_0 is a parameter determining the freeze-out volume:

$$V = \frac{4\pi r_0^3 A_0}{3} \tag{3.27}$$

and A_0, Z_0, A_i, Z_i are the mass and atomic numbers of the decaying nucleus and of the fragments, respectively.

The Fermi break-up model treats all possible partitions of the decaying nucleus on the equal footing, assuming r_0 quantity as the only free parameter. Usually its value is fixed to 1.4 fm. The number of possible partitions increases very strongly with the mass of the decaying nucleus, what leads to cumbersome calculations for heavier nuclei, thus the Fermi break-up model is rarely used for nuclei with the mass number A_0 larger than 18.

In the computer program ROZPAD of Magiera [83], realizing the Fermi break-up model, the Monte Carlo sampling is used to evaluate the $\frac{d\sigma}{d\Omega dE}$. First, the sampling of a given decay channel n is performed using probabilities determined by equation (3.22). Then, the n-body event $(\vec{p}_1, ..., \vec{p}_n)$ is generated according to Fermi Lorentz-invariant phase space using subroutine GENBOD from the CERN library (adapted from FOWL - CERN W505 by F. James in 1974). The momenta are transformed from the CM reference system of the decaying nucleus to the LAB reference system and the appropriate histograms of events are produced.

3.2.4 Statistical multifragmentation model - SMM

The main idea of the *Statistical Multifragmentation Model* [74] is that a very large number of degrees of freedom is involved in high excitation of the nuclei. Thus instead studying the detailed dynamics of the decay the probabilities of different decay channels are estimated assuming the statistical equilibrium of the excited system.

The decaying nucleus is characterized by its ***volume V*** and ***excitation energy*** E_0 besides the ***mass*** A_0 ***and atomic*** Z_0 ***quantum numbers***. Three different sets of variables describing the state of the system at the break-up are used in the SMM:

- The most complete set includes the masses A_i, charges Z_i, momenta $\vec{p}_i$, excitation energies ϵ_i, angular momenta s_i and the coordinates of centres of mass $\vec{r}_i$ of all the fragments. The state characterised by these variables is called ***the break-up configuration F***:

$$F: \{A_i, Z_i, \vec{p}_i, \epsilon_i, s_i, \vec{r}_i, i \leqslant M\} \tag{3.28}$$

  where M is the total number of fragments (including nucleons).

- Since the fragments are observed only at very large distances in comparison to dimension of the nucleus at the break-up, such a full set of variables is not needed. The state may be described by smaller set of variables, i.e., mass numbers A_i, atomic numbers Z_i and momenta $\vec{p}_i$ of all the fragments. This set of variables is called ***the break-up event***, and may be replaced by even smaller set of variables because the assumption of thermal equilibration of the decaying nucleus determines momentum distributions of fragments to be of the Maxwellian shape with the common temperature parameter. Then it is possible to sample lengths of the momenta from this distribution by Monte Carlo method as well as to choose isotropically the directions of the momenta in the rest system of the decaying nucleus.

- The most truncated set of variables, called ***the break-up partition*** is a set of multiplicities $N_{A,Z}$

$$f: \{N_{A,Z};\ 1 \leqslant A \leqslant A_0, 0 \leqslant Z \leqslant Z_0\} \tag{3.29}$$

  arranged in a matrix of A_0 rows and Z_0+1 columns which determines number of different fragments (A, Z) appearing in the decay.

  All partitions have to preserve mass number and atomic number, i.e.,:

$$\sum_{(A,Z)} N_{A,Z}\ A = A_0, \quad \sum_{(A,Z)} N_{A,Z}\ Z = Z_0, \quad \sum_{(A,Z)} N_{A,Z}\ = M_f \tag{3.30}$$

  where M_f is total multiplicity of fragments in partition f.

As it was mentioned at begin of this section, it is assumed in the statistical model of the reaction, that the decaying nucleus is thermalized, what means that all microscopic states of the nucleus are considered to be equally probable. Thus the nucleus may be characterized by the common temperature T. This greatly facilitates the calculations in which different sets of variables discussed above may be used. Usually only most crude system of variables, i.e. the break-up partitions are taken explicitly into consideration assuming that integration/summing over all other coordinates is done implicitly.

Three various types of statistical ensembles are considered for this purpose:

(1) Microcanonical ensemble where all break-up partitions, break-up events, and break-up configurations obey strictly the conservation laws of energy, momentum, angular momentum, mass, and charge number.

For light nuclei or for heavy nuclei decaying exclusively into partitions with small multiplicity ($M_f \leqslant 4$) all partitions can be directly sorted in the calculation. This is equivalent to *the Fermi break-up model* discussed in the previous section.

When the multiplicity of partitions increases over $M_f = 4$ for heavy nuclei (for excitation energies larger than $\sim$ 3 MeV/nucleon it frequently appears to be larger than 4) such method is not applicable because total number of partitions becomes enormously large. Then the partitions have to be sampled by Monte Carlo method using the following probabilities:

$$W_f^{mic} = \frac{\exp\left[S_f\left(E_0, V, A_0, Z_0\right)\right]}{\sum\limits_{\{f\}} \exp\left[S_f\left(E_0, V, A_0, Z_0\right)\right]} \tag{3.31}$$

In this formula S_f is entropy of partition f of the nucleus (A_0, Z_0) excited to energy E_0, decaying from the freeze-out volume V.

The partition energy E_f is dependent on the temperature T and volume V of the system:

$$E_f\left(T, V\right) = E_f^{tr}\left(T, V\right) + \sum_{(A,Z)} E_{AZ}\left(T, V\right)\ N_{AZ} + E_0^C\left(V\right) \tag{3.32}$$

where $E_f^{tr}\left(T, V\right)$ is the translational energy, $E_{AZ}\left(T, V\right)$ is the average energy of the group of N_{AZ} fragments of (A, Z) type including the internal energy and Coulomb clusterization energy. The $E_0^C\left(V\right)$ is the Coulomb energy:

$$E_0^C\left(V\right) = \frac{3}{5}\frac{Z_0 e^2}{R} \ \text{ with R} = \left(\frac{3\text{V}}{4\pi}\right)^{1/3}. \tag{3.33}$$

The condition

$$E_f\left(T_f, V\right) = E_0 \tag{3.34}$$

may be used to determine temperature T_f of the partition, and then the entropy S_f defines the probability W_f^{mic} of the partition f by the formula (3.31). Since entropy S is proportional to logarithm of number of states of the system, the exponential function in the formula (3.31) is analogous to the formula (3.22) of the Fermi break-up model.

(2) Canonical ensemble preserves total mass - A_0 and atomic - Z_0 numbers for all partitions. However, the total energy fluctuates from partition to partition and only its average value (over partitions) is equal to E_0:

$$\left\langle E_f\left(T, V\right)\right\rangle \equiv \sum_{\{f\}} E_f\left(T, V\right)\ W_f = E_0 \tag{3.35}$$

The assumption of established thermal equilibrium means that the ensemble of partitions is characterized by the same, constant temperature T. This may be interpreted that the decaying system is a part of a bigger system which provides a thermal bath for the studied system, assuring possibility to keep the constant temperature.

In the canonical ensemble the probabilities of different break-up partitions are given by a Gibbs distribution:

$$W_f^{can} = \frac{\exp\left[-F_f\left(T, V, A_0, Z_0\right)/T\right]}{\sum\limits_{\{f\}} \exp\left[-F_f\left(T, V, A_0, Z_0\right)/T\right]} \tag{3.36}$$

where F_f is the free energy of the partition f.

The temperature determines the equilibrium (Maxwellian) momentum distribution of fragments. Thus, the Monte Carlo sampling of the momenta of fragments can be done from this distribution after choosing the partition according to probabilities given by equation (3.36) or (3.31).

In the SMM model it is assumed that all nuclear fragments except the lightest ones ($A \leqslant 4$) may be treated as spherical drops of the nuclear matter. Thus the free energy F_{AZ} of the individual fragment of (A, Z) kind is calculated using the drop model and is consisted of several additive contributions:

$$F_{AZ} = F_{AZ}^{B} + F_{AZ}^{sym} + F_{AZ}^{S} + F_{AZ}^{C} \tag{3.37}$$

where the terms with indices B, sym, S, and C represent bulk, symmetry, surface, and Coulomb contributions, respectively. Details of method of evaluation of these contributions are given in the review publication of Bondorf et al. [74].

(3) Macrocanonical (grand canonical) ensemble

In this ensemble not only the total energy E_f, but also the total number of nucleons A, and the total charge Z, fluctuate from partition to partition, thus only average values of these quantities are conserved:

$$\langle A_f \rangle \equiv \sum_{AZ} \langle N_{AZ} \rangle A = A_0, \quad \langle Z_f \rangle \equiv \sum_{AZ} \langle N_{AZ} \rangle Z = Z_0 \tag{3.38}$$

The probabilities of break-up partitions in the macrocanonical ensemble are given by the formula:

$$W_f^{mac} = \frac{\exp\left(-\Omega_f\left(T, V, \mu, \nu\right)\right)}{\sum\limits_{\{f\}} \exp\left(-\Omega_f\left(T, V, \mu, \nu\right)\right)} \tag{3.39}$$

where Ω_f is a thermodynamical potential of a partition f:

$$\Omega_f\left(T, V, \mu, \nu\right) = F_f\left(T, V\right) - \mu A_f - \nu Z_f \tag{3.40}$$

The chemical potentials μ and ν may be found from equations (3.38).

The macrocanonical ensemble has a specific advantage, that some of the calculations can be performed analytically. Furthermore the probability distribution of fragment multiplicities may be approximated by the Poisson distribution

$$p\left(N_{AZ}\right) = \frac{\exp\left(-\omega_{AZ}\right)\ \left[\omega_{AZ}\right]^{N_{AZ}}}{N_{AZ}!} \tag{3.41}$$

and then the probability of given partition may be written in the factorized form:

$$W_f^{mac} = \frac{\prod\limits_{(A,Z)} \left[\frac{(\omega_{AZ})^{N_{AZ}}}{N_{AZ}!}\right]}{\prod\limits_{(A,Z)} \exp\left(\omega_{AZ}\right)} \tag{3.42}$$

where

$$\omega_{AZ} = g_{AZ} \frac{V_f}{\lambda_T^3} A^{3/2} \exp\left[-\frac{F_{AZ}\left(T, V\right) - \mu A - \nu Z}{T}\right] \tag{3.43}$$

with g_{AZ} equal to the spin degeneracy of the ground state of fragment (A, Z), F_{AZ} equal to internal free energy of such a fragment, and λ_T defined as so called "thermal wave length":

$$\lambda_T = \frac{h}{\sqrt{m_N T}}. \tag{3.44}$$

Here symbols h, m_N, and V_f denote the Planck constant, the nucleon mass, and the "free" volume of the partition f for translational motion of fragments in the decaying nucleus, respectively. The free volume V_f is defined as $V - V_0$, where V_0 is the volume occupied by fragments

in the total volume V of the decaying nucleus.

Of course, the mean multiplicity $\langle N_{AZ} \rangle$ of the partition (A,Z) and its variance $\sigma^2(N_{AZ})$ are equal to ω_{AZ}:

$$\langle N_{AZ} \rangle = \sigma^2 \left(N_{AZ} \right) = \omega_{AZ} \tag{3.45}$$

due to properties of the Poisson distribution (3.41).

Number of possible partitions increases very quickly with the mass number of the excited nucleus. For example, it is equal to 1.9×10^8 for $A_0 = 100$ and 3.9×10^{12} for $A_0 = 200$. Thus the direct sampling of all partitions is practically possible only for light nuclei. If such a direct sampling is realized (for light nuclei or for heavy nuclei at so low excitation energies that only small multiplicities of the fragments; $M \leqslant 4$ are possible) and deexcitation of the fragments as well as their propagation in the Coulomb field is not taken explicitly into consideration, then the SMM model is equivalent to the Fermi break-up model.

When the number of the partitions is larger and larger, the direct sampling has to be replaced by searching for representative subset of partitions which is selected by the Monte Carlo method from the full set of possible partitions. The practical methods of the partition sampling are described in the review article of Bondorf et al. [74].

After selection of the partition, excitation energies and momenta of the fragments have to be generated. It is done in the following manner: First, the temperature T_f associated with the partition f is found from equation (3.34), then the excitation energy $E^*_{AZ}(T_f)$ of each fragment (A, Z) is evaluated assuming the equipartition of energy:

$$\begin{aligned} E^*_{AZ}(T_f) &\equiv E_{AZ}(T_f) - E_{AZ}(0) \approx \\ &\approx \frac{T_f^2}{\epsilon_0} A + \left(\beta(T_f) - T_f \frac{d\beta(T_f)}{dT_f} - \beta(0) \right) \end{aligned} \tag{3.46}$$

where $\beta(0) \approx 18$ MeV is the surface coefficient in the Bethe-Weizsaecker formula, $\beta(T_f)$ depends on the temperature in the neighbourhood of the critical temperature $T_c = 18$ MeV (at which the surface tension vanishes) in the following way:

$$\beta(T) = \beta(0) \left[\frac{T_c^2 - T^2}{T_c^2 + T^2} \right]^{5/4} \tag{3.47}$$

and $\epsilon_0 \equiv A/a$, where a is equal to the single-particle level density at the Fermi energy ϵ_F. For ideal Fermi gas $\epsilon_0 = (4/\pi^2)\epsilon_F \approx 16$ MeV.

In the next step a generation of the fragment momenta is realized under an assumption of the thermodynamical equilibrium, thus directions of momenta are isotropically distributed in

the centre of mass of the decaying nucleus. The length of the momentum vector is found by sampling of the kinetic energy E of each fragment, which in the equilibrated system obeys the Boltzmann-Maxwell distribution with the common temperature T_f for all fragments of given partition f:

$$\frac{dN_{AZ}}{dE} \propto \sqrt{E}\ \exp\left(-\frac{E}{T_f}\right) \tag{3.48}$$

The total kinetic energy of all fragments $E_f^T(T_f)$ should fulfill the equality:

$$E_f^T\left(T_f\right) = \frac{3}{2}\ \left(M_f - 1\right) T_f \tag{3.49}$$

where M_f denotes the total multiplicity of fragments in partition f. This is achieved by proper selection of the last two momenta for the set of M_f fragments.

The SMM allows to take into account the Coulomb interaction of fragments after decay but such calculations need also information on the positions of fragments at moment of the decay. These positions are randomly chosen over the break-up volume V with the condition of not overlapping of the fragments.

Further refinement of the model as, e.g., evaporation of particles from the hot fragments, and details of the methods used for numerical realization of the SMM model may be found in the work of Bondorf et al. [74]

Chapter 4

PISA experiment

4.1 Experimental setup

The PISA experiment has been performed on the internal beam of COSY (COoler SYnchrotron) of the Research Centre in Juelich. The apparatus and experimental procedure have been described in previous publications [2, 84] thus in the present work only details, characteristic for the studied reactions are discussed.

Self-supporting Carbon and Aluminium targets of thickness 80 μg/cm^2 and 170 μg/cm^2, respectively, were bombarded by internal proton beam of COSY. Three beam energies were used: 1.2, 1.9, and 2.5 GeV. To assure the same experimental conditions for all beam energies the COSY operated in so called supercycle mode. In this mode several cycles were alternated for each requested beam energy, consisting of protons injection from JULIC cyclotron to COSY ring, their acceleration with the beam circulating in the ring below the target, and irradiating the target by slow movement of the beam in the upward direction. Due to application of supercycle mode of target irradiation all conditions of the experiment except the energy of the proton beam remained unchanged. This allowed to minimize the effect of systematic uncertainties on the energy dependence of measured cross sections.

Double differential cross sections $\frac{d\sigma}{d\Omega dE}$ were measured at seven scattering angles: 15.6° , 20° , 35° , 50° , 65° , 80° , and 100° . The mass and charge identification of detected particles was realized by Δ E - E method using telescopes consisted of silicon semiconductor detectors supplied (in four cases) by thick CsI scintillator detectors, which were used to detect high energy light charged particles passing through the silicon detectors. The scattering chamber and position of the detector telescopes are schematically presented in fig. 4.1. The range of energy of measured ejectiles is listed in tables 4.1 and 4.2 for Aluminium and Carbon targets, respectively.

Further details of the detector telescopes, i.e., their geometrical dimensions, distance from the target, the solid angles, etc., can be found in PhD thesis of Piskor-Ignatowicz [84]. The $\frac{d\sigma}{d\Omega dE}$ were measured for the following products: p, d, t, ^{3,4,6}He, ^{6,7,8,9}Li, ^{7,9,10}Be, ^{10,11,12}B and C

for the Aluminium target whereas for the Carbon target following nuclides; ^{9}Li,^{9,10}Be, Boron, and Carbon isotopes had to small statistics to be extracted from the raw data.

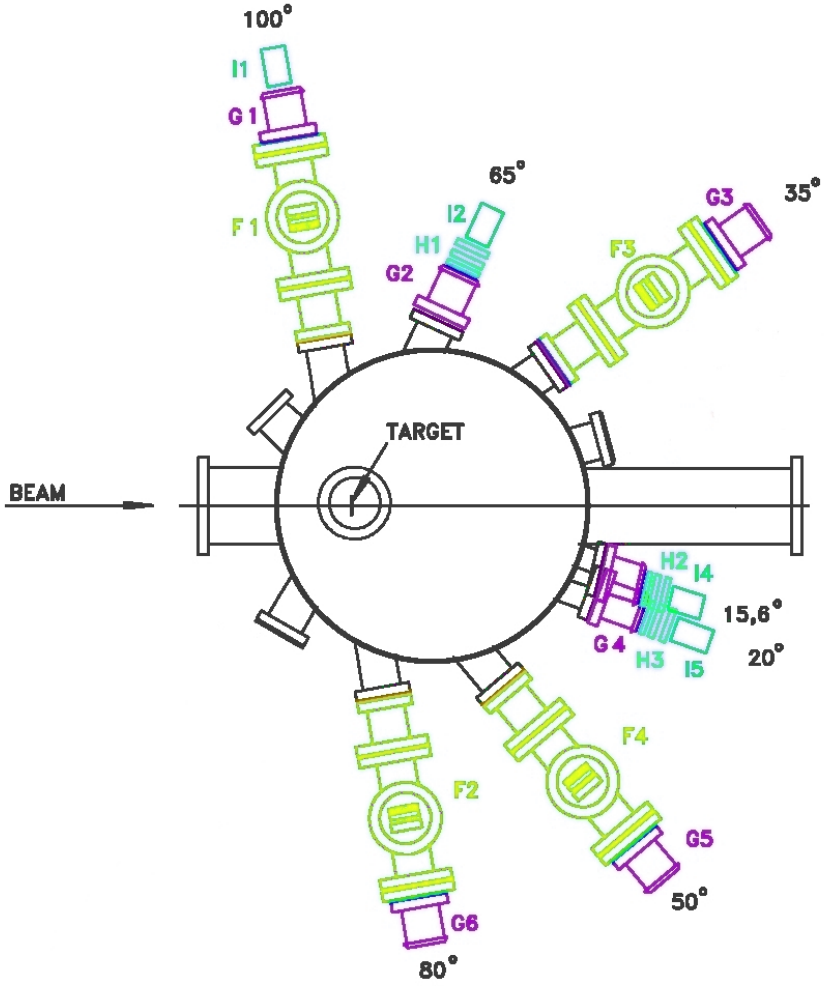

Figure 4.1: Detector setup of PISA experiment. Detectors were placed at 7 telescope arms at: 15.6°, 20°, 35°, 50°, 65°, 80°, and 100° in respect to the beam direction. Symbols F1-F4 denote cooled Si-telescopes placed in vacuum of the scattering chamber, I1-I5 depict CsI (scintillator) detectors, H1-H3 - air positioned Si-telescopes, G1- G7 represent flanges closed with stainless steel foils used to protect the high vacuum of the scattering chamber.

Table 4.1: Energy ranges (in MeV) of detected particles from p+Al collisions in PISA experiment. Rows of the table correspond to different particles and columns represent different angles of detector telescopes.

Ejectile	Angle[degrees]						
	15.6	20	35	50	65	80	100
p	7.0-162.0	7.5-162.5	3.5-22.0	3.5-23.5	7.5-161.5	3.5-6.5	9.5-161.5
d	9.5-208.5	9.5-212.0	4.5-34.5	4.5-30.5	8.5-213.0	4.5-9.5	13.5-212.5
t	10.5-220.0	10.5-232.5	4.5-39.0	4.5-34.5	9.5-239.5	5.5-7.5	14.5-160.5
^{3}He	21.5-285.0	21.5-269.5	8.5-91.5	8.5-94.5	21.5-288.0	12.5-20.5	9.5-155.5
^{4}He	23.5-163.5	23.5-140.5	9.5-121.5	9.5-120.0	23.5-177.5	13.5-24.5	10.5-114.5
^{6}He	26.5-40.0	26.5-43.5	10.6-86.5	10.5-83.5	26.5-85.5	15.5-27.0	11.5-50.0
^{6}Li	42.5-146.0	42.5-137.5	17.5-137.5	15.5-159.5	42.5-118.5	18.5-50.5	18.5-90.5
^{7}Li	45.5-138.0	45.5-143.5	17.5-112.5	16.5-110.5	44.5-106.5	20.5-55.5	19.5-76.0
^{8}Li	47.5-95.5	47.5-94.5	18.5-77.0	17.5-75.5	46.5-83.5	21.5-53.5	19.5-55.0
^{9}Li	49.5-70.0	50.5-69.5	20.5-44.0	17.5-35.5	49.5-52.5	22.0-36.0	21.5-39.5
^{7}Be	62.5-130.0	62.5-116.5	20.5-108.5	21.5-80.5	61.5-106.5	27.5-69.0	25.5-73.5
^{9}Be	68.5-97.5	69.5-97.5	26.5-89.5	24.5-62.5	68.0-74.5	29.5-68.5	27.5-61.0
^{10}B	91.5-111.5	92.5-110.5	35.5-84.0	30.5-79.5		38.5-62.5	36.5-60.5
^{11}B	94.0-101.5	95.5-108.5	35.5-82.5	30.5-71.5	100.5	39.5-67.5	37.5-72.5
^{12}B			36.5-48.5	34.5-57.5		48.5-53.5	40.5

Table 4.2: Energy ranges (in MeV) of detected particles from p+C collisions in PISA experiment. Rows and columns of the table have the same meaning as in table 4.1

Ejectile	Angle[degrees]						
	15.6	20	35	50	65	80	100
p	7.5-162.0	7.5-162.5	3.5-21.5	3.5-23.5	7.5-161.5	3.5-6.5	9.5-163.5
d	9.5-208.5	9.5-212.5	4.5-34.5	4.5-31.0	8.5-213.0	4.5-9.5	13.5-110.5
t	10.5-112.5	10.5-115.5	4.5-39.5	4.5-34.0	9.5-66.5	4.5-10.0	14.5-45.5
^{3}He	21.5-69.5	21.5-90.0	8.5-74.5	8.5-86.5	21.5-87.0	12.5-21.0	9.5-72.5
^{4}He	23.5-107.5	23.5-105.5	9.5-92.5	8.5-113.5	23.5-101.0	13.5-25.0	10.5-75.5
^{6}He	26.5-40.5	26.5-35.5	10.5-19.5	10.5-23.5	26.0-33.5	15.5-27.0	11.5-21.5
^{6}Li	42.5-77.0	42.5-78.0	17.5-67.5	15.5-44.5	42.5-75.5	18.5-45.0	18.5-39.0
^{7}Li	45.5-54.5	45.5-73.5	17.5-46.5	16.5-53.0	44.5-66.0	20.5-47.5	19.5-31.5
^{8}Li	47.5-49.5	47.0-50.0	18.5-24.0	17.5-23.0		23.5-29.5	19.5
^{7}Be	62.0-67.5	66.5	25.5-46.5	21.5-45.5		27.5-43.5	25.5-39.5
^{9}Be			27.0-30.5	29.5		29.0	

4.2 Normalization

The absolute normalization of the data in such an experiment may be done by simultaneous measuring of known and unknown cross sections. It happened that the information on the differential cross sections measured for proton induced reactions on Carbon and Aluminium targets is scarce at beam energies used in the present experiment. Thus, the normalization of double differential cross sections could not be achieved by straightforward comparison of present and literature data. As it is discussed below, the normalization of differential cross sections from p+Al reactions was obtained by integration of $\frac{d\sigma}{d\Omega dE}$ from our experiment to be compared to known *total* cross sections from the literature. On the other hand, the p+C *differential* cross sections were compared to literature data, however these data were taken at different energies than those used in the present experiment. This procedure was based on the assumption that at such high energies the limiting fragmentation hypothesis [17] is fulfilled, i.e. the differential cross sections for such light target like C do not vary with the energy.

4.2.1 p+Al collisions

The absolute normalization of the data, measured for Al target was obtained by comparison of total cross section $\sigma_{a.u.}$ of ^{7}Be production, derived from measured differential cross sections, with value of this cross section known from the literature [13].

The following procedure has been applied to extract the not normalized production cross section $\sigma_{a.u.}$ from the spectra $\frac{d\sigma}{d\Omega dE}$ measured at seven scattering angles: 15.6° , 20° , 35° , 50° , 65° , 80° , and 100° . It was found that the angular and energy dependence of $\frac{d\sigma}{d\Omega dE}$ can be well reproduced by simple formula representing isotropic emission from two sources moving forward along the beam. Each source emitting particles with Maxwellian energy distribution was characterized by its velocity β, temperature T, height of the Coulomb barrier between ^{7}Be and the source remnant – described by parameter k, and by emission intensity σ (for details see Appendix B). The σ parameter has the meaning of the energy and angle integrated differential cross section attributed to given source. Thus, the not normalized cross section $\sigma_{a.u.}$ of ^{7}Be production is equal to sum of parameters σ for both sources:

$$\sigma_{a.u.} = \sigma_1 + \sigma_2 \tag{4.1}$$

Best values of the parameters were found by fitting full set of the ^{7}Be spectra (seven scattering angles) with the same set of parameters. The fits lead to ambiguous results because the experimental spectra were not measured in full energy range allowed by kinematics. Low energy particles were not detected what was caused by energy thresholds of detector telescopes. This lack of information on low energy part of spectra could strongly influence the value of the energy integrated cross section since the spectra have Maxwellian shape with the maximum lying in the neighbourhood of the energy cut-off. Fortunately, it turned out that the spread of values of σ parameters was smaller than 10 % among the sets of parameters which have the

same, best χ^2 values obtained for various combinations of fixed Coulomb barrier parameters k_1 and k_2. The final values of the σ parameters of both sources were taken as an arithmetic mean of results obtained for equivalent quality fits, i.e., those which have the same, smallest χ^2 value.

Table 4.3: The set of total cross sections of ^{7}Be production used for the absolute normalization of p+Al reaction data. In the first column the proton beam energy is listed, in the second column the literature value of the production cross section $\sigma_{lit}(^7\mathrm{Be})$ is depicted whereas the not normalized cross section $\sigma_{a.u.}$ from present experiment and its error are shown in next two columns. The last two columns contain normalization factor $f \equiv \sigma_{lit}/\sigma_{a.u.}$ and its error.

T_p[GeV]	σ_{lit} [mb]	$\sigma_{a.u.}$ [a.u.]	$\sigma(\sigma_{a.u.})$ [a.u.]	f	$\sigma(f)$
1.2	8.0	477	42	0.0168	0.0015
1.9	9.5	288	26	0.0330	0.0030
2.5	10.1	255	24	0.0396	0.0037

The error of normalization factor quoted in the table (4.3) does not take into consideration the inaccuracy of the literature value of the production cross section $\sigma_{lit}(^7\mathrm{Be})$ which is believed to be smaller than 10 % [13].

4.2.2 p+C collisions

As it is presented in fig. 4.2 the total cross sections for alpha particle production in p+C collisions, published in the literature, are constant above 1 GeV proton beam energy.

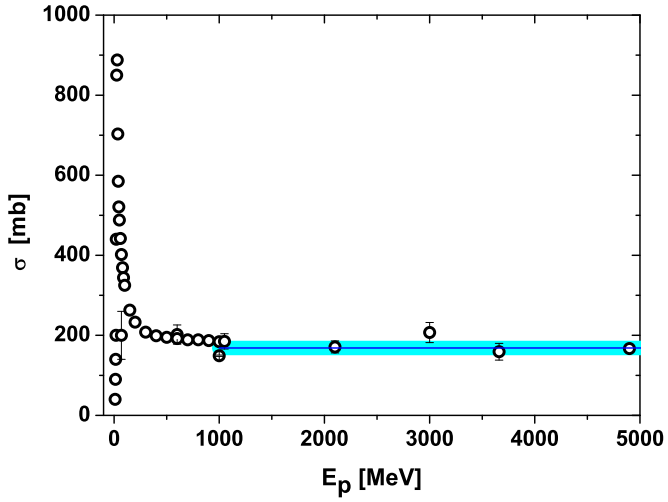

Figure 4.2: Beam energy dependence of total production cross section of alpha particles in p+C collisions. The thin horizontal line represents the average value of cross sections measured for proton energies larger than 1 GeV and the shadowed bar depicts the spread of experimental values (standard deviation).

Treating this fact as manifestation of the validity of limiting fragmentation hypothesis [17] it may be conjectured that the differential cross sections for alpha article production also do not vary with beam energy. Taking this fact as granted the differential cross sections measured in the present experiment were absolutely normalized comparing them with data obtained at proton beam energy 2.1 GeV by Westfall et al. [69].

The spectrum of alpha particles determined at 90 degree, presented in fig. 2 of ref. [69], was used as reference data. Since the spectra in PISA experiment were measured at other angles (15.6, 20, 35, 50, 65, 80 and 100 degree to the beam direction) the interpolation of data known 80 and 100 degree was performed.

Finally, the following normalization factors were obtained:**0.1317(56)**, **0.1629(70)** and **0.210(12)** for beam energy 1.2, 1.9, and 2.5 GeV, respectively. As can be seen, the errors of normalization factors are small, equal to 4 – 6 %. These errors contain only the statistical uncertainty of the PISA experiment. Taking into consideration 10 % uncertainty of absolute normalization of data quoted in ref. [69] the overall error of the present normalization is about 12 %.

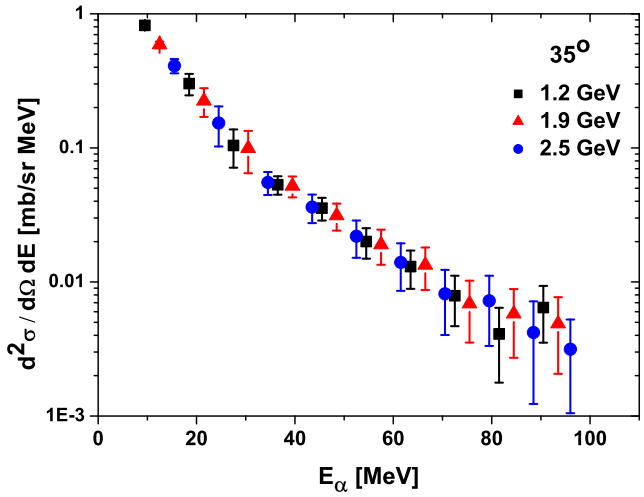

Figure 4.3: Spectra of alpha particles measured at the same scattering angle (35°) for three proton beam energies; 1.2, 1.9, and 2.5 GeV (square, triangle, and circle, respectively) and C target.

As can be seen on fig. 4.3 the shape of alpha particle spectra is the same at three beam energies used in the present experiment. This confirms correctness of the assumption concerning validity of limiting fragmentation hypothesis also for differential cross sections.

4.3 Comparison of results with literature data

The quality of the absolute normalization of the present experiment may be judged from comparison of the obtained data with the data from literature. The differential cross sections for proton induced spallation on such light targets like C and Al were rarely measured in the proton energy range studied in this work (cf. Appendix A).

4.3.1 p+Al collisions

To our knowledge only one measurement of light charged particle spectra as well as intermediate mass fragment spectra is present in the literature for Aluminium target at proton beam energies similar to those used in the present study. This is the paper of Westfall et al. [69] dealing with reactions performed at 4.9 GeV proton energy. This energy is higher than those used in the present work, however, it is known that the total production cross sections vary only slightly for this target at proton beam energies larger than 1 GeV (cf. chapter 2). Thus, it is reasonable to compare present data with results obtained by Westfall et al. Such a comparison is depicted

on figure 4.4 for hydrogen and helium isotopes, and figure 4.5 for lithium, beryllium and boron isotopes. As can be seen, the shape and magnitude of the spectra is in excellent agreement for helium isotopes as well as for all heavier ejectiles. However, the slope of the spectra of hydrogen isotopes and the absolute magnitude of the cross sections from the present measurement do not fit well with those obtained in the work of Westfall et al. This disagreement may indicate that the differential cross sections of hydrogen isotopes production still vary with beam energy in the studied energy range. A similar conclusion could be derived from inspection of fig. 2.6 where the total production cross sections for tritons seem to increase for beam energies up to 6 GeV.

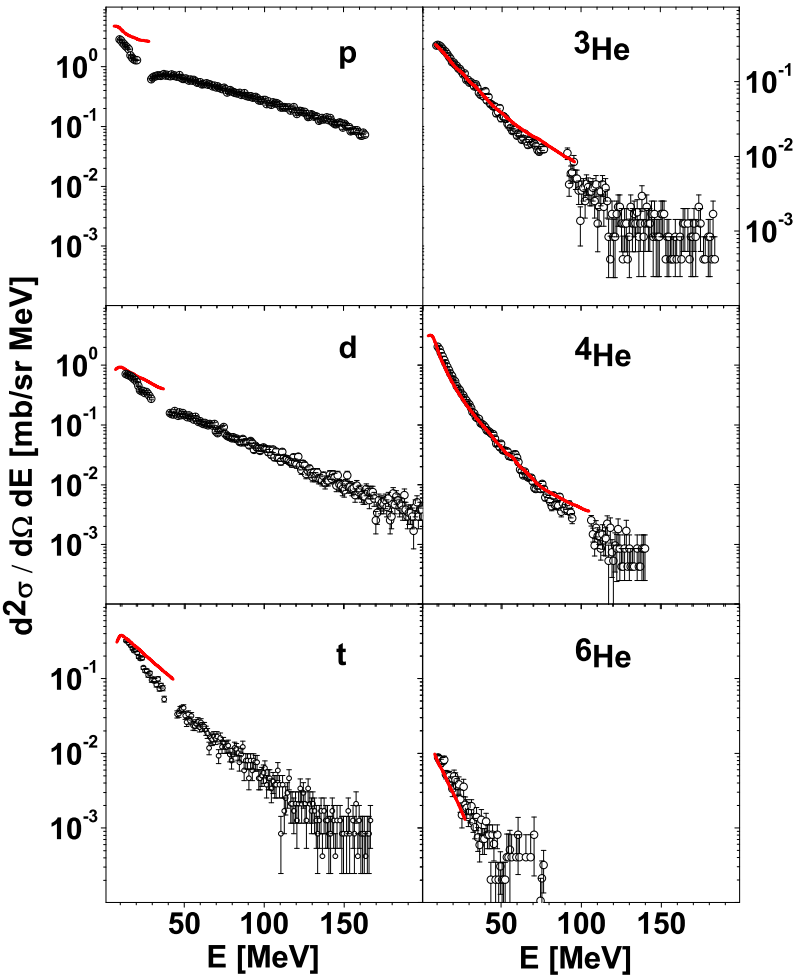

Figure 4.4: Experimental spectra of H and He isotopes from the present work (circles) measured at 100° in Al+p collisions at proton beam energy 2.5 GeV and data from ref. [69] measured at 90° at proton energy 4.9 GeV (lines).

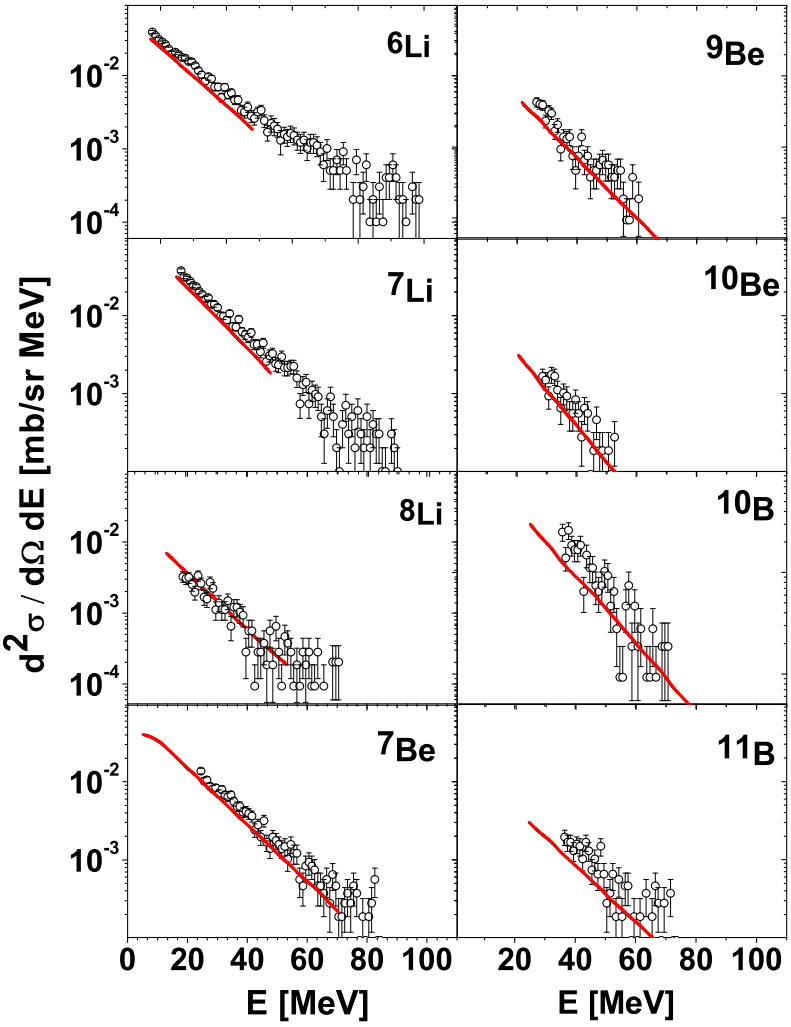

Figure 4.5: Experimental spectra of Li, Be, and B from the present work (circles) measured at 100° in Al+p collisions at proton beam energy 2.5 GeV and data from ref. [69] measured at 90° at proton energy 4.9 GeV (lines).

4.3.2 p+C collisions

Differential cross sections for products of p+^{12}C collisions were measured at 1.0 GeV by Andronenko et al. [85] and Westfall et al. [69] at 2.1 GeV. The spectrum of alpha particles from the latter experiment, measured at 90° was used for normalization of our data (cf. chapter 4.2). Thus the good agreement shown in fig. 4.6 of the present spectrum of the alpha particles obtained for 100° with that measured by Westfall et al. at 90°, is a result of this normalization. However, good agreement of Helium data of Andronenko et al. with the present data is

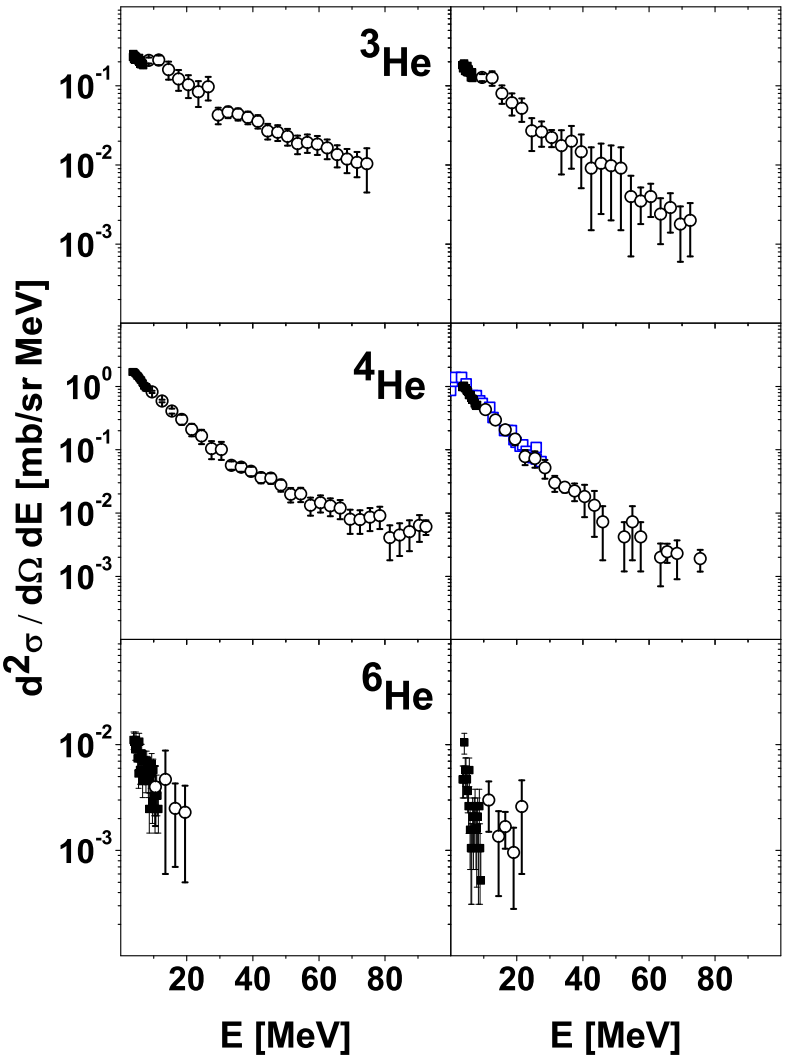

Figure 4.6: Experimental spectra of He isotopes from the present work (circles) measured at 35° (left column) and 100° (right column) in C+p collisions at proton beam energy 1.2 GeV and data from ref. [69] measured at 90° at proton energy 2.1 GeV (empty squares) as well as data from ref. [85] (full squares) measured at 30° (left column) and 126° (right column) at proton beam energy 1.0 GeV

confirmation of consistency of results of all these experiments in spite of very different method of measurements used in these investigations. The experiment of Andronenko et al. applied Bragg curve detectors together with the time-of-light method for identification of mass

and charge of the ejectiles. Therefore the range of energies of particles detected in their experiment is narrower than that of the present experiment. Furthermore the stopping power of gas in the Bragg detectors is smaller than that of the silicon detectors, thus the energy threshold of their experiment is smaller than threshold in the present experiment. Nevertheless it seems that the spectra from both experiments match well together. This is especially well visible at 30° spectra of Andronenko et al. compared to present spectra measured at very close angle - 35°. The agreement of Andronenko spectra measured at 126° with the present spectra measured at 100° is poorer, however, the difference of both detection angles may explain this fact.

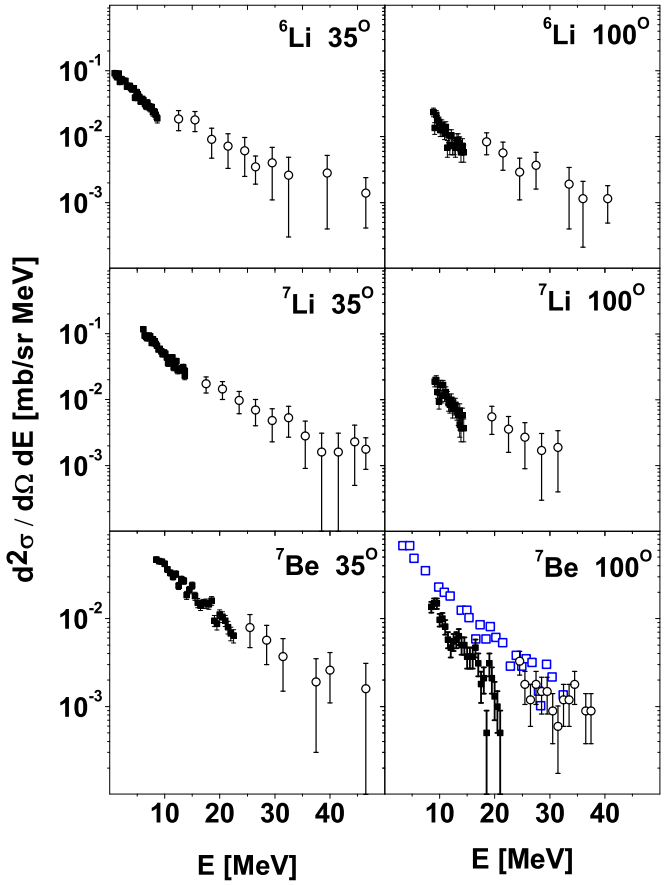

Figure 4.7: Experimental spectra of ^{6}Li, ^{7}Li and ^{7}Be from the present work (circles) measured at 35° (left column)and 100° (right column) in C+p collisions at proton beam energy 1.2 GeV and data from ref. [69] measured at 90° at proton energy 2.1 GeV (empty squares) as well as data from ref. [85] (full squares) measured at 30° (left column) and 126° (right column) at proton beam energy 1.0 GeV

The spectra of ^{6}Li, ^{7}Li, and ^{7}Be measured by Andronenko et al. [85] and Westfall et al. [69] also agree with the present data as can be seen in fig. 4.7. Such a good agreement is also visible for elementally identified Li spectra of Westfall et al., presented in fig. 4.8 together with the present results summed over isotopically identified Li ejectiles.

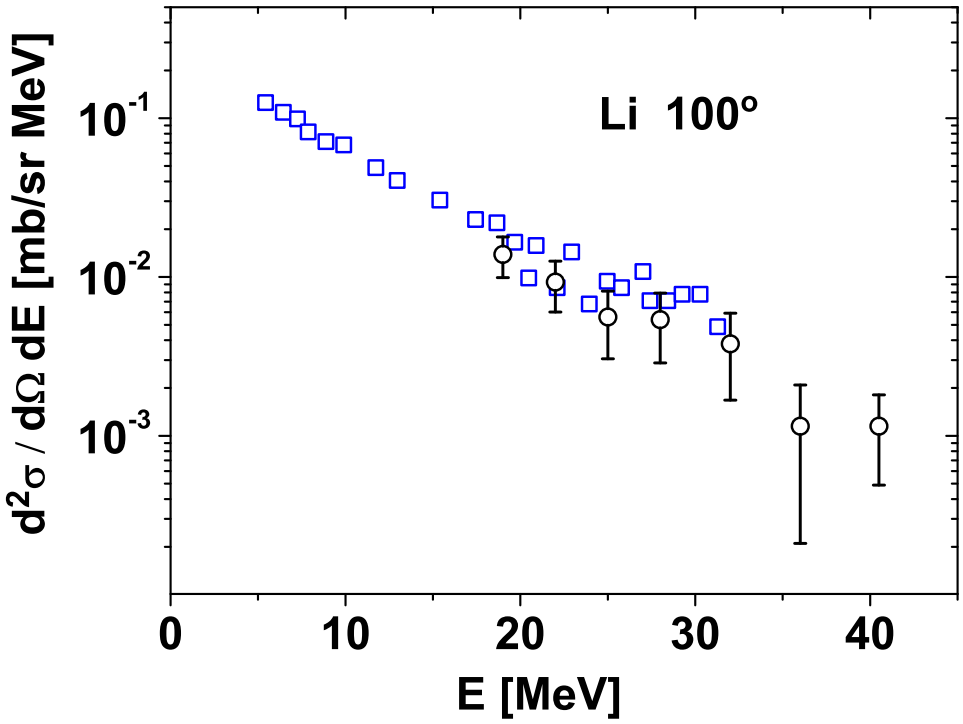

Figure 4.8: Experimental spectrum of Li ejectiles from the present work (circles) measured at 100° in C+p collisions at proton beam energy 1.2 GeV and data from ref. [69] measured at 90° at proton energy 2.1 GeV (empty squares)

In summary, the present data on the double differential production cross sections $\frac{d\sigma}{d\Omega dE}$ from the p+^{12}C collisions, normalized to Westfall et al. [69] α-particle differential cross sections, agree well with available literature cross sections, providing that the data are energy independent in the studied energy range as it is expected from the limiting fragmentation hypothesis.

Chapter 5

Results of measurements

In the present experiment double differential cross sections have been measured for two target nuclei: ^{27}Al and ^{12}C, for three proton beam energies: 1.2, 1.9, and 2.5 GeV. Spectra of light charged particles (p,d,t,^{3}He, and ^{4}He) as well as of intermediate mass fragments (^{6}He,^{6,7,8,9}Li,^{7,9,10}Be, and ^{10,11,12}B) were measured for Al target at seven scattering angles: 15.6°, 20° , 35° , 50° , 65° , 80° , and 100° . The spectra of the same ejectiles (with exception of ^{9,10}Be and B isotopes) were measured for ^{12}C target at the same scattering angles.

It turned out that the data vary very smoothly with the beam energy and with the scattering angle. Therefore, only selected - typical spectra of the ejectiles are presented in the figures below to illustrate the character of beam energy and angular dependencies, separately for ^{27}Al and for ^{12}C targets. For both targets the light charged particle spectra have different character than those for intermediate mass fragments, thus they are shown in two different figures, first for ^{27}Al and later for ^{12}C target.

The following general observations may be summarized after the inspection of figures shown below in which characteristic properties of the data are well visible:

- It may be stated, that the spectra of products from p+^{12}C collisions vary less with the beam energy than those from p+^{27}Al collisions. This is in agreement with observed in the literature fact (cf. section 2.1), that the approaching of the limiting fragmentation energy region appears at lower beam energies for lighter of these two targets.

- The beam energy variation of the spectra of light charged particles (LCPs) is more pronounced than variation of cross sections for intermediate mass fragments (IMFs). This is true for both targets, ^{27}Al and ^{12}C and is due, perhaps, to the fact that the LCPs approach the limiting fragmentation energy region at higher beam energies than the IMFs.

- The angular variation of the spectra of LCPs seems to be also more pronounced than that for intermediate mass fragments. Furthermore, the high energy tails of LCP spectra extend to higher energies than those for IMFs.

5.1 p+Al system

The beam energy variation of spectra of LCPs (hydrogen isotopes) from p+^{27}Al collisions are shown in Fig. 5.1. As can be seen all cross sections increase monotonically by 20 - 30 % when the beam energy varies from 1.2 to 2.5 GeV. Two regions of the ejectile energies may be distinguished in the picture: The spectra of low energy particles (energy smaller than about 30 - 40 MeV) are more steep than the high energy, exponential tails of the spectra.

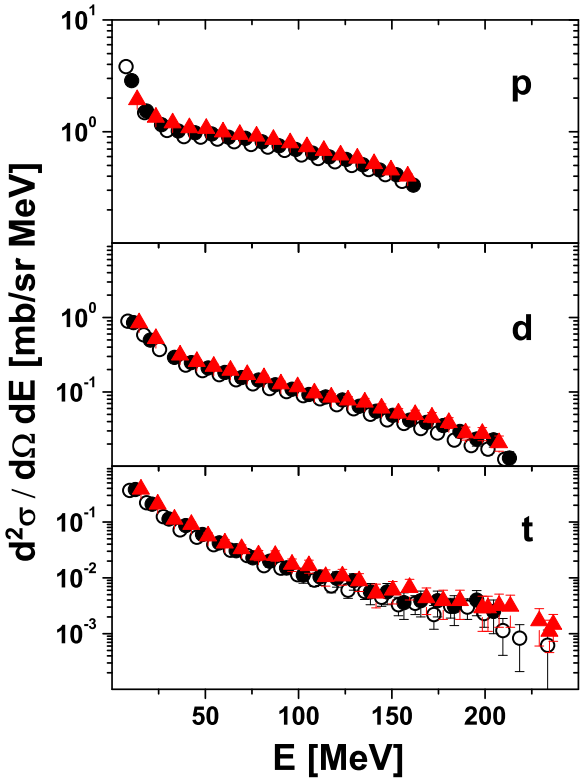

Figure 5.1: Spectra of hydrogen isotopes measured at 65° for p+Al collisions at three proton beam energies: 1.2 (empty circles), 1.9 (full circles), and 2.5 GeV (triangles). The proton, deuteron, and triton spectra are presented in the upper, the middle and the lower panel of the figure, respectively.

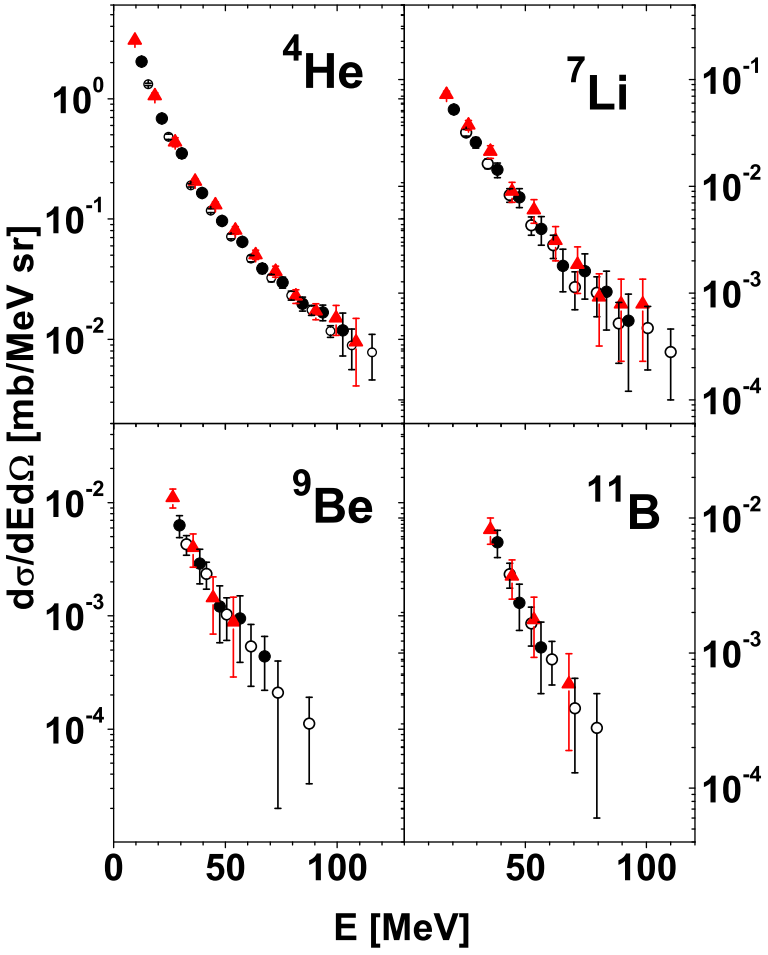

Figure 5.2: Spectra of ^{4}He, ^{7}Li, ^{9}Be, ^{11}B, measured at 35° for p+Al collisions at three proton beam energies: 1.2 (empty circles), 1.9 (full circles), and 2.5 GeV (triangles) .

The beam energy dependence of the spectra for intermediate mass fragments from p+^{27}Al collisions is presented in the Fig. 5.2. Two characteristic properties may be easily noticed:

- The absolute value of the cross sections varies very slightly with the increasing beam energy. This increase is stronger for lighter ejectiles (^{4}He, ^{7}Li) whereas the data for heavier IMFs are in the limits of the errors independent of the beam energy.
- The shape of the spectra for heavier IMFs does not indicate a presence of two different energy regions as it was for LCPs. The spectra of the α-particles, however, still have similar character as those for the Hydrogen isotopes.

The angular dependence of the spectra of light charged particles from p+^{27}Al collisions is presented in Fig. 5.3. A strong angular dependence is visible for all the spectra. This is especially pronounced for the high energy tails of the spectra. These tails become more steep with increasing scattering angle and the cross sections are then more concentrated in the lower energy region. Such a behaviour of the spectra may be explained by the emission of particles from the source which moves with a significant velocity in the forward direction. The low energy part of the spectra varies also with the scattering angle but not as strongly as the high energy tail. Thus, it may be expected that for this energy region the main effect of angular variation may be due to the angular dependence of the same component which dominates at high ejectile energies and gives some background also for small energies.

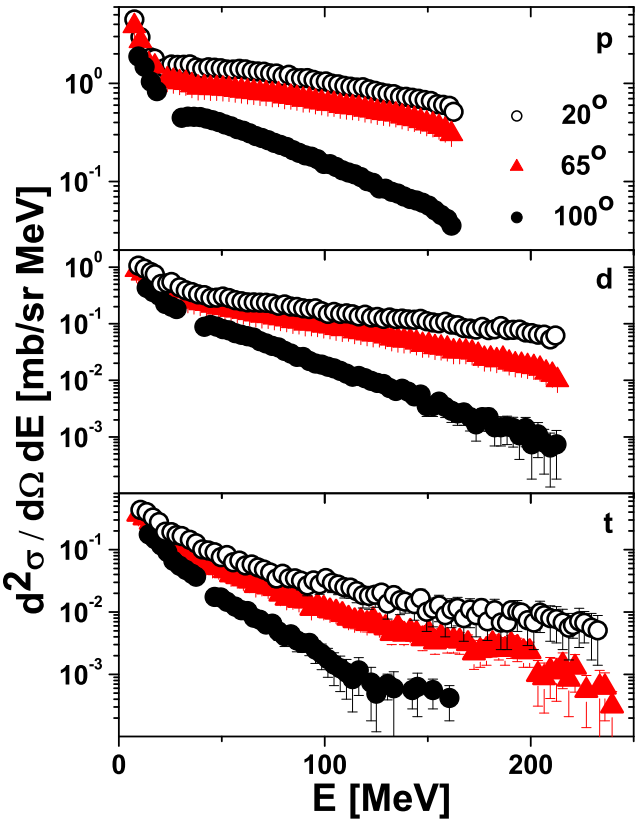

Figure 5.3: Spectra of hydrogen isotopes measured for p+Al collisions at proton beam energy 1.2 GeV for three emission angles: 20° (empty circles), 65° (full triangles), and 100° (full circles). Proton, deuteron, and triton spectra are shown in the upper, the middle, and the lower panel of the figure.

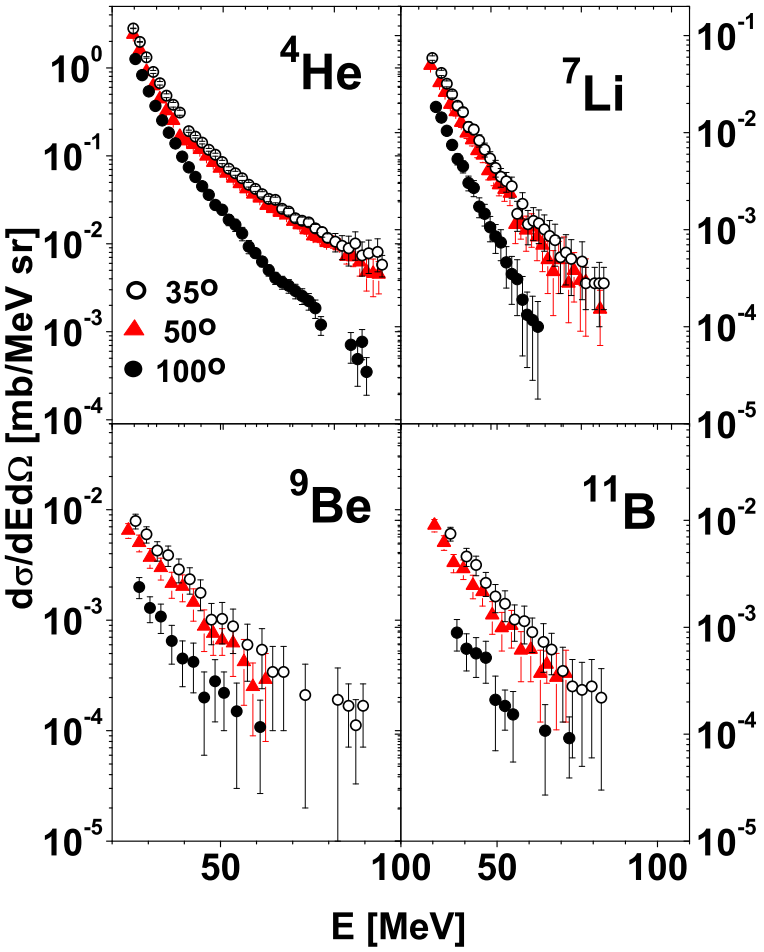

Figure 5.4: Spectra of ^{4}He, ^{7}Li, ^{9}Be, and ^{11}B measured for p+Al collisions at proton beam energy 1.2 GeV for three emission angles: 35° (empty circles), 50° (full triangles), and 100° (full circles).

The spectra of ^{4}He and of intermediate mass fragments like ^{7}Li, ^{9}Be, and ^{11}B from p+^{27}Al collisions also vary with scattering angle. It should be, however, pointed out that this angular dependence is different for ^{4}He and ^{7}Li from that for heavier intermediate mass fragments. The angular dependence of the spectra of lighter ejectiles is almost the same as that observed for light charged particles. For heavier intermediate mass fragments the shape of the spectra does not change with the scattering angle, however, the absolute value of the cross section decreases strongly (even by order of magnitude) at larger angles. Such a qualitative behaviour of the spectra establishes a challenge for any theoretical description of the reaction mechanism.

5.2 p+C system

Energy dependence of the spectra for light charged particles from p+^{12}C collisions is illustrated by Fig. 5.5 where the data measured at 65° are presented. As can be seen the spectra are identical in the limit of errors for all three beam energies: 1.2, 1.9, and 2.5 GeV. In all spectra two qualitatively different energy regions may be distinguished. The low energy part of the spectrum (energies smaller than approximately 30 MeV) with steeper slope, and the high energy exponential tail. Such a behaviour is very similar to that observed for the Aluminium target (cf. section 5.1).

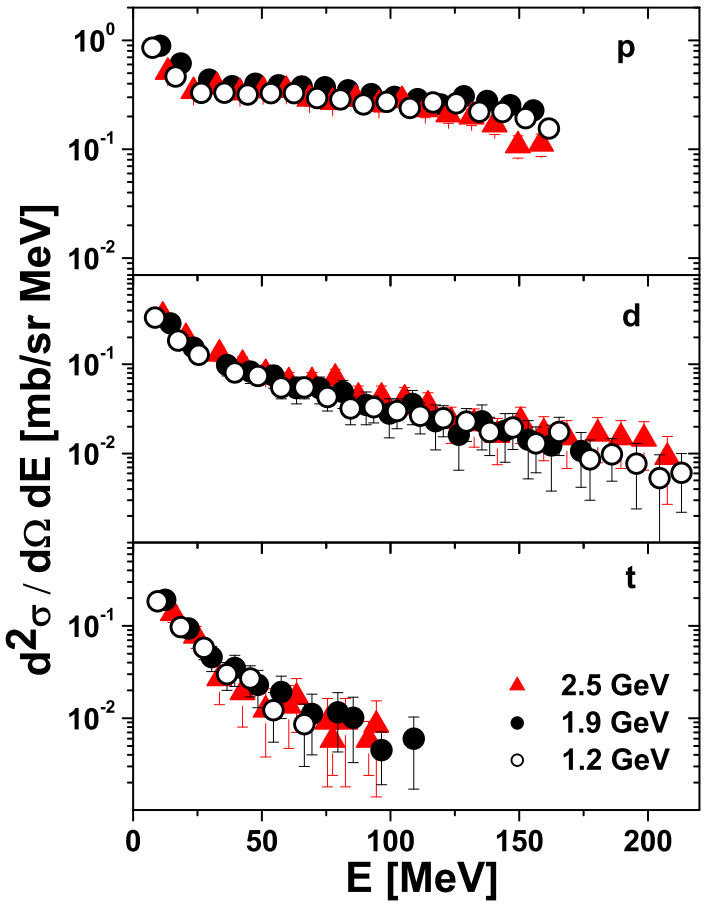

Figure 5.5: Spectra of hydrogen isotopes measured at 65° for p+C collisions at three proton beam energies: 1.2 (empty circles), 1.9 (full circles), and 2.5 GeV (triangles). Proton, deuteron, and triton spectra are shown in the upper, the middle, and the lower panel of the figure.

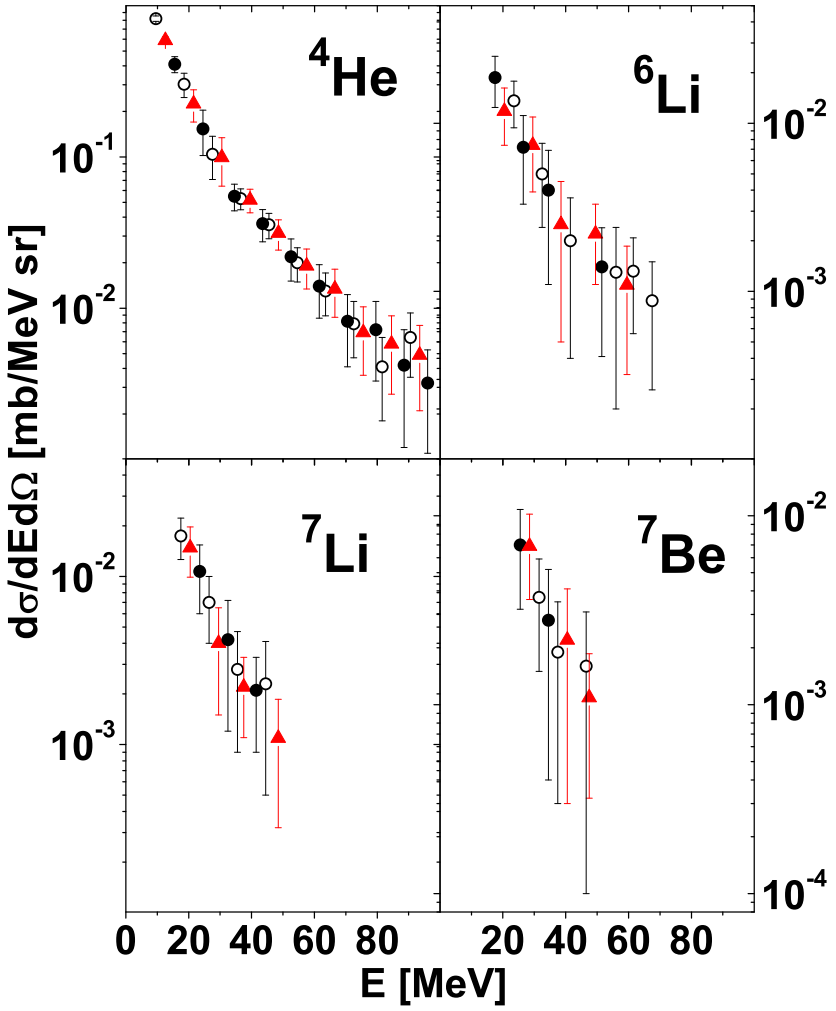

Figure 5.6: Spectra of ^{4}He, ^{6}Li, ^{7}Li, ^{7}Be, measured at 35° for p+C collisions at three proton beam energies: 1.2 (empty circles), 1.9 (full circles), and 2.5 GeV (triangles) .

The cross sections measured for heavier ejectiles (^{4}He, ^{7}Li, ^{9}Be, ^{11}B) on the ^{12}C target are energy independent, i.e. the cross sections at 1.2, 1.9, and 2.5 GeV have the same values in the limit of errors. Note, that for ^{12}C target such an energy independence of ^{4}He production was observed in the literature (cf. section 2) and was used in the absolute normalization of the cross sections from the present experiment (cf. section 4). Energy independence of other cross sections observed with the above normalization confirms that all intermediate mass fragments fulfill the limited fragmentation hypothesis in the studied beam energy range.

The angular dependence of the light charged particle spectra from p+^{12}C collisions is represented by Fig. 5.7, where the data for protons, deuterons, and tritons are depicted. Similarly like for ^{27}Al, the spectra consist of two parts with different angular dependence. The absolute value of the cross sections in the low energy part of the spectra, which extends to 25 - 30 MeV decreases with the scattering angle but the shape of the spectrum does not change. On the other hand, the cross sections in the high energy part of the spectra decrease with the energy and the slope of the spectra strongly increases.

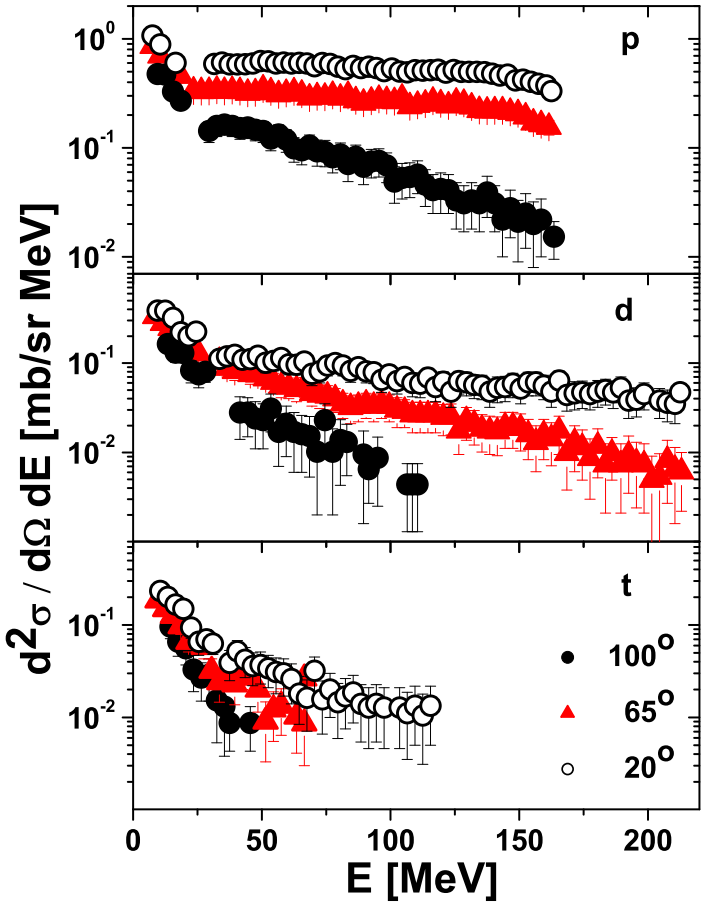

Figure 5.7: Spectra of hydrogen isotopes measured for p+C collisions at proton beam energy 1.2 GeV for three emission angles: 20° (empty circles), 65° (full triangles), and 100° (full circles). Proton, deuteron, and triton spectra are shown in the upper, the middle, and the lower panel of the figure.

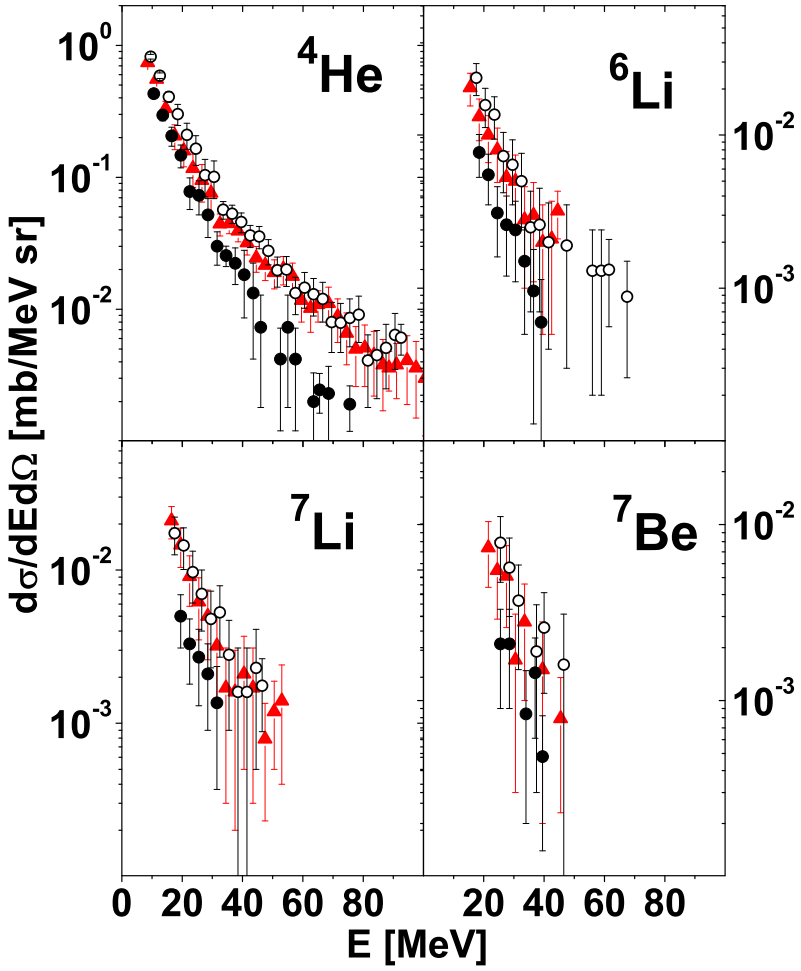

Figure 5.8: Spectra of ^{4}He, ^{6}Li, ^{7}Li, and ^{7}Be measured for p+C collisions at proton beam energy 1.2 GeV for three emission angles: 35° (empty circles), 50° (full triangles), and 100° (full circles).

The angular dependence of the ^{4}He spectra and to some extend also the spectra of ^{6}Li behave in similar manner like those for the Hydrogen isotopes. The ^{7}Li and ^{7}Be spectra do not change their shape for different scattering angles but the absolute value of the cross sections decreases with the angle. This is again similar behaviour to that observed for intermediate mass fragments in the case of p+^{27}Al collisions. The main difference consists in the fact that angular variation of the absolute value of the cross sections is larger for Al target than for C target.

Chapter 6

Theoretical analysis

> *" A rich experience gained in the last decade shows that no one particular model is able to give a satisfactory description of the formation, evolution and decay of highly excited nuclear systems in the course of a nuclear reaction at intermediate and high energies. The development of various approaches describing some selected features of the reaction seems to be the most fruitful way of tackling the problem. A decisive role in this situation is played by the systematic comparison of theoretical models with each other and with experimental data."*
>
> J.P Bondorf et al., Physics Reports 257 (1995) 133-221

The analysis of the data obtained in the present experiment was realized in several steps:

(1) At first the analysis in the frame of traditional, two-step model – discussed in section 6.1 – has been applied: The first stage of the reaction was described by an intranuclear cascade of nucleon-nucleon and nucleon-pion collisions allowing for coalescence of nucleons into light charged particles, and the second stage of the reaction was treated as evaporation of particles from an excited remnant of the intranuclear cascade.

It turned out, as it is described below, that the angular distributions as well as the energy spectra were not reproduced properly by the model. The deviations of the model cross sections from the data were most prominent in the tails of the energy distributions. This is true for both target nuclei, i.e. ^{12}C and ^{27}Al. Therefore, it was assumed that another reaction mechanism should be taken into consideration.

(2) Since this mechanism manifests itself in high energy part of the spectra it is reasonable to conjecture, that the mechanism searched for is typical for highly excited nuclei. The natural candidate for this additional mechanism is the statistical multifragmentation of remnants of the intranuclear cascade appearing when the excitation energy per nucleon is larger than some limiting value. Thus, the theoretical analysis based on the two-step model was repeated for IMFs treating in a different way the remnants of the first stage of the reactions when they are excited to low or to high excitation energy. This analysis

is discussed in section 6.2. It was assumed that the deexcitation of former remnants proceeds by a sequential evaporation of particles and that the latter remnants are subject of a multifragmentation. The multifragmentation was treated in the frame of a simple, statistical formalism of so called Fermi break-up [73]. It will be shown in section 6.2, that multifragmentation of highly excited remnant nuclei combined with evaporation of IMFs from low excited nuclei describes well the data for IMFs.

Such a good description of the data has not been achieved for light charged particles (LCPs). It turned out that the LCP data measured at forward scattering angles were strongly underestimated by predictions of the model discussed above. This suggested that still another mechanism of emission of LCPs at forward scattering angles should be taken into consideration.

(3) This mechanism was treated phenomenologically as the emission from the fast, hot, forward–moving source - so called "fireball". Since in such an approach the impinging proton, which knocks-out the fireball does not interact with the remnant nucleus, it is reasonable to assume that the target remnants after fireball emission have similar properties (mass, charge, excitation energy) as target remnants after the intranuclear cascade of nucleon-nucleon collisions. Then the second step of the reaction, i.e., evaporation and/or multifragmentation of excited target remnants should be practically the same for both mechanisms contributing to the first stage of the reaction. This means that the results of analysis of IMF production remain valid, the same as discussed in section 6.2, however, the data for LCPs should be analyzed taking into consideration scaling down of contribution from intranuclear cascade (by factor $f < 1$) and adding contribution from the fireball emission.

Details of this analysis are presented in section 6.3.

6.1 Two-step traditional model

The fast stage of the proton induced reaction has been described by INCL model (cf. section 3.1.1), treating the proton - nucleus interaction as a set of nucleon-nucleon collisions initiated by the impinging proton with target nucleons, which move in a static mean field. The standard values of parameters of the model, recommended by authors of the computer program INCL4.3 [55, 56], were used in the present analysis.

The nucleon-nucleon collisions lead to energy deposition in the nucleus as well as to emission of fast nucleons and LCPs (due to coalescence of target nucleons with outgoing nucleon). It was assumed that excited target remnants are equilibrated after the first step of the reaction. Then, in the second step of the reaction an evaporation of nucleons and complex particles was allowed from the excited remnants of the target. This stage of reaction was described by GEM2 model of Furihata [70, 71]. Again, the standard values of the model parameters were used as recommended by Furihata [71].

6.1.1 p+Al collisions

The theoretical spectra (lines) of Hydrogen, Helium, Lithium, Beryllium, and Boron isotopes evaluated for p+Al collisions at proton beam energy 1.2 GeV are presented together with experimental data (dots) in figures 6.1,6.2, 6.3, 6.4, and 6.5, respectively. Fluctuations of the theoretical lines have no physical meaning. They appear due to limited statistics of the Monte Carlo method of calculations used in the theoretical model.

It is evident that the traditional model fails to describe properly the data:

- Spectra of LCPs, i.e. Hydrogen and Helium ejectiles, measured at forward angles (15° - 65°) are ***underestimated*** by the model by factor 2 – 4.

- Experimental spectra of LCPs measured at 100° have larger slope at highest energies than that predicted by the model and therefore they are there ***overestimated*** by the model.

- Experimental spectra of IMFs have smaller slope than that of the model spectra, and the absolute values of the experimental cross sections are larger than theoretical cross sections in full range of measured ejectile energies.

Such quantitative and qualitative disagreement observed for reactions induced by p+ Al collisions suggests that an important reaction mechanism was not taken into account in the traditional reaction model.

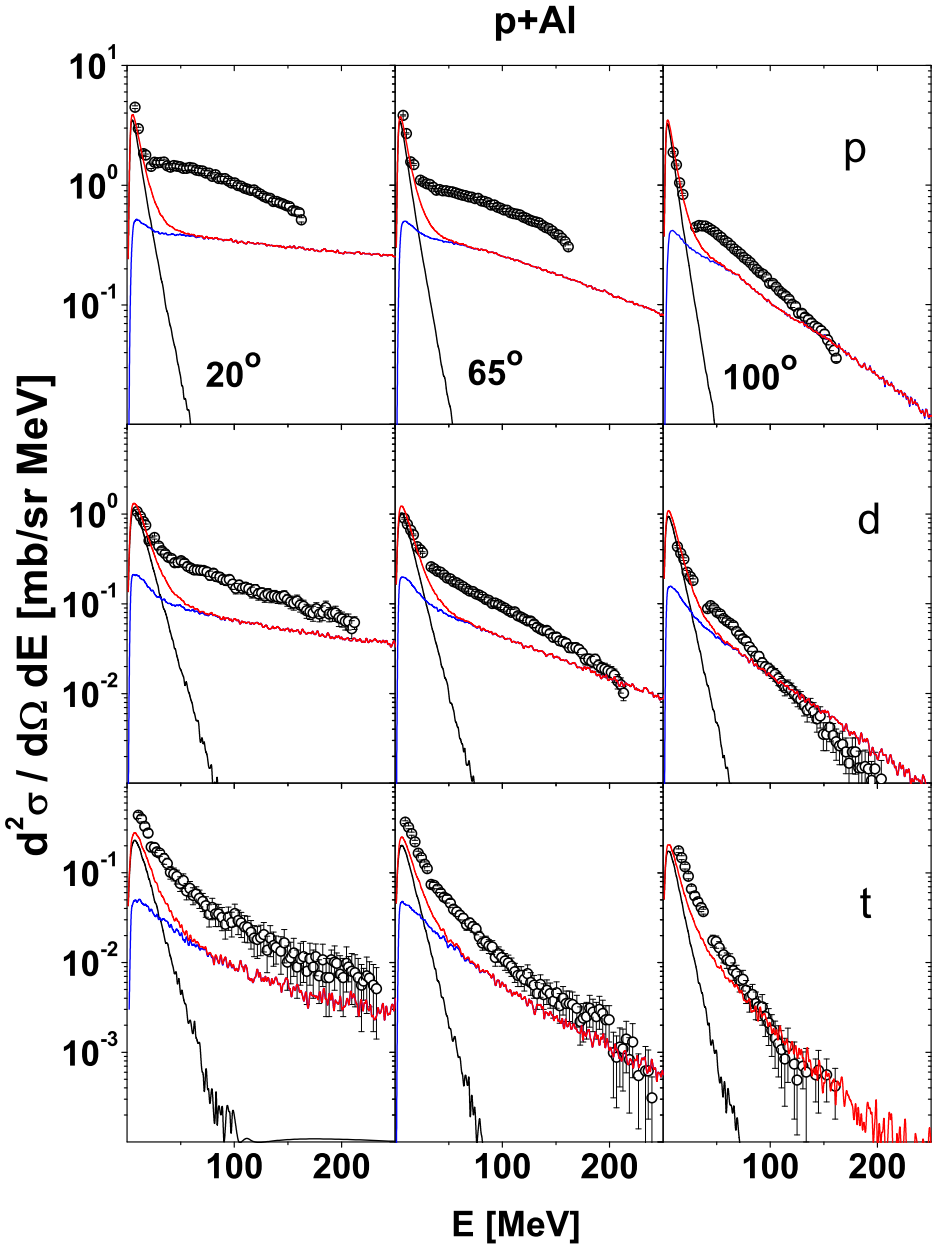

Figure 6.1: Experimental spectra (dots) of protons (upper row), deuterons (middle row), and tritons (lower row) measured for p+Al collisions at Tp=1.2 GeV. Left, middle, and right columns present data measured at 20°, 65°, and 100°, respectively. Blue line represents intranuclear cascade calculations performed with INCL4.3 computer program [55,56], which include coalescence of nucleons emerging from the reaction into complex particles. Black line shows contribution of evaporation of particles from excited remnant nuclei – products of the intranuclear cascade. The red line depicts sum of both contributions.

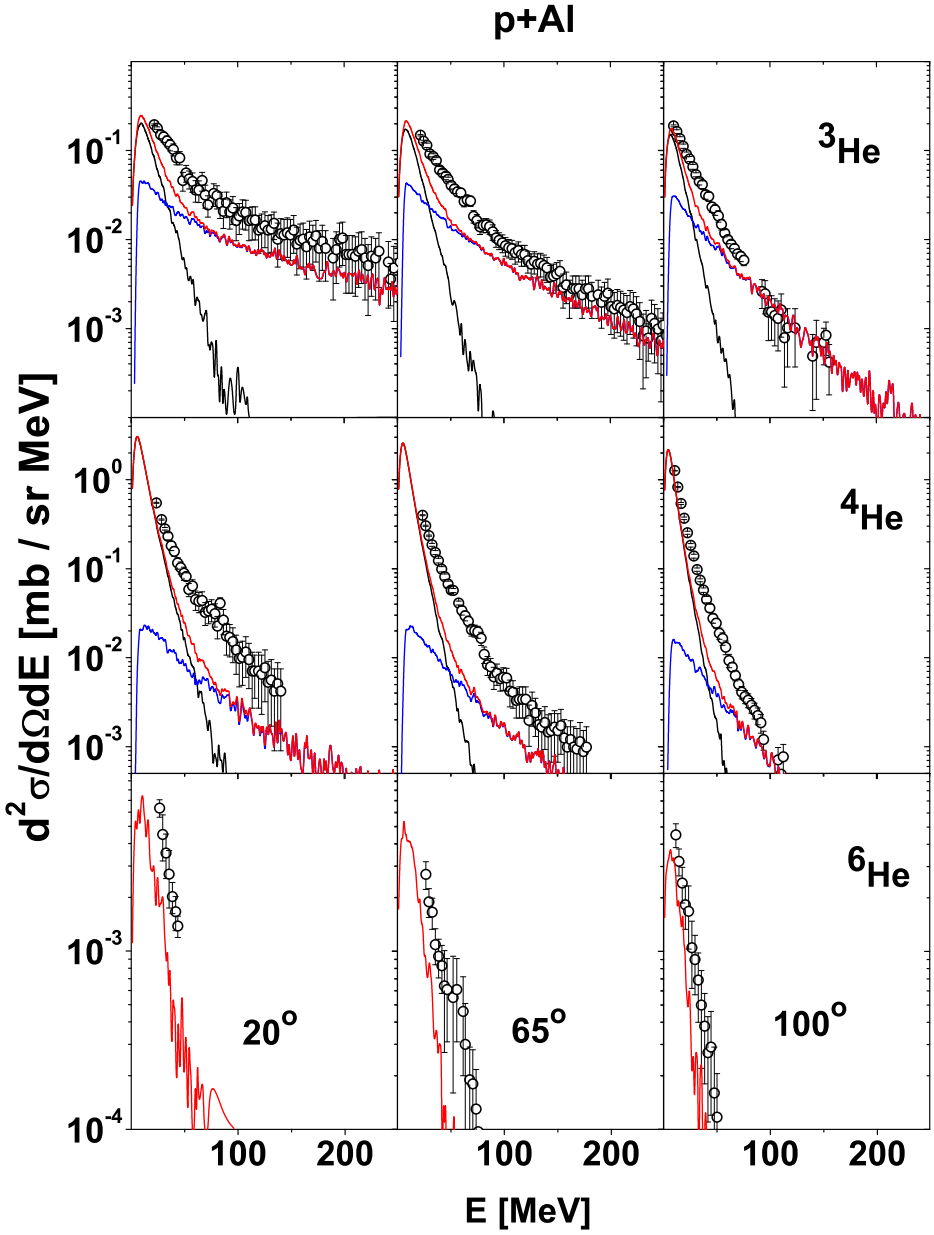

Figure 6.2: The same as on fig. 6.1 but for ^{3}He (upper row), ^{4}He (middle row), and ^{6}He (lower row).

Note that the red line for ^{6}He and heavier ejectiles does not present sum of different processes but the evaporation contribution (i.e. GEM model), only. This comment is also valid for next

figures, where spectra of Li, Be, and B isotopes are presented.

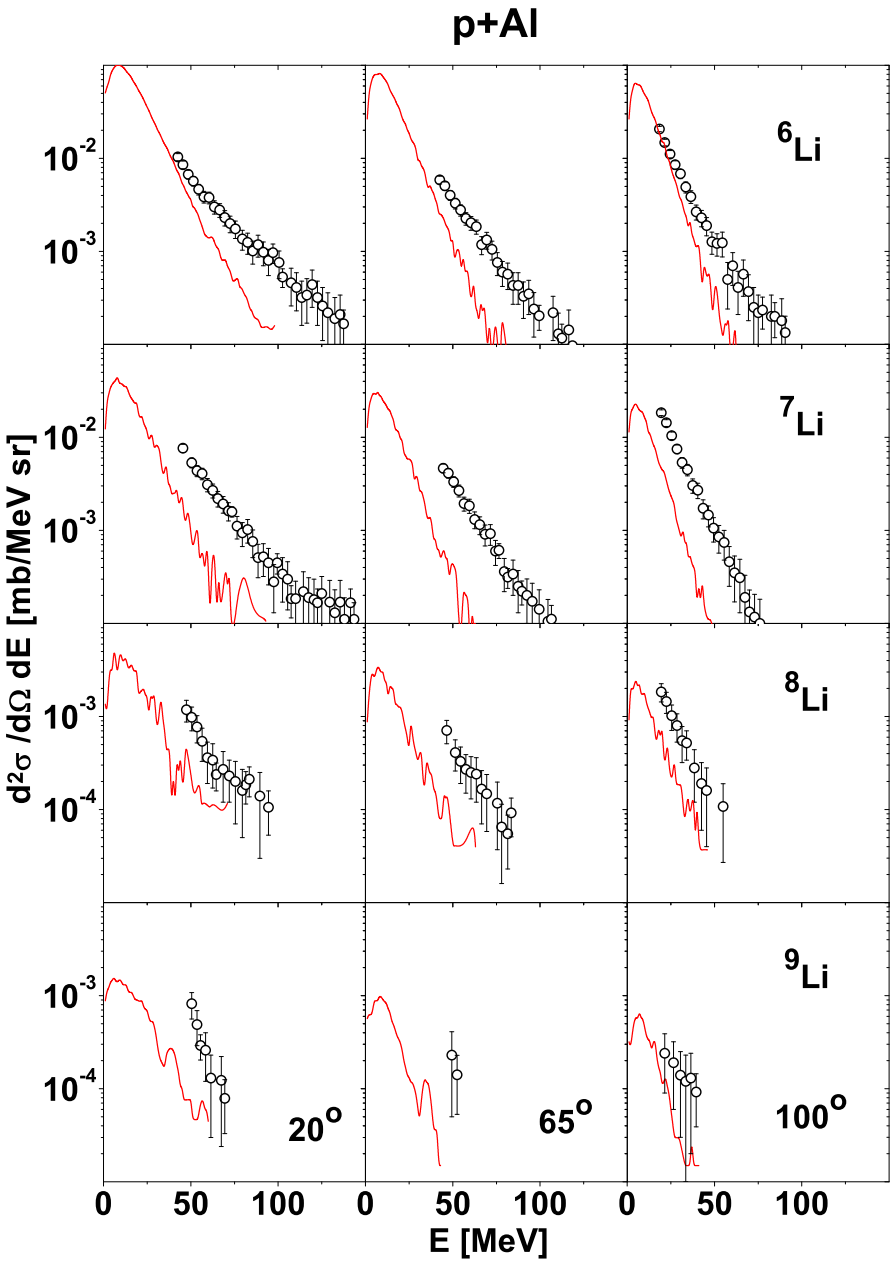

Figure 6.3: The same as on fig. 6.1 but for ^{6}Li (upper row), ^{7}Li, ^{8}Li (middle rows), and ^{9}Li (lower row).

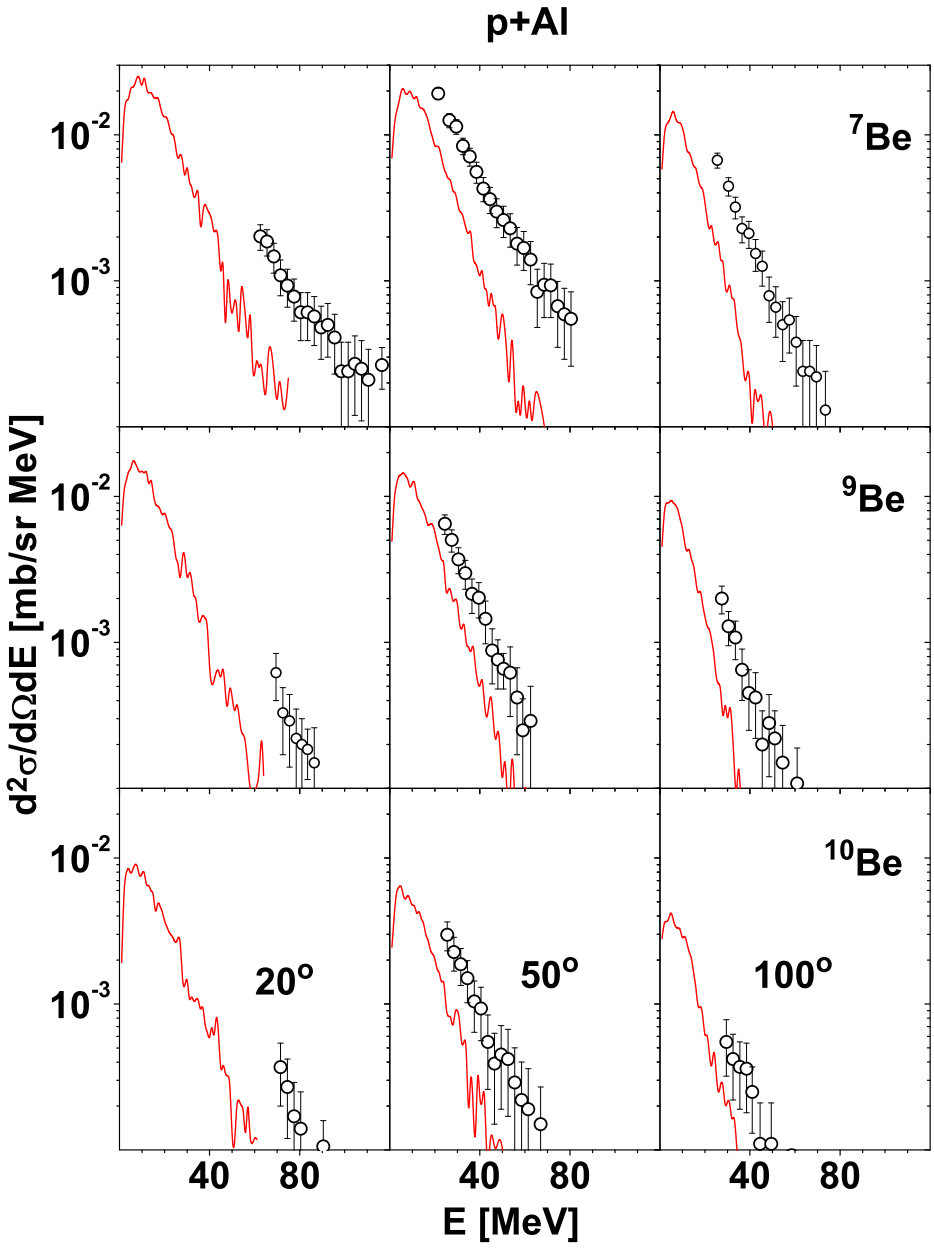

Figure 6.4: The same as on fig. 6.1 but for ^{7}Be (upper row), ^{9}Be (middle row), and ^{10}Be (lower row). The left, middle, and right column represent the spectra at 20° , 50° , and 100° , respectively.

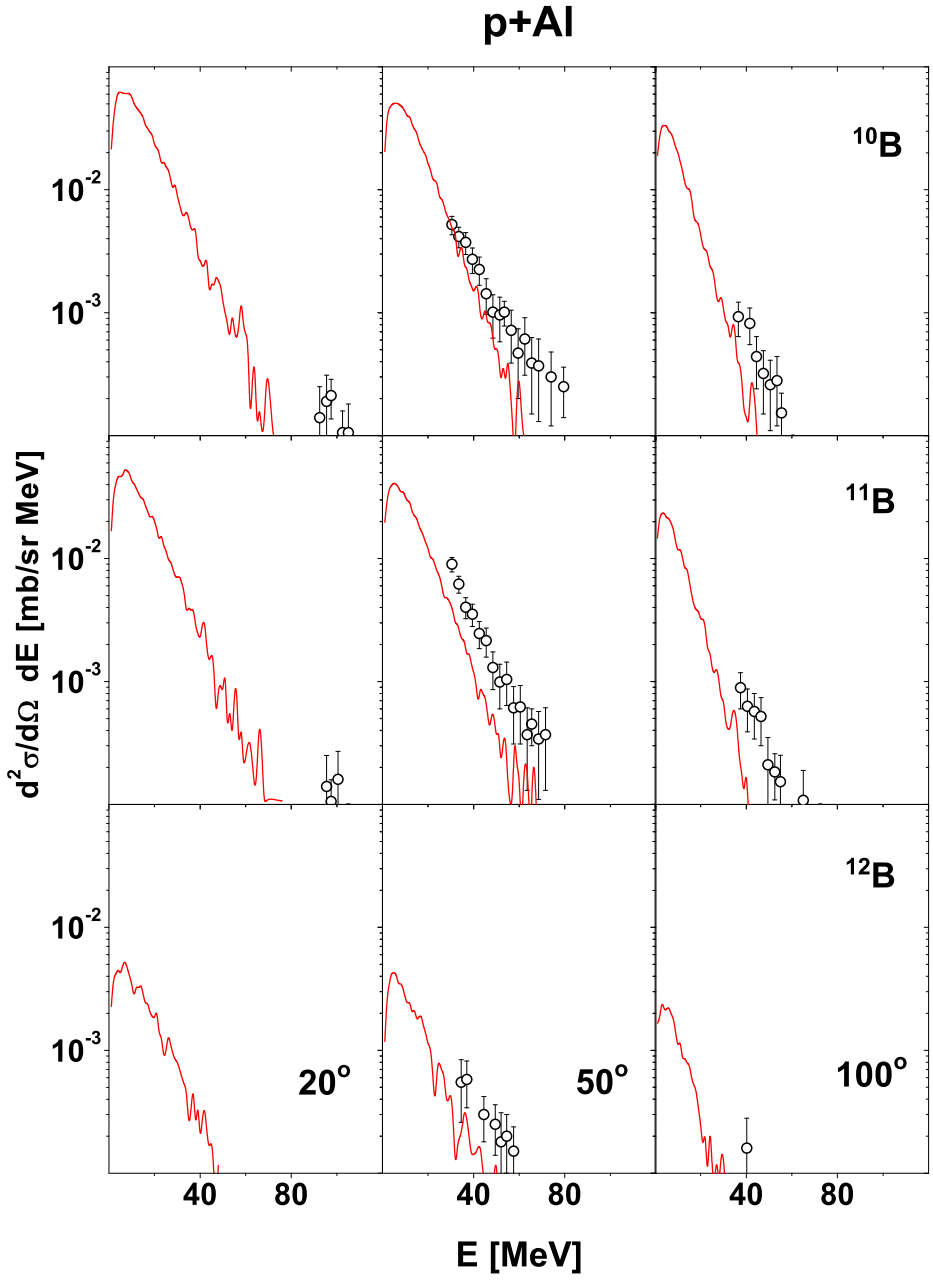

Figure 6.5: The same as on fig. 6.1 but for ^{10}B (upper row), ^{11}B (middle row), and ^{12}B (lower row). The left, middle, and right column represent the spectra at 20° , 50° , and 100° , respectively.

6.1.2 p+C collisions

Analogous spectra for isotopes of Hydrogen, Helium, Lithium, and ^{7}Be for p+C collisions at proton beam energies are shown in figures 6.6, 6.7, and 6.8, respectively.

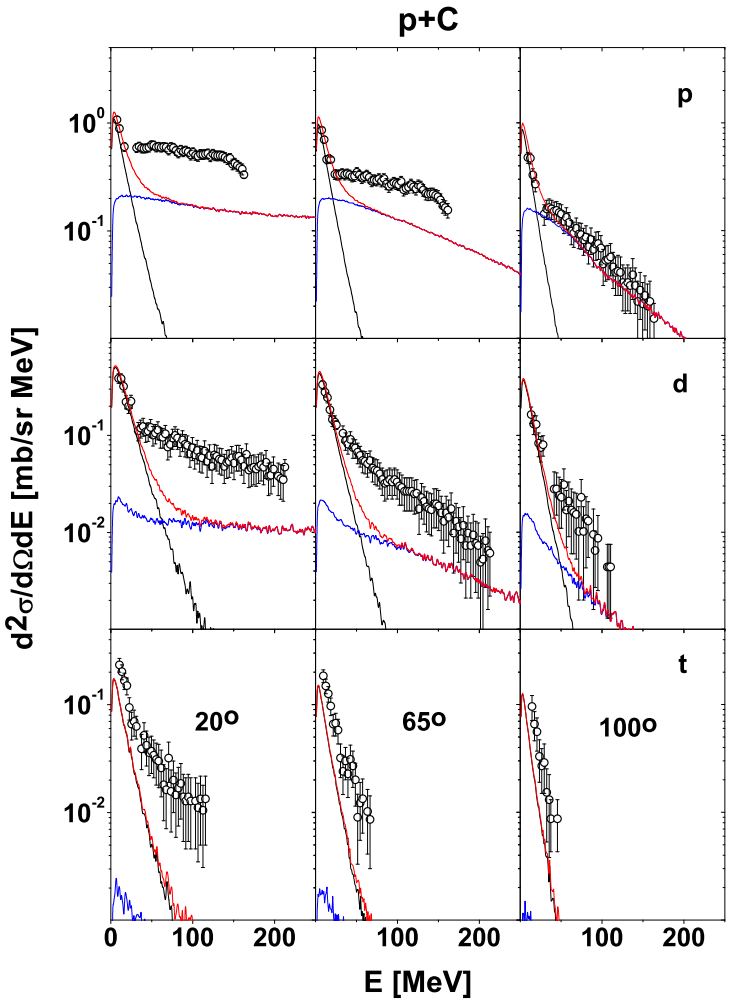

Figure 6.6: Experimental spectra (dots) of protons (upper row), deuterons (middle row), and tritons (lower row) measured for p+C collisions at Tp=1.2 GeV. Left, middle, and right columns present data measured at 20°, 65°, and 100°, respectively. Blue line represents intranuclear cascade calculations performed with INCL4.3 computer program [55,56], which include coalescence of nucleons emerging from the reaction into complex particles. Black line shows contribution of evaporation of particles from excited remnant nuclei – products of the intranuclear cascade. The red line depicts sum of both contributions.

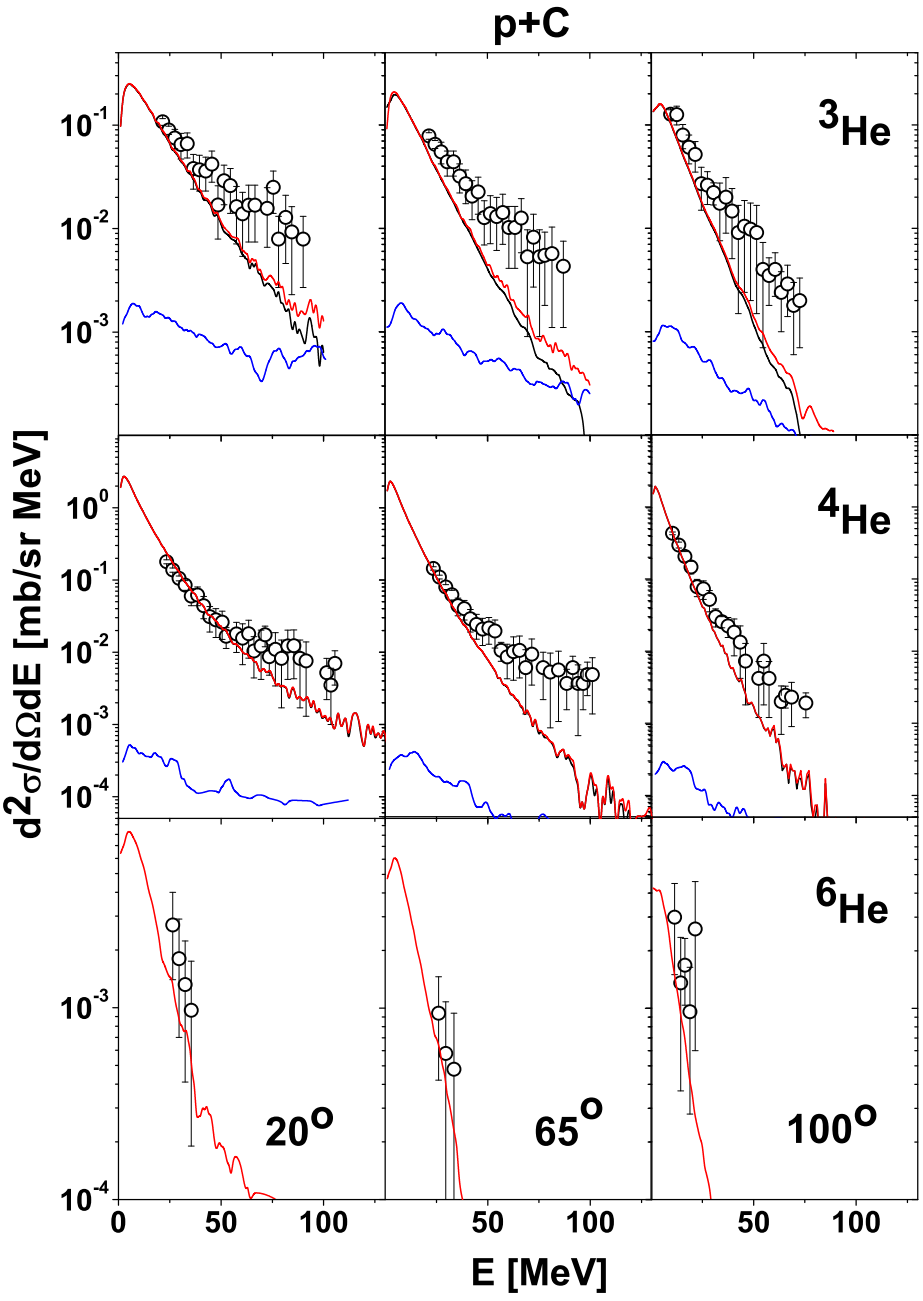

Figure 6.7: The same as on fig. 6.6 but for ^{3}He (upper row), ^{4}He (middle row), and ^{6}He (lower row). The oscillations of the theoretical lines have no physical meaning. They appear because of limited statistics of time consuming Monte Carlo calculations.

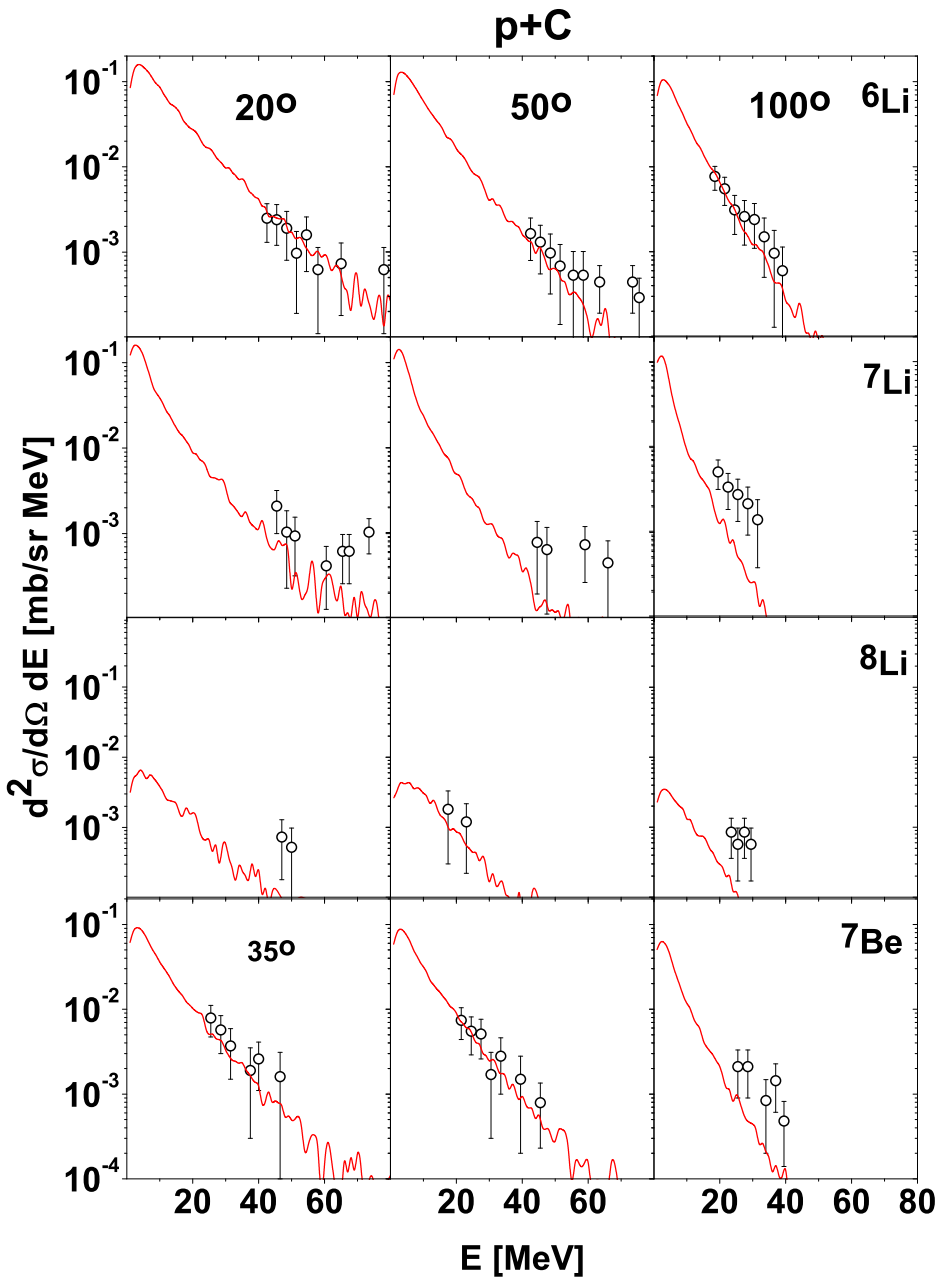

Figure 6.8: The same as on fig. 6.6 but for ^{6}Li (upper row), ^{7}Li and ^{8}Li (middle rows), and ^{7}Be (lower row). Note that the red line presents the evaporation contribution only (GEM model).

As it is shown in figs 6.6 and 6.7, the traditional two-step model is not able to reproduce

spectra and angular distributions of light charged particles, however, it works much better for intermediate mass fragments. Such a conclusion may be derived from fig. 6.8 where the main part of the spectra is reasonably well described by the model. The largest deviations are seen for the highest energies of IMFs, where the slope of experimental spectra is less steep than that predicted by the model.

6.2 Multifragmentation

The emission of IMFs from p+Al collisions was treated as evaporation from and multifragmentation of excited nuclei - remnants of the first stage of the reaction. It was assumed that sequential emission of IMFs, i.e. the evaporation of a single particle in each step, dominates when the remnants of the cascade are excited to rather low energies whereas the remnants excited to high energies split into many pieces thus they are subject of multifragmentation which is considered as a simultaneous process. ***The critical excitation energy per nucleon*** $(E^*/A)_{cr}$, i.e. the smallest value of excitation energy per nucleon at which multifragmentation appears was treated as free parameter. Another free parameter was the so called ***freeze-out radius*** r_0. It has the following meaning; these parts of the nucleus, which appear to be outside of the sphere with radius $r_0 A^{1/3}$ and with a center inside the nucleus do not interact by attractive nuclear force but feel only a repulsive Coulomb interaction. A denotes the mass number of decaying nucleus.

The evaporation of particles from excited remnants which have an excitation energy smaller than the critical value $(E^*/A)_{cr}$ was evaluated by means of the GEM2 computer program [70,71] (see also detailed description in section 3.2.1) with standard values of parameters whereas the multifragmentation of nuclei with excitation energy larger than $(E^*/A)_{cr}$ was calculated as Fermi break-up using the computer program ROZPAD [83] (see also detailed description in section 3.2.3).

6.2.1 Multifragmentation in p+Al system

The free parameters of the model; freeze-out radius r_0 and critical excitation energy $(E^*/A)_{cr}$ were searched for by comparison of theoretical spectra to experimental data for ^{6}He, ^{6,7,8,9}Li, ^{7,9,10}Be, and ^{10,11,12}B. Chi-square values were evaluated summing over all data listed above for several fixed values of r_0 parameter and several values of critical excitation energy $(E^*/A)_{cr}$. The obtained values of the chi-square are shown in the upper panel of figs 6.9, 6.10, and 6.11 for proton beam energies 1.2, 1.9, and 2.5 GeV, respectively.

The following properties of the chi-square dependence are clearly visible:

- Broad minima of the chi-square treated as a function of critical excitation energy $(E^*/A)_{cr}$ are present for each fixed r_0 parameter. The chi-square value increases very strongly when critical excitation energy decreases to values smaller than $\approx$ 5 MeV/nucleon. This behaviour points to the fact that the nuclei at such low excitation energies are not subject of multifragmentation but rather evaporate particles sequentially. This increase of chi-square is caused by a disagreement of the shape of the experimental spectra at lowest ejectile energies and the shape of the spectra predicted by the multifragmentation mechanism. The slope of experimental spectra at lowest energies is much steeper than that from the multifragmentation mechanism (cf. e.g. spectra of ^{6}Li and ^{7}Li in Fig. 6.13).

- Minimal value of the chi-square for each value of the r_0 parameter is presented as a

function of critical excitation energy $(E^*/A)_{cr}$ in the middle panel of the figures. As can be seen this dependence may be well approximated by a concave parabolic function, which minimum allows to choose the best fit value of the critical energy for each fixed r_0, respectively.

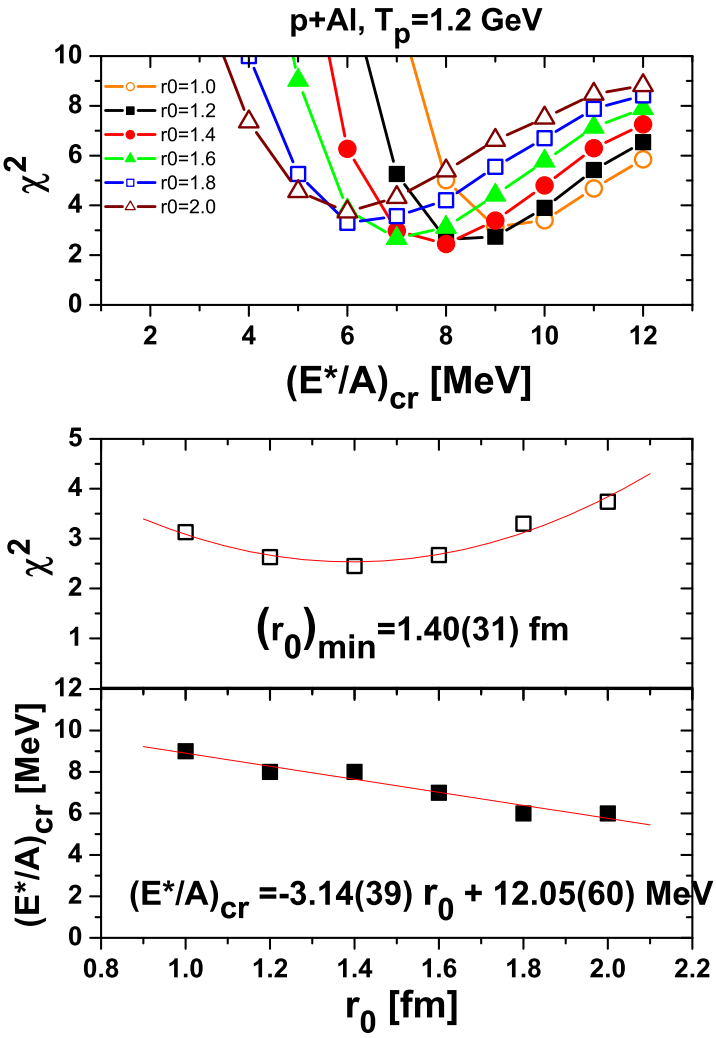

Figure 6.9: Upper panel: the chi-square value evaluated for all IMFs as a function of $(E^*/A)_{cr}$ at several fixed values of r_0 parameter for p+Al collisions at T_p=1.2 GeV. Middle panel: minimal chi-square of the functions $\chi^2((E^*/A)_{cr})$ presented above for each fixed r_0 parameter versus r_0. Lower panel: $(E^*/A)_{cr}$ parameter for the best chi-square value versus corresponding r_0 parameter.

- This best fit $(E^*/A)_{cr}$ parameter value is correlated with the value of the r_0 parameter,

what can be observed in the lower panel of figs 6.9, 6.10, and 6.11. Such a correlation has clear intuitive meaning: Increasing volume of an excited nucleus leads to lowering of its density and facilitates decomposition of the nucleus into several pieces thus a multifragmentation may appear at lower excitation energy of the decaying nucleus.

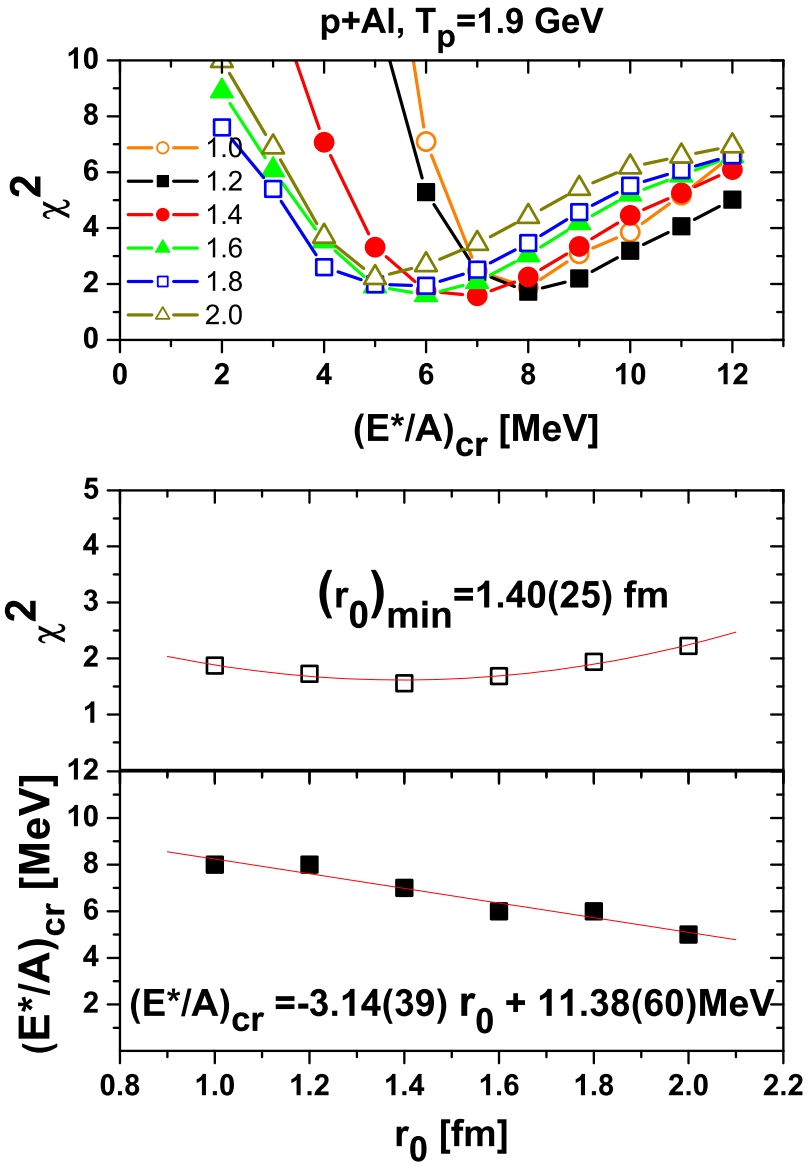

Figure 6.10: The same as in fig. 6.9 but for the beam energy equal 1.9 GeV.

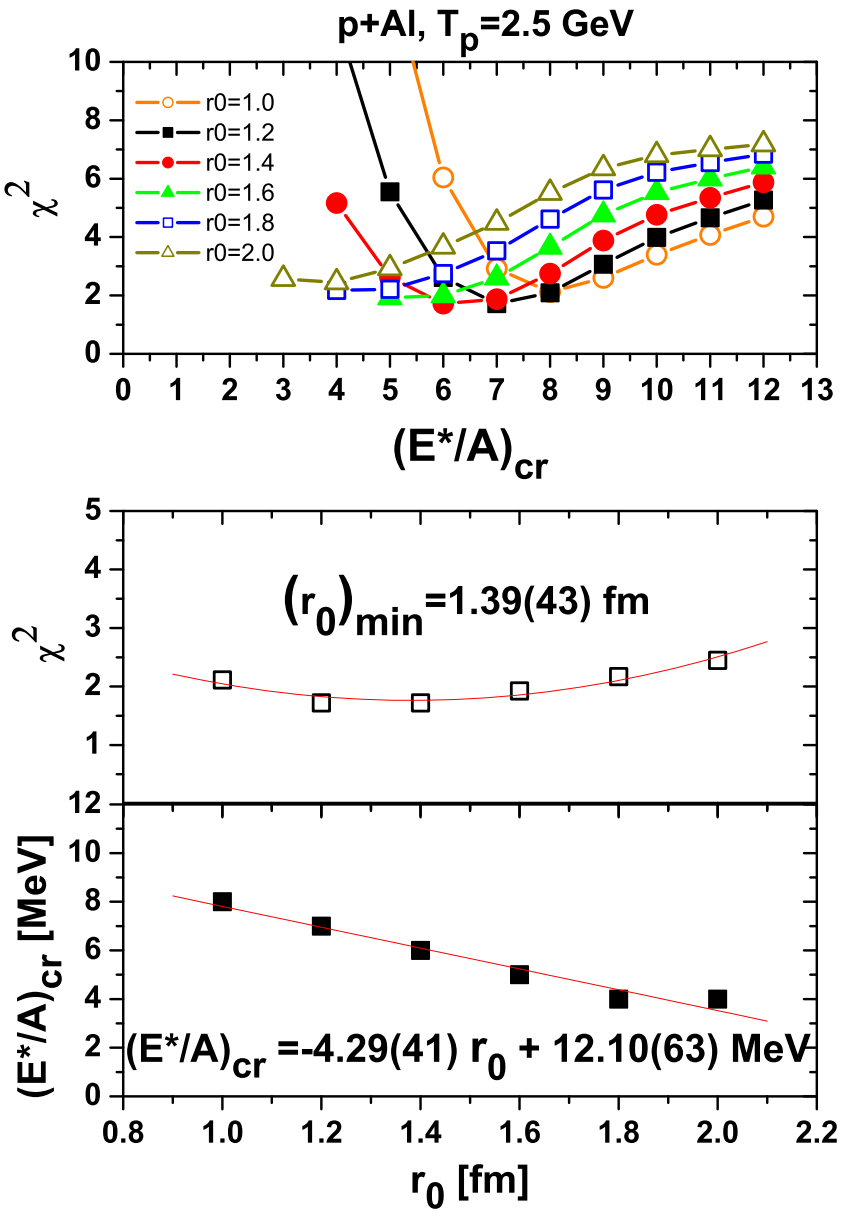

Figure 6.11: The same as in fig. 6.9 but for the beam energy equal 2.5 GeV.

As can be seen in figs 6.9, 6.10, and 6.11 the best fit value of the reduced radius r_0 ***– 1.40(31) fm, 1.40(25) fm, and 1.39(43)fm for beam energy 1.2, 1.9, and 2.5 GeV, respectively – is in the limits of error the same for all three beam energies.*** Thus fixing the parameter r_0 at $\boldsymbol{r_0 = 1.40(20)\ \mathbf{fm}}$ allows to find the best fit value of the second parameter - the critical excitation energy $(E^*/A)_{cr}$ - from the linear relation between

these two parameters shown in the lowest panel of the figures. ***It was found that the critical excitation energy is also almost the same in the studied beam energy range. It is equal to 7.7(8) MeV/nucleon, 7.0(8) MeV/ nucleon, and 6.1(9) MeV/nucleon for 1.2, 1.9, and 2.5 GeV beam energy, respectively.***

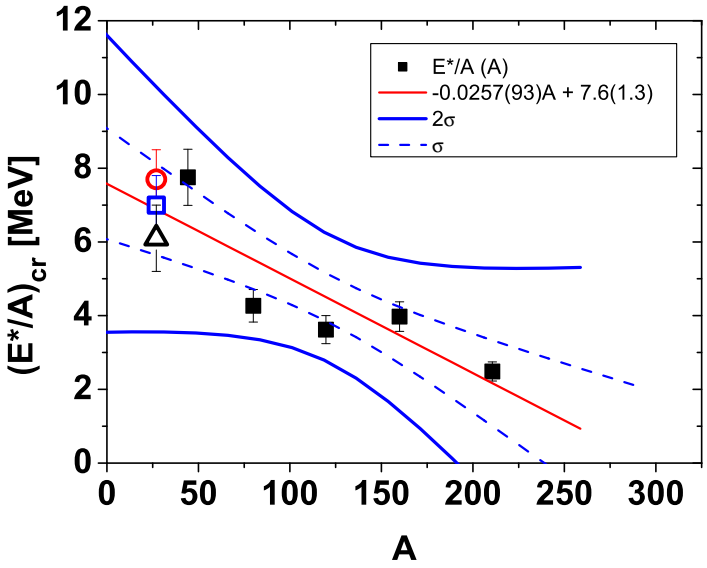

Figure 6.12: The full symbols represent the compilation of critical excitation energies per nucleon as a function of mass number of decaying nuclei [49], the solid line shows the linear regression of these data whereas the dashed and solid hyperbolas correspond to one- and two-standard deviation confidence intervals of the regression line, respectively. The empty symbols depict the critical excitation energy values used in the present analysis for p+Al collisions; circle, square, and triangle correspond to 1.2, 1.9, and 2.5 GeV beam energy, respectively.

It is interesting to compare the critical energy for fragmentation with values quoted by Natowitz et al. [49] in their compilation of multifragmentation reaction for various nuclear systems. ***The present values of critical energy fit perfectly to the compilation of Natowitz et al. as can be seen in fig. 6.12.***

The quality of the description of experimental data for p+Al collisions may be judged from inspection of figs 6.13 - 6.17 where the data measured at proton beam energy equal to 1.2 GeV are shown. As can be seen the contribution of multifragmentation to the spectra (shown by green solid line in the figures) is negligible for protons, small for other LCPs, but it is crucial for spectra of IMFs. ***It turned out that the sum of evaporation and multifragmentation reproduces very well the full spectra of*** ^{6}**He,** ^{6,7,8,9}**Li,** ^{7,9,10}**Be, and** ^{10,11,12}**B. It should be emphasized that all these spectra are evaluated assuming the same parameters:** $r_0 = 1.4$ **fm** ***and*** $(E^*/A)_{cr} = 7.7$ **MeV**.

An equally good description of IMF data was achieved for higher beam energies (1.9 and 2.5 GeV) using the same value of r_0 parameter and appropriate critical excitation energies.

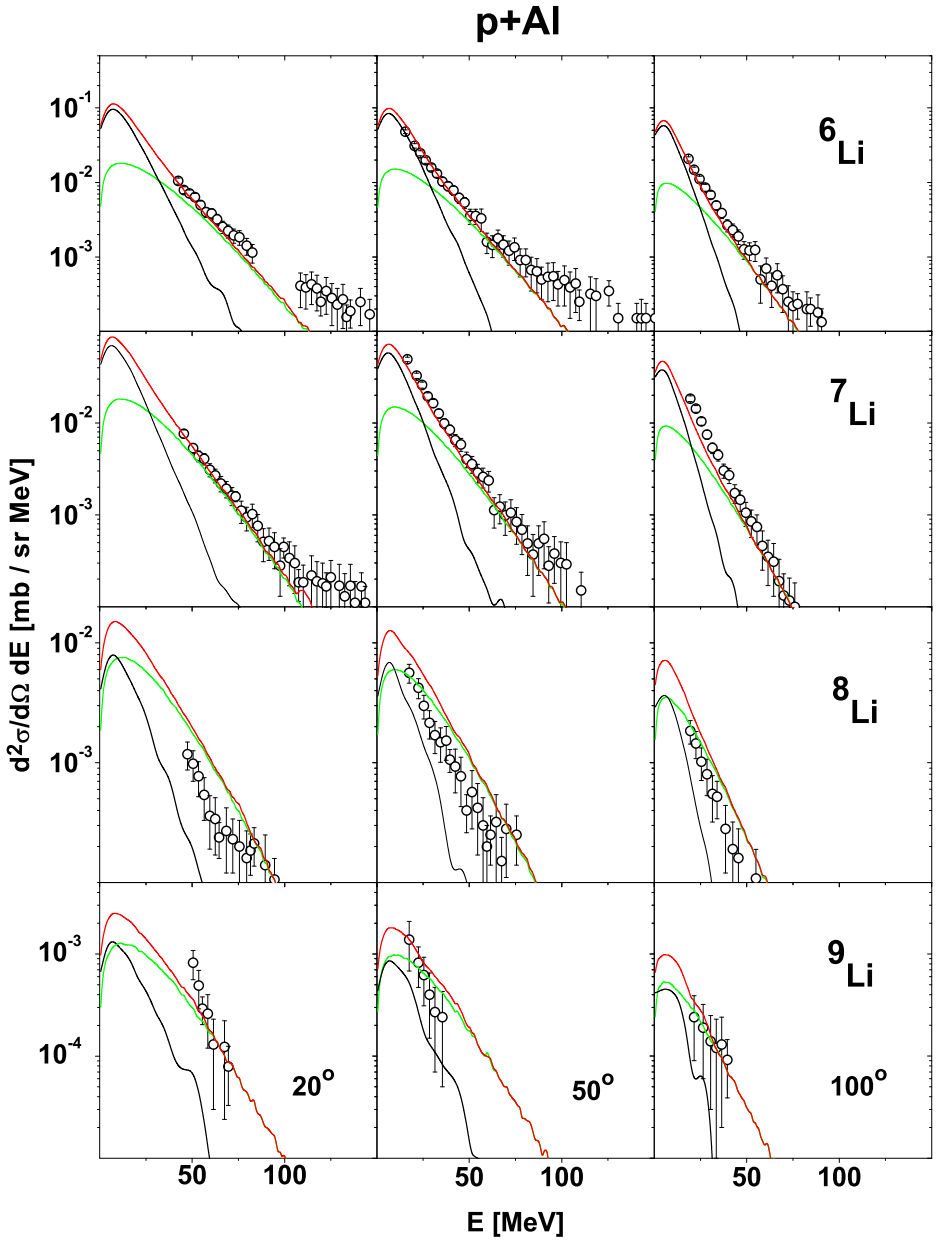

Figure 6.13: Experimental spectra (dots) of ^{6}Li (upper row), ^{7}Li, ^{8}Li (middle rows), and ^{9}Li (lowest row) measured for p+Al collisions at Tp=1.2 GeV. Left, middle, and right columns present data measured at 20°, 50°, and 100°, respectively. The black line represents evaporation from remnant nuclei of intranuclear cascade evaluated with the GEM2 computer program [70,71]. The green line shows contribution of multifragmentation of excited remnant nuclei evaluated in the frame of Fermi break up model by means of the computer code ROZPAD [83]. The red line depicts the sum of both contributions.

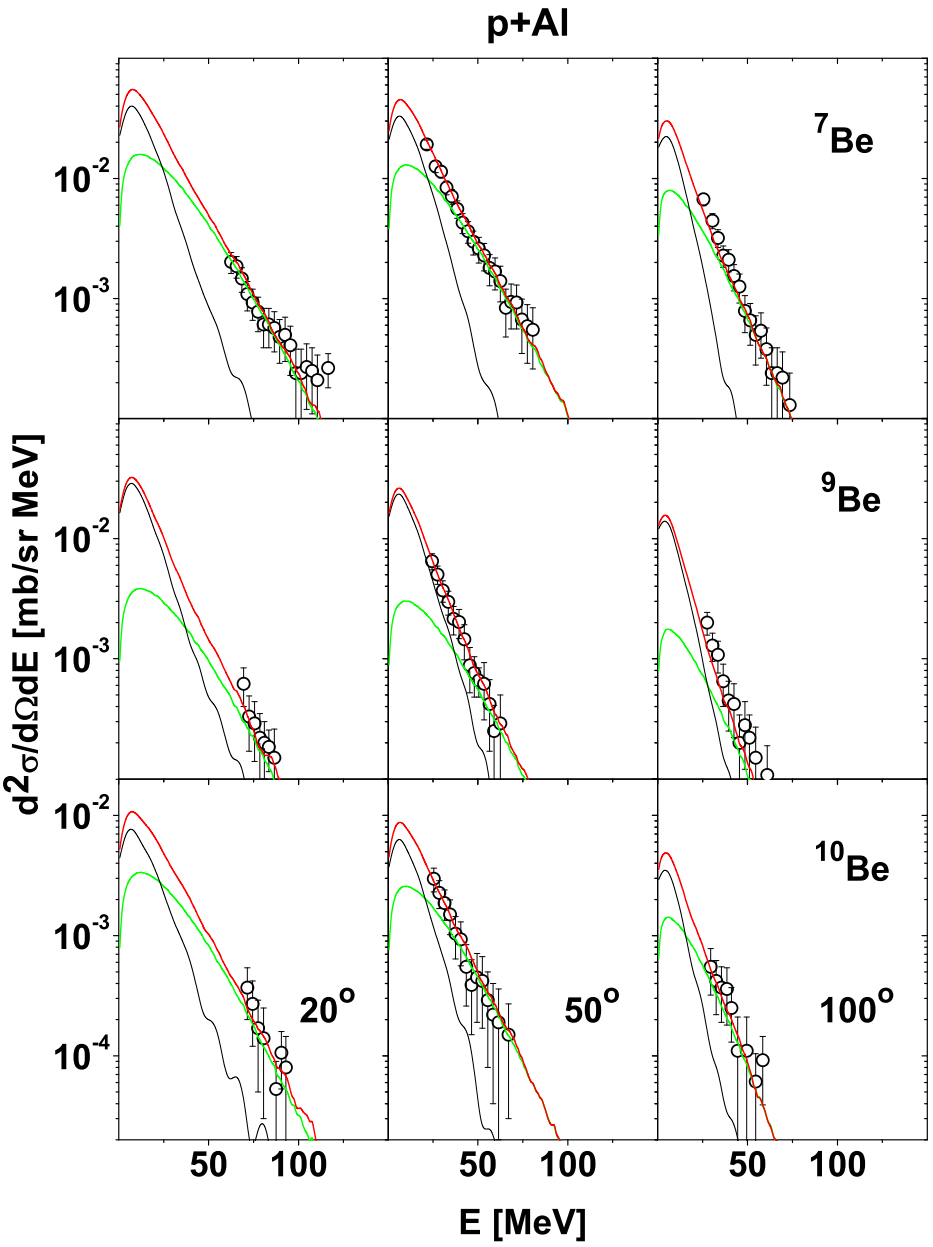

Figure 6.14: The same as on fig. 6.13 but for ^{7}Be (upper row), ^{9}Be (middle row), and ^{10}Be (lowest row).

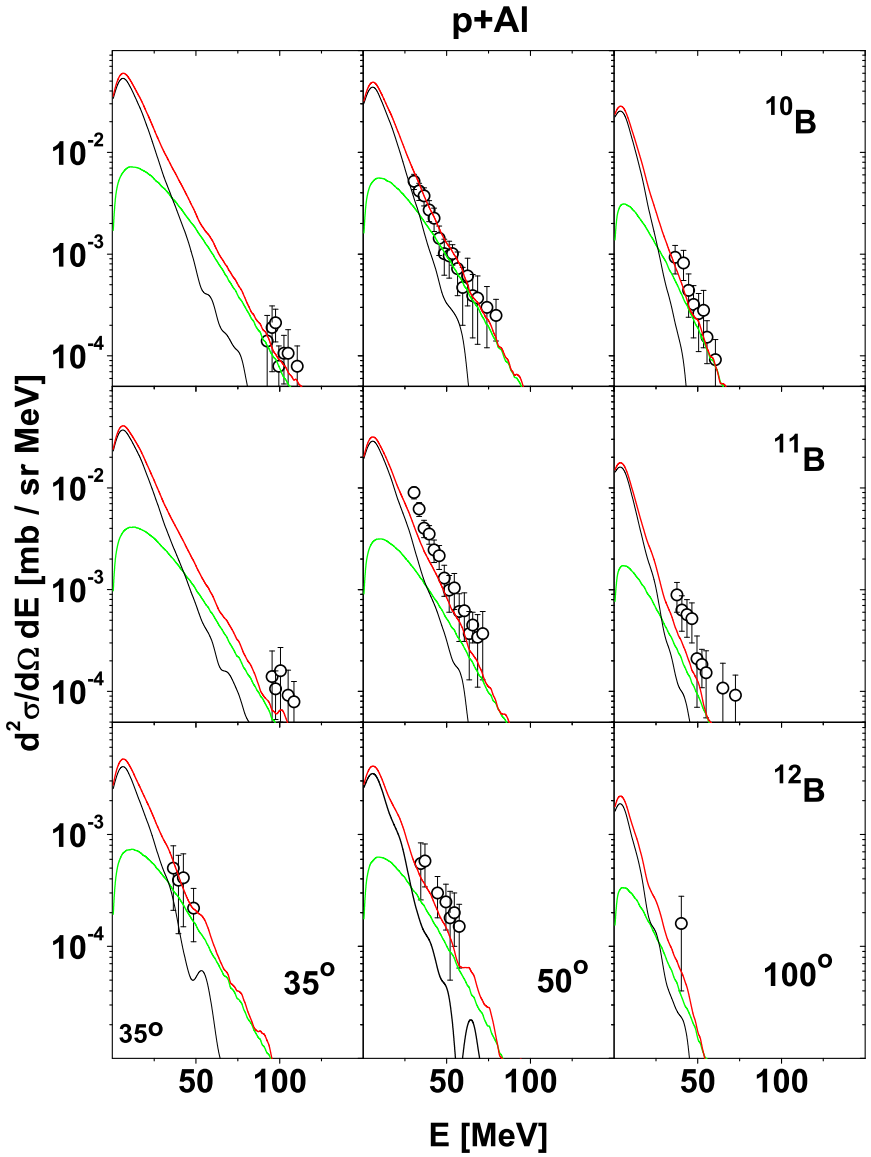

Figure 6.15: The same as on fig. 6.13 but for ^{10}B (upper row), ^{11}B (middle row), and ^{12}B (lowest row). The left panel for ^{12}B represents spectra at 35° whereas for ^{10}B and ^{11}B left panels depict results obtained at 20° .

The experimental IMF spectra measured at higher beam energies have very similar shape as those measured at 1.2 GeV and differ only in the magnitude of the cross sections. Therefore their description is very similar to that presented in figs 6.13, 6.14, and 6.15 thus only representative data and calculations for the beam energy 1.2 GeV are shown. The cross sections for IMF production are collected in the table 6.1.

Table 6.1: Total production cross sections of intermediate mass fragments for p+Al collisions at three proton beam energies: 1.2, 1.9, and 2.5 GeV. In the first column the symbol of the ejectile is listed, in the second column the beam energy is depicted, and in the following columns the production cross section due to sequential evaporation, production cross section due to the multifragmentation, the sum of both cross sections and the relative contribution of the multifragmentation are presented.

particle	energy [GeV]	σ_{GEM} [mb]	σ_{FBM} [mb]	σ_{Tot} [mb]	σ_{FBM}[%]
^{6}He	1.2	0.57	1.03	1.60	64
	1.9	0.45	1.68	2.13	79
	2.5	0.34	2.33	2.67	87
^{6}Li	1.2	9.81	4.28	14.09	30
	1.9	7.35	7.02	14.37	49
	2.5	5.60	9.32	14.92	62
^{7}Li	1.2	3.57	4.04	7.61	53
	1.9	2.72	6.61	9.33	71
	2.5	1.95	9.40	11.35	83
^{8}Li	1.2	0.37	1.55	1.92	81
	1.9	0.28	2.55	2.83	90
	2.5	0.21	3.71	3.92	95
^{9}Li	1.2	0.056	0.24	0.296	81
	1.9	0.046	0.42	0.466	90
	2.5	0.033	0.62	0.653	95
^{7}Be	1.2	2.19	3.56	5.75	62
	1.9	1.66	6.17	7.83	79
	2.5	1.24	7.98	9.22	87
^{9}Be	1.2	1.63	0.78	2.41	32
	1.9	1.30	1.37	2.67	51
	2.5	0.99	2.20	3.19	69
^{10}Be	1.2	0.78	0.64	1.42	45
	1.9	0.63	1.13	1.76	64
	2.5	0.45	1.91	2.36	81
^{10}B	1.2	5.86	1.39	7.25	19
	1.9	4.81	2.65	7.46	36
	2.5	3.73	4.23	7.96	53
^{11}B	1.2	4.36	0.77	5.13	15
	1.9	3.52	1.50	5.02	30
	2.5	2.57	2.71	5.28	51
^{12}B	1.2	0.44	0.15	0.59	25
	1.9	0.38	0.31	0.69	45
	2.5	0.29	0.63	0.92	68

The analysis of light charged particle spectra is discussed separately below because it turned out that the mechanism of reactions leading to production of light charged particles is more complicated than that for IMFs.

It is interesting to investigate the energy dependence of the production mechanism of the intermediate mass fragments. This is caused to the large extent by the energy dependence of the critical value $(E^*/A)_{cr}$ found from the fit to the experimental data of two competing mechanisms; the evaporation of particles at low excitation energies, and the multifragmentation at energies above the critical value. The total production cross sections for these ejectiles are collected in table 6.1. The following conclusions can be derived from inspection of this table:

- Evaporation cross sections decrease quickly with the beam energy for all IMFs on the contrary to increasing of multifragmentation cross sections. These monotonic dependencies lead to fast increase of the *relative* contribution of fragmentation to the total cross section.

- The multifragmentation contribution dominates for all ejectiles at the highest beam energy. It exhausts at least 51% of the total cross section (for ^{11}B) but for selected ejectiles it reaches even 95% (for ^{8}Li and ^{9}Li).

- The sum of both contributions increases with the beam energy but not so quickly as the fragmentation cross sections because of decreasing of the evaporation contribution. The ratio of the total production cross section at beam energy 2.5 GeV to that at 1.2 GeV varies from about 1.1 for ^{6}Li and ^{11}B to about 2.2 for ^{9}Li.

The analysis of the light charged particle data for p+Al collisions was performed by adding evaporation and multifragmentation contributions, evaluated with the same r_0 and $(E^*/A)_{cr}$ parameters as those used for intermediate mass fragments, to the cross section originating from the first step of the reaction, i.e. to the cascade (for protons) and coalescence (for complex LCPs) cross sections. The results of this analysis are presented in figs 6.16 and 6.17 for Hydrogen and Helium isotopes, respectively.

As can be seen in these figures ***there is a clear disagreement of the model differential cross sections and the experimental data for all LCPs***. The experimental data at small scattering angles are much larger than the predictions of the model. The disagreement decreases with the scattering angle and with the mass of the ejectile. The ^{6}He particle data are very well reproduced by evaporation and fragmentation mechanism but cross sections for all lighter particles indicate a lack of some contribution smoothly varying with the scattering angle and with the energy of the ejectile. The search for an explanation of this effect by the contribution of emission of LCPs from a "fireball" is described in the section 6.3.

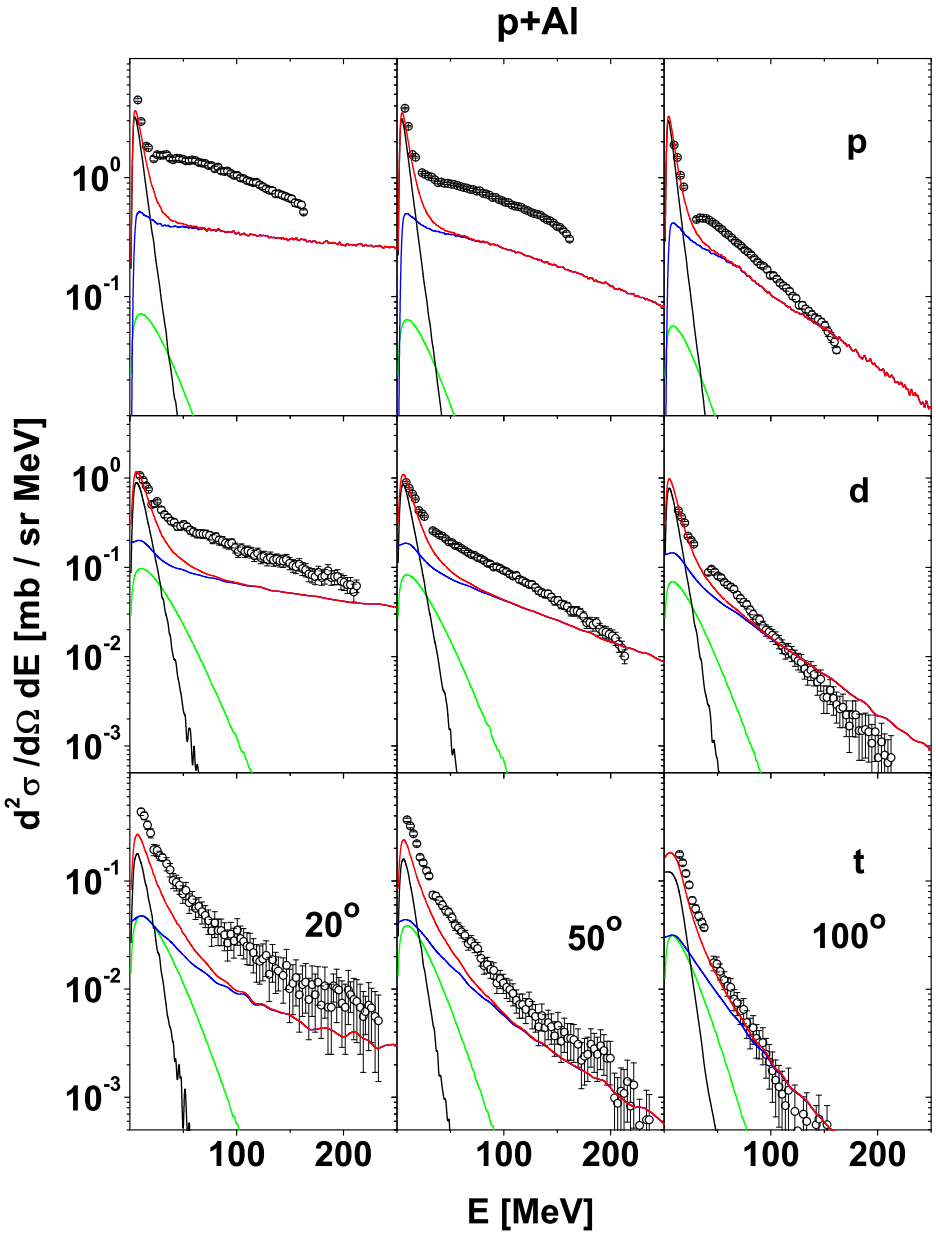

Figure 6.16: Experimental spectra (dots) of protons (upper row), deuterons (middle rows), and tritons (lowest row) measured for p+Al collisions at Tp=1.2 GeV. Left, middle, and right columns present data measured at 20°, 65°, and 100°, respectively. The black line represents evaporation from remnant nuclei of intranuclear cascade evaluated with GEM2 computer program [70,71]. The green line shows contribution of multifragmentation of excited remnant nuclei evaluated with the frame of Fermi break up model by means of computer code ROZPAD [83]. The blue line represents results of calculations with the INCL4.3 computer code [55,56] whereas the red line depicts the sum of all contributions.

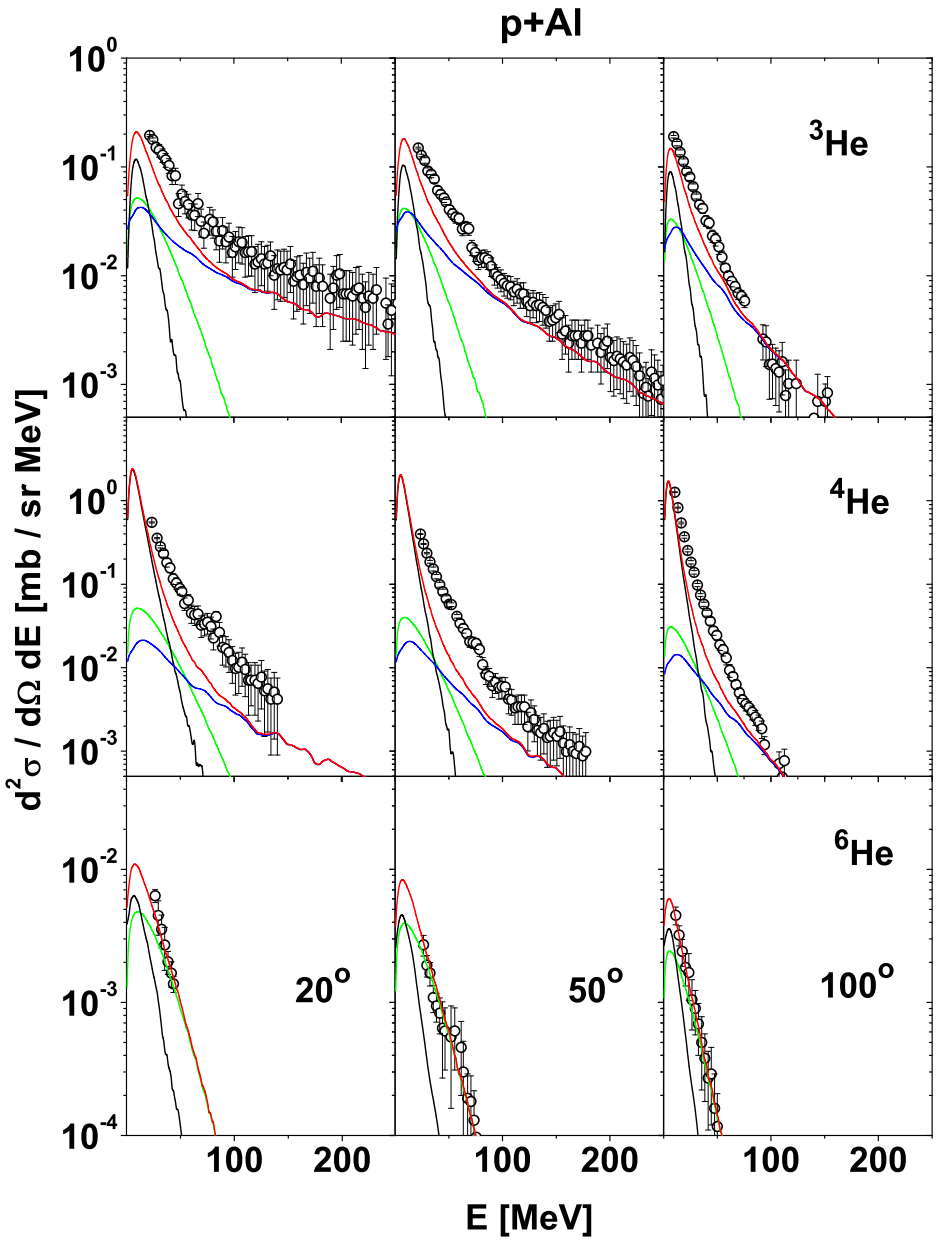

Figure 6.17: Same as fig. 6.16 but for ^{3}He (upper row), ^{4}He (middle row), and ^{6}He (lower row)

6.2.2 Multifragmentation in p+C system

The analysis of the data for intermediate mass fragments which were measured for the p+^{12}C system, i.e. for ^{6}He, ^{6,7,8}Li and ^{7}Be has been done according to the same procedure as the analysis for p+^{27}Al. The dependence of the chi-square on the r_0 and $(E^*/A)_{cr}$ parameters obtained in this analysis is shown in figs 6.18, 6.19, and 6.20 for proton beam energy 1.2, 1.9, and 2.5 GeV, respectively.

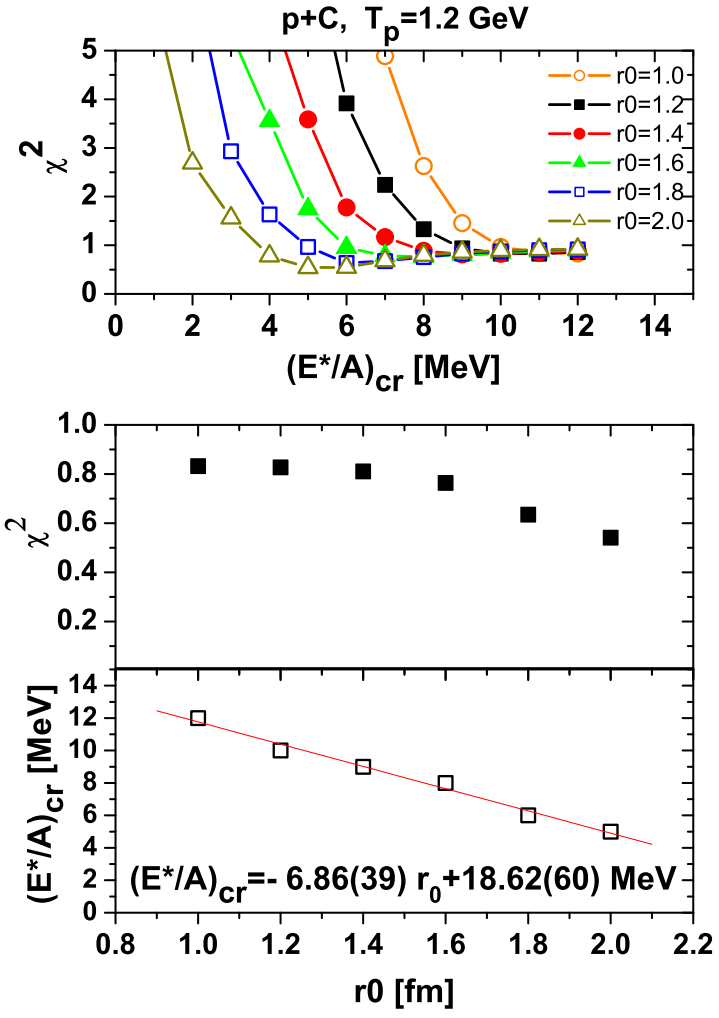

Figure 6.18: Upper panel: Chi-square evaluated for all detected IMFs, i.e., ^{6}He, ^{6,7}Li and ^{7}Be as a function of $(E^*/A)_{cr}$ parameter for several fixed values of r_0 for p+C collisions at T$_p$=1.2 GeV. Middle panel: minimal chi-square of the functions χ^2 $((E^*/A)_{cr})$ presented above for each fixed r_0 parameter versus r_0. Lower panel: $(E^*/A)_{cr}$ parameter for the best chi-square value for each r_0 parameter versus corresponding r_0 value.

As can be seen, there is no minimum of the chi-square in the studied range of the r_0 parameter. Chi-square values per degree of freedom are smaller than unity for all values of r_0, thus the description is good in each case. It means, however, that the fit is not sensitive to r_0 parameter value what indicates small contribution of the studied effect - multifragmentation - to the reaction cross section. Furthermore, a strong increase of the chi-square visible for small values of the critical excitation energy $(E^*/A)_{cr}$ for each value of r_0 parameter suggests that at small excitation energies another emission mechanism, presumably sequential evaporation, dominates. This again points to a big contribution of the evaporation because most of the nuclei - remnants of the fast stage of the reaction - are excited to small energies.

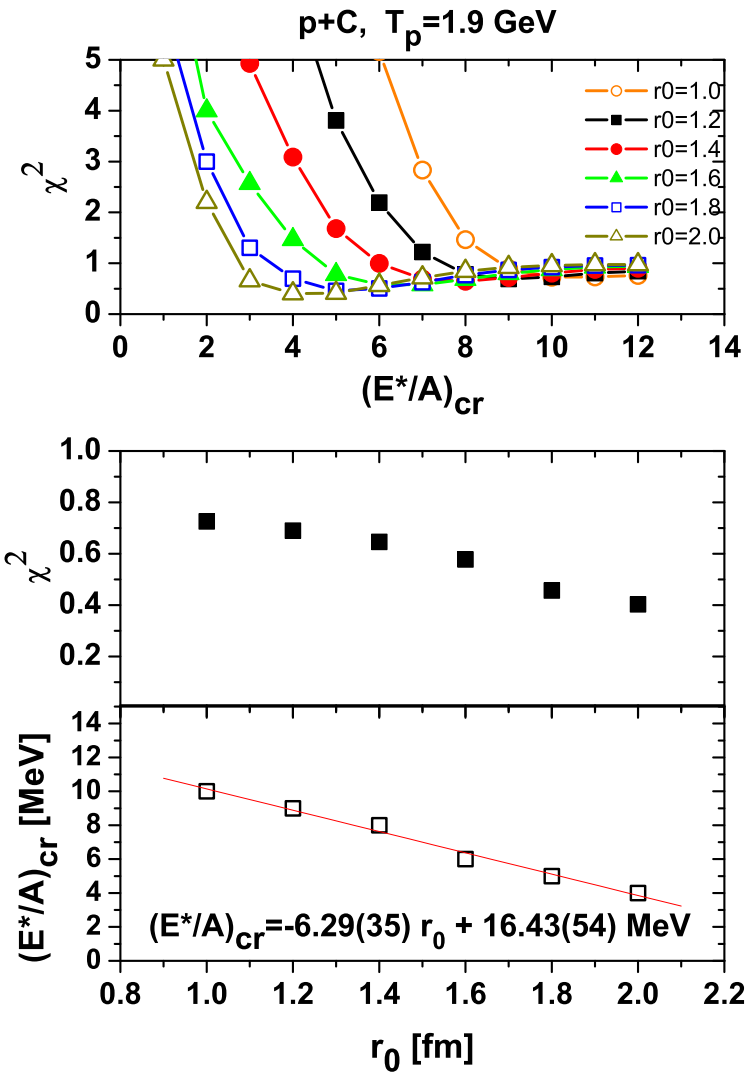

Figure 6.19: The same as in fig. 6.18, but for p+C collisions at T_p=1.9 GeV.

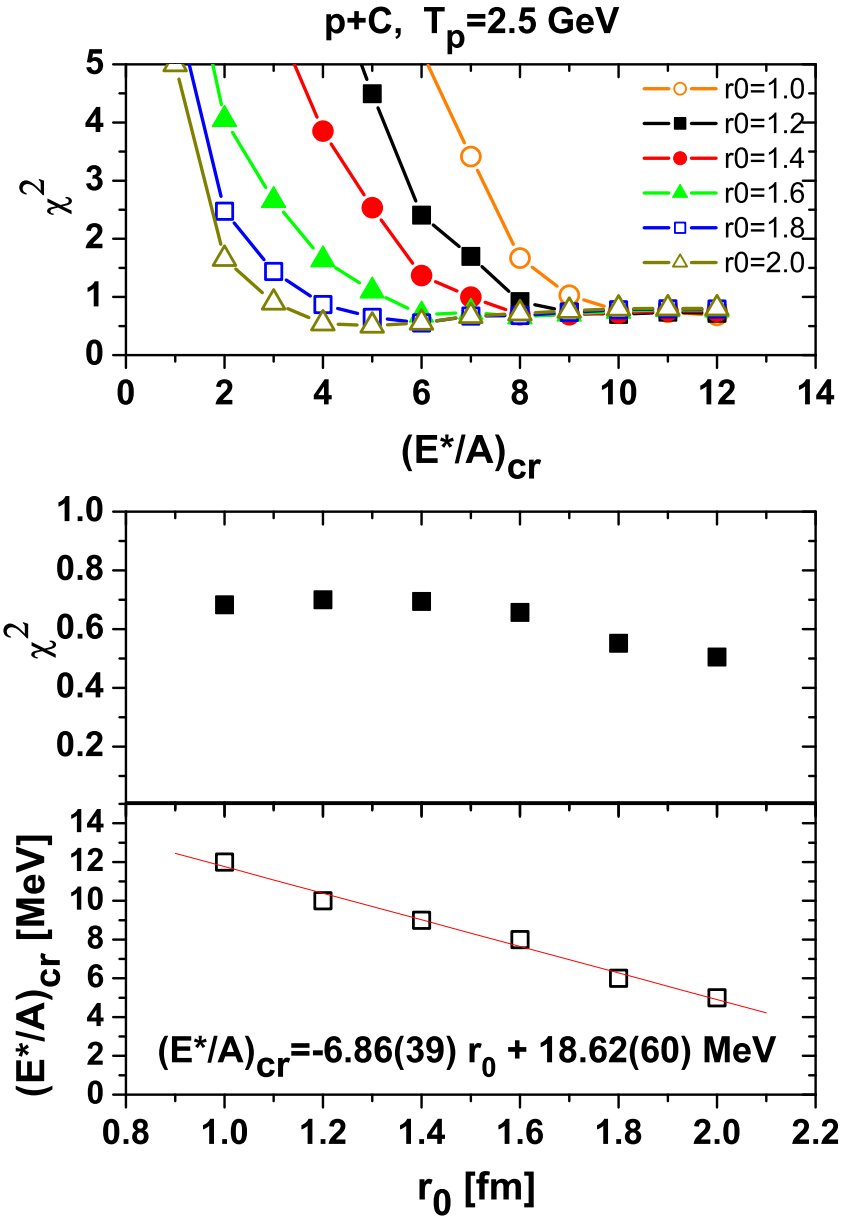

Figure 6.20: The same as in fig. 6.18, but for p+C collisions at T_p=2.5 GeV.

In such a situation, the chi-square method is not able to select physical values of r_0 and $(E^*/A)_{cr}$ parameters, especially in view of a strong ambiguity of both parameters. Thus, the following reasoning was applied for the selection of values of the parameters:

It was assumed that for the p+C system the same reduced radius r_0 is appropriate as that used for p+Al system, i.e. r_0=1.4 fm. This value of r_0 is usually applied in the description

of multifragmentation of light nuclei by the Fermi break-up model (cf. recommended value of this parameter in the GEANT-4 computer toolkit; [86]). Then, it was possible to choose an appropriate value of the critical excitation energy from the observed dependence of this parameter on the r_0.

The following values of the critical excitation energy have been found: 9.0(8), 7.6(7), and 8.6(8) MeV/nucleon for beam energy 1.2, 1.9, and 2.5 GeV, respectively. These values fit very well to the compilation of the atomic mass dependence of the critical excitation energy for multifragmentation as published by Natovitz et al. [49]. Values of the critical excitation energy obtained in the present analysis are shown in fig. 6.21 together with those from ref. [49].

While using the standard value of the r_0 parameter such good agreement of the obtained values of the critical excitation energy can be treated as an argument in favour of an internal consistency of the present analysis.

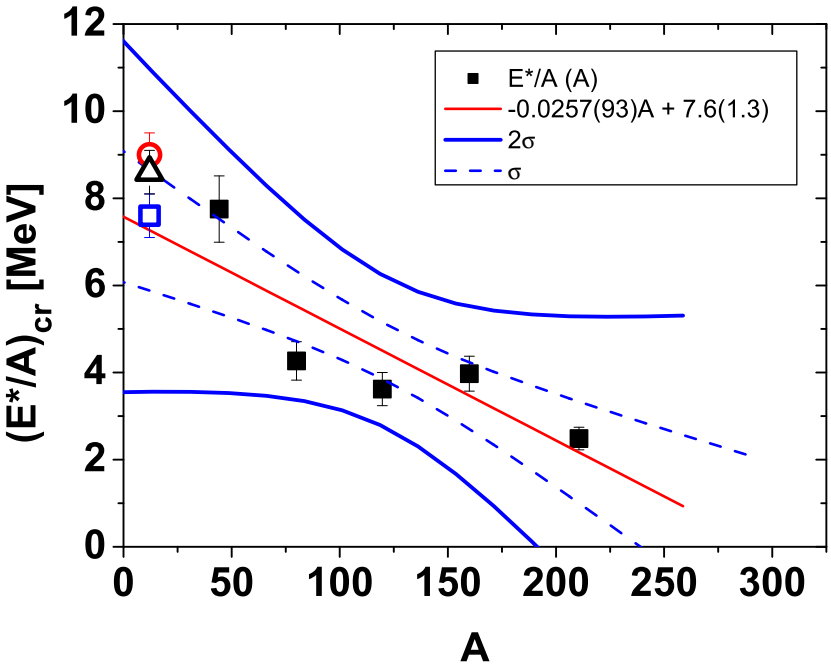

Figure 6.21: Atomic mass dependence of the critical excitation energy $(E^*/A)_{cr}$ for multifragmentation of atomic nuclei. The full symbols represent results of the compilation of Natovitz et al. [49]. The straight line shows the linear regression of these data whereas the dashed- and solid-lines present one- and two-standard deviation confidence intervals of the regression line, respectively. The open symbols - circle, square, and triangle depict results of the present analysis of p+^{12}C at three proton beam energies; 1.2, 1.9, and 2.5 GeV, respectively.

The quality of the description of the IMF data from p+C collisions may be judged from

the inspection of figure 6.22 where the experimental cross sections for ^{6}Li, ^{7}Li, ^{8}Li, and ^{7}Be are presented together with results of the two-step model in which evaporation and multifragmentation were taken into consideration for the second stage of the reaction. The fluctuations of the lines have no physical meaning and result from small statistics of Monte Carlo method of model calculations.

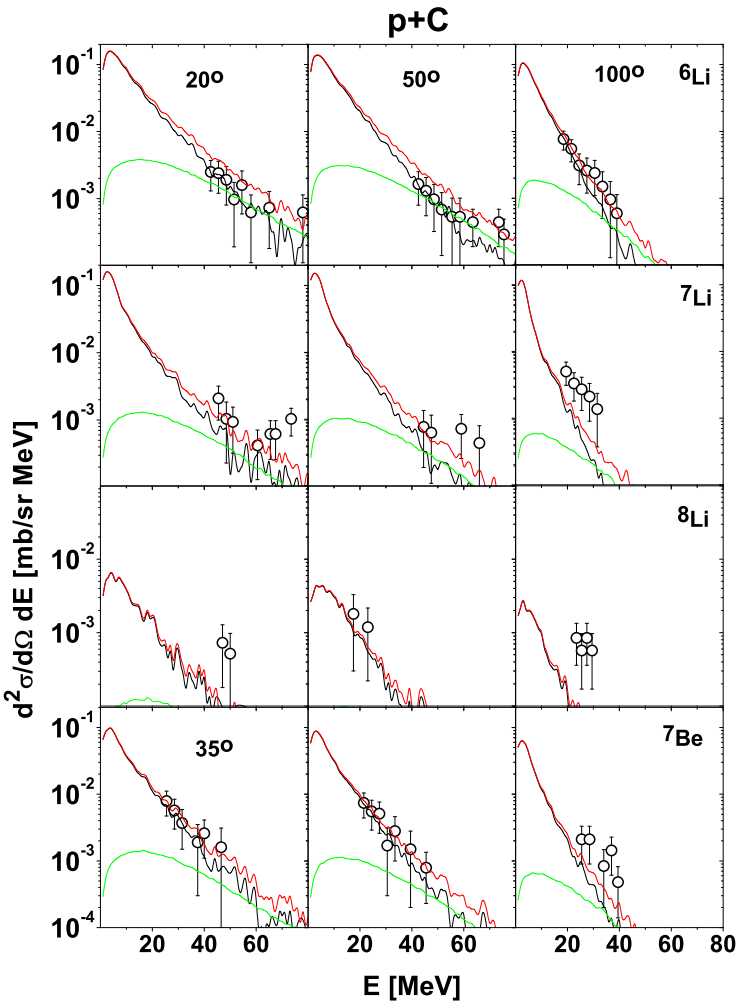

Figure 6.22: The experimental spectra (open circles) for production of ^{6}Li (upper row), of ^{7}Li, ^{8}Li (middle rows), and of ^{7}Be (lowest row) in p+ ^{12}C collisions for three scattering angles: 20° (left column), 50° (middle column), and 100° (right column). The lowest scattering angle for ^{7}Be is equal to 35° instead of 20° because of better statistics in the spectrum measured at 35° . The black line represents the evaporation cross section, the green line depicts the contribution from multifragmentation and the red line shows the sum of both cross sections.

As it was already stated in section 6.1 the IMF data are quite well reproduced by the

traditional two-step model, which takes into consideration the nucleon-nucleon cascade as the first stage of the reaction and the evaporation of ejectiles as the second stage. The inclusion of multifragmentation improves slightly the description of the data, as can be seen in fig. 6.22 but the evaporation is a dominant process in the second stage of the reaction.

This qualitative conclusion may be formulated in more quantitative manner by the analysis of total production cross sections, which are listed in table 6.2 for all studied intermediate mass fragments for three proton beam energies. As can be seen the contribution of multifragmentation is typically of the order of several percent with the exception of ^{6}He for which multifragmentation exhausts approximately 20 % of the total production cross section.

The present conclusion concerning the dominance of evaporation of IMF in p+^{12}C collisions is in accordance with results of Furihata [70], which showed that nucleon-nucleon cascade coupled with generalized evaporation model is able to reproduce the total cross sections for ^{7}Be production in p+^{16}O collisions for a broad range of beam energies.

Table 6.2: Total production cross sections of intermediate mass fragments for p+C collisions at three proton beam energies: 1.2, 1.9, and 2.5 GeV. In the first column the symbol of the ejectile is listed, in the second column the beam energy is depicted, and in the following columns the production cross section due to sequential evaporation, production cross section due to multifragmentation, the sum of both cross sections and the relative contribution of the multifragmentation are presented.

particle	energy [GeV]	σ_{GEM} [mb]	σ_{FBM} [mb]	σ_{Tot} [mb]	σ_{FBM}[%]
^{6}He	1.2	0.78	0.16	0.94	17
	1.9	0.74	0.27	1.01	27
	2.5	0.75	0.15	0.9	17
^{6}Li	1.2	13.50	0.89	14.39	6
	1.9	12.62	1.47	14.09	10
	2.5	12.68	0.66	13.34	5
^{7}Li	1.2	9.25	0.28	9.53	3
	1.9	8.78	0.53	9.31	6
	2.5	8.63	0.25	8.88	3
^{8}Li	1.2	0.42	0.025	0.445	6
	1.9	0.41	0.055	0.465	12
	2.5	0.40	0.021	0.421	5
^{7}Be	1.2	6.95	0.30	7.25	4
	1.9	6.80	0.57	7.37	8
	2.5	6.81	0.25	7.06	4

Multifragmentation contribution to the LCP data from p+C collisions is almost

negligible for Hydrogen isotopes as it is seen in fig. 6.23 but becomes quite significant for Helium isotopes - cf. fig. 6.24. In both cases, i.e., for Hydrogen and Helium data, the high energy tail of the spectra is not described well by the assumed model, with the exception of ^{6}He cross section, what is almost not significant, because of poor data here.

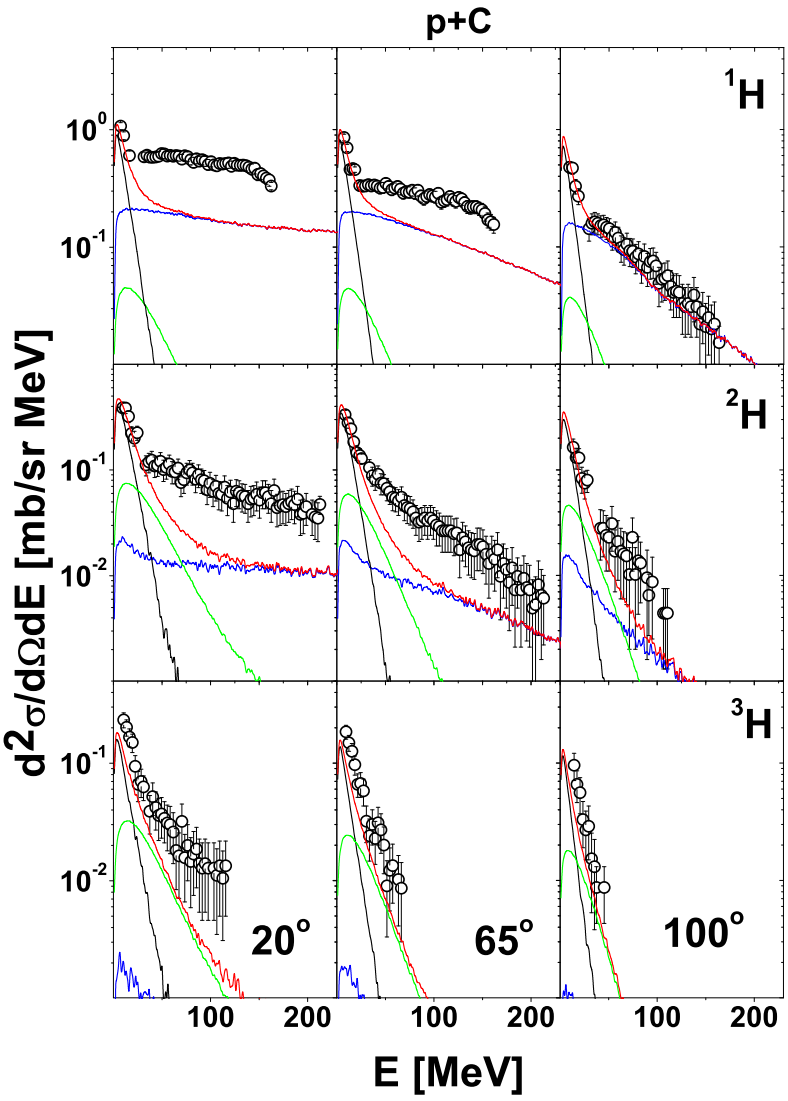

Figure 6.23: The experimental spectra (open circles) for production of ^{1}H (upper row), of ^{2}H, (middle row), and of ^{3}H (lowest row) in p+ ^{12}C collisions for three scattering angles: 20° (left column), 65° (middle column), and 100° (right column). The black line represents evaporation cross section, the blue line is attributed to INCL results (nucleon-nucleon cascade for protons and coalescence for deuterons and tritons), the green line depicts the contribution from multifragmentation and the red line shows the sum of all cross sections.

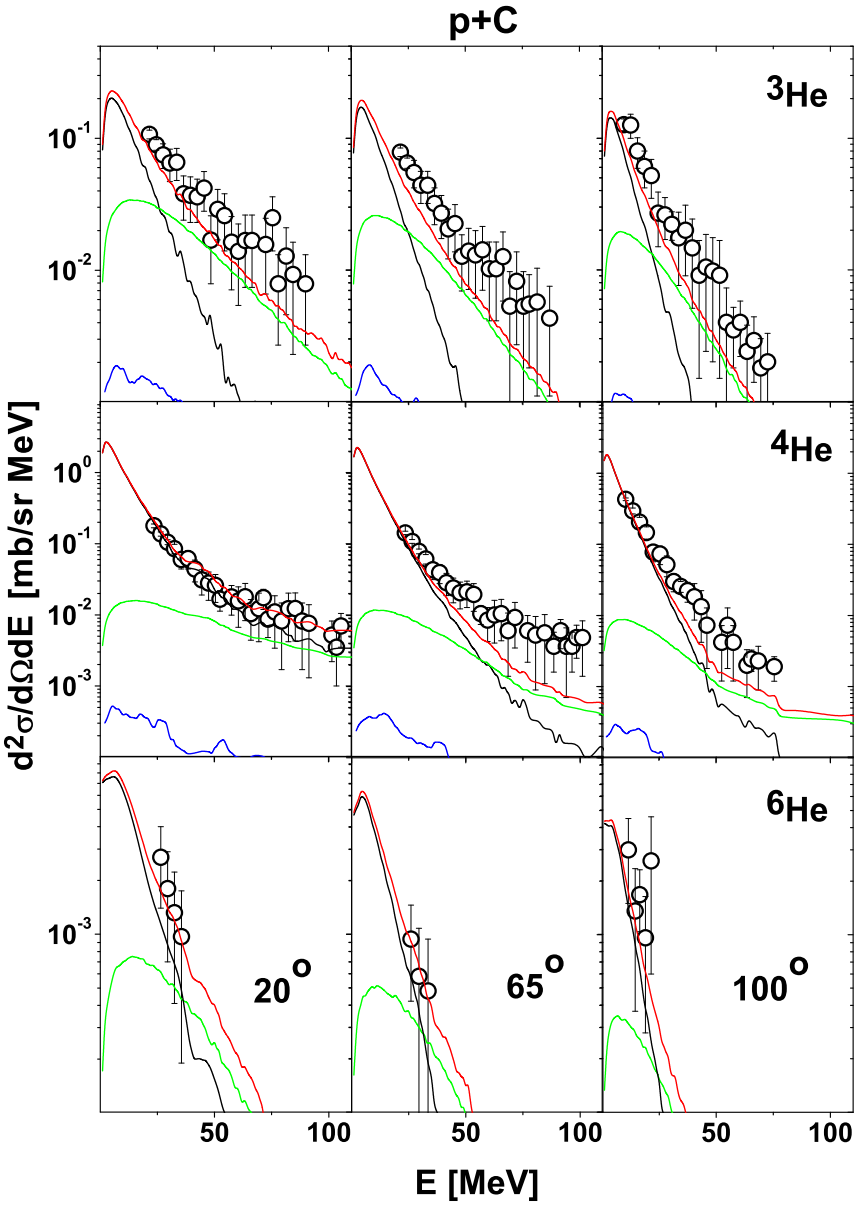

Figure 6.24: The same as in fig. 6.23 but for isotopes of Helium: ^{3}He,^{4}He, and ^{6}He.

It seems, that similarly like for ^{27}Al target, another reaction mechanism plays an important role in the p+^{12}C collisions under consideration. The candidate for this mechanism is the emission of light charged particles from a "fireball" - fast and hot source, consisted of several nucleons, moving in the forward direction. This mechanism will be discussed in the next section.

6.3 Fireball emission

The analysis of differential cross sections for reactions in p+Al as well as in p+C systems reveals that the energy and angular dependencies are not reproduced by the two step model of the reaction for light charged particle emission. Such unsatisfactory situation appears even if the coalescence of nucleons into composite particles - in the first stage of the reaction, as well as competition of evaporation and multifragmentation - in the second stage of the reaction are taken into account. Differences between the data and predictions of the two-step model are largest for protons and decrease with increasing mass of the ejectile. Moreover, the disagreement is stronger for small angles and almost vanishes at the angle 100° . These qualitative relationships between data and theoretical cross sections indicate, that another reaction mechanism, which favours forward directed emission of the lightest ejectiles has to be taken into consideration. Such a process has been introduced in a phenomenological way as an emission of LCPs from a fast and hot source - the "fireball", moving along the beam direction.

Differential cross sections of this emission have been calculated using formulae given in the Appendix B. These formulae contain free parameters which values were searched to assure a good fit to the data. The quality of the data description is good as can be judged from chi-square values listed in Tables 6.3 (for p+Al) and 6.4 (for p+C), as well as from the inspection of Figs 6.25, 6.26 (for p+Al) and Figs 6.27, 6.28 (for p+C).

The following properties of the fireball emission of light charged particles are common for both studied nuclear systems - p+Al and p+C:

- The effect is largest for protons and decreases with the mass of ejectile becoming the smallest for the emission of α-particles. This is well visible in Figs 6.25, 6.26, 6.27, and 6.28 as well as in Tables 7.1 and 7.2.

- The fireball contribution is largest for small angles and decreases with the scattering angle. This can also be seen in Figs 6.25, 6.26, 6.27, 6.28.

- The inspection of the above figures leads to the conclusion that the fireball emission affects the spectra of Hydrogen isotopes mainly at energies smaller than 150 - 200 MeV whereas for the Helium ejectiles this energy range is limited to energies smaller than approximately 100 MeV.

- The velocity β and the apparent temperature T of the fireball decrease with the mass of emitted particles. The only exception is the α-particle emission in the p+C system, for which larger β and T of the fireball are needed than the same quantities for lighter Helium isotope - ^{3}He (cf. Tables 6.3 and 6.4).

6.3.1 Fireball in p+Al system

The search for parameters k, β, T and σ characterizing the fireball has been performed by fitting simultaneously experimental spectra of light charged particles measured at all seven scattering angles for a given ejectile and a given proton beam energy. The theoretical cross section has been calculated as a sum of contributions originating from both, the first and the second stage of the reaction.

The former cross sections were evaluated on the basis of two competing mechanisms: the intranuclear cascade and the fireball emission. The contribution of the intranuclear cascade has been evaluated by INCL4.3 computer program [55, 56], which enables coalescence of nucleons in composite particles.

Since the intranuclear cascade model cross sections are absolutely normalized by assuming that each projectile - target collision leads to the intranuclear cascade, there is no room for some other process initiated by the proton impinging on to the target. Thus, to allow for collision of the proton from the beam with a group of nucleons inside the target some scaling down of the intranuclear cascade cross sections must be introduced. It was realized phenomenologically, i.e. multiplying the INCL cross sections by a factor f which was treated as a free parameter. Its value was determined in the analysis of the deuteron data but for other ejectiles the scaling factor was fixed at the same values as those found for deuterons.

The cross sections corresponding to the second stage of the reaction include the sequential evaporation of particles from remnants of the first step of the reaction – excited to low energies (lower than the critical energy per nucleon discussed in the section 6.2), and the multifragmentation of the highly excited remnants.

The parameters of the fireball obtained from the fit are listed in Table 6.3 together with the cross sections characterizing other reaction mechanisms contributing to p+Al collisions.

Values of *the scaling factor* vary between 0.55 and 0.84 for the studied beam energies suggesting that the first step of the reaction proceeds mainly via an intranuclear cascade mechanism. The inclusive cross sections of the proton and the α-particle emission from the fireball are, however, larger than the respective cross sections from the intranuclear cascade (protons) and from the coalescence of nucleons escaping from the intranuclear cascade (α-particles). Such an effect does not contradict the conclusion derived from the value of the scaling factor of prevailing role of the intranuclear cascade mechanism because the inclusive cross sections are dependent also on multiplicities of the emitted particles.

The k *parameter*, which determines the height of the effective barrier between the ejectile and the fireball (in units of the height of the barrier between ejectiles and target nuclei) is small for all ejectiles, what is natural because the fireball is much smaller than the target nucleus.

The *apparent temperature* T as well as the *velocity* β of the fireball, decrease with the mass of the ejectiles. Decreasing of these two parameters may be interpreted as indication of two effects:

(i) increasing of the average mass of the fireball with the mass of the ejectile, what for a given average momentum transfer to the fireball leads to decreasing its velocity with its mass, and

(ii) strong modification of the apparent temperature by recoil of the emitting source.

ad (i) The increasing of a mass of the fireball is obvious in view of the fact, that the mass of the fireball must be larger than mass of observed ejectile. For example, the lightest particles - protons can be emitted by a fireball consisted of two nucleons (p+p or p+n) whereas this light fireball cannot emit deuterons and heavier particles. On the other hand, fireballs consisted of three or more nucleons are able to emit protons as well as heavier particles.

ad (ii) Since the mass of the ejectile A is comparable to the mass of the fireball A_S, the observed (apparent) temperature T of the fireball is modified by the recoil being related to the true temperature τ by relation: $T = \tau \cdot (1 - A/A_S)$. This means that the apparent temperature T is always smaller than the true temperature τ and this difference increases for heavier fireballs (thus for heavier ejectiles), because then A/A_S is closer to unity.

It should be emphasized that the temperature parameter is so large that the fireball cannot exist outside the target nucleus and must emit particles.

The *cross section* for emission from the fireball increases with the beam energy for all ejectiles (cf. Table 6.3). Furthermore, the relative contribution of the fireball emission increases with the beam energy.

The model spectra are compared with the experimental data in figures 6.25 and 6.26 for p, d, t, and ^{3}He, ^{4}He, and ^{6}He, respectively. As can be seen the description of the experimental data was significantly improved for all light charged particles.

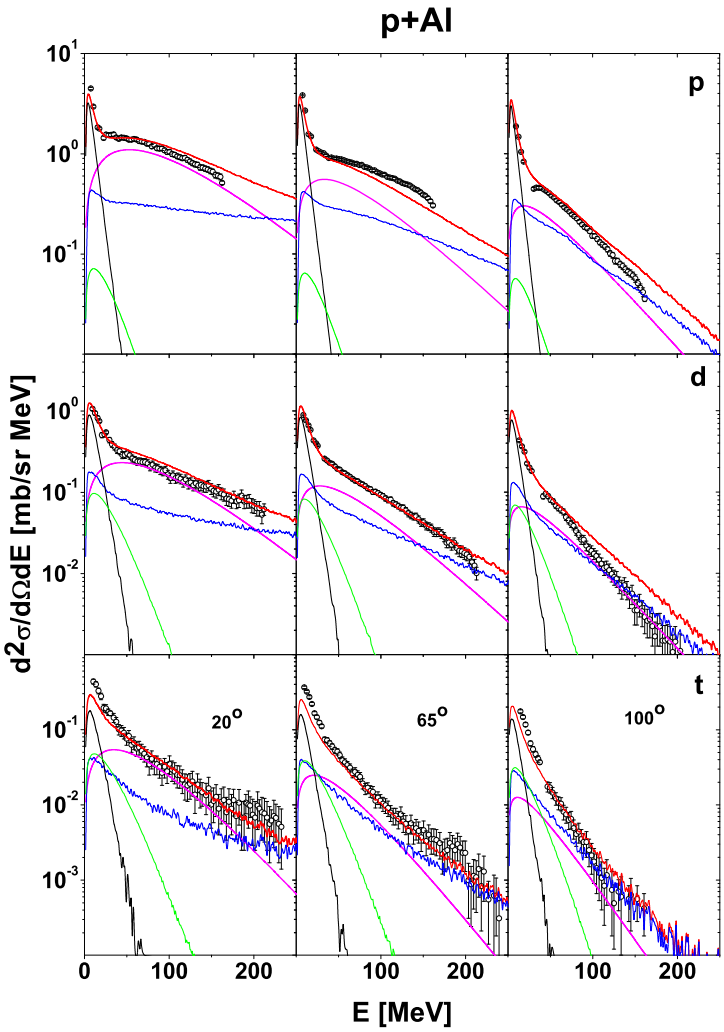

Figure 6.25: Experimental spectra (dots) of protons (upper row), deuterons (middle row), and tritons (lowest row) measured for p+Al collisions at proton beam energy T_p=1.2 GeV. Left, middle, and right columns present data measured at 20° , 65° , and 100° , respectively. The black line represents evaporation from remnant nuclei of intranuclear cascade calculated with the GEM2 computer program [70, 71]. The green line shows the contribution of the multifragmentation of excited remnant nuclei evaluated in the frame of the Fermi break up model by means of the computer code ROZPAD [83]. The blue line represents results of calculations with INCL4.3 computer code [55, 56], the magenta line shows the contribution from the fireball emission whereas the red line depicts the sum of all contributions.

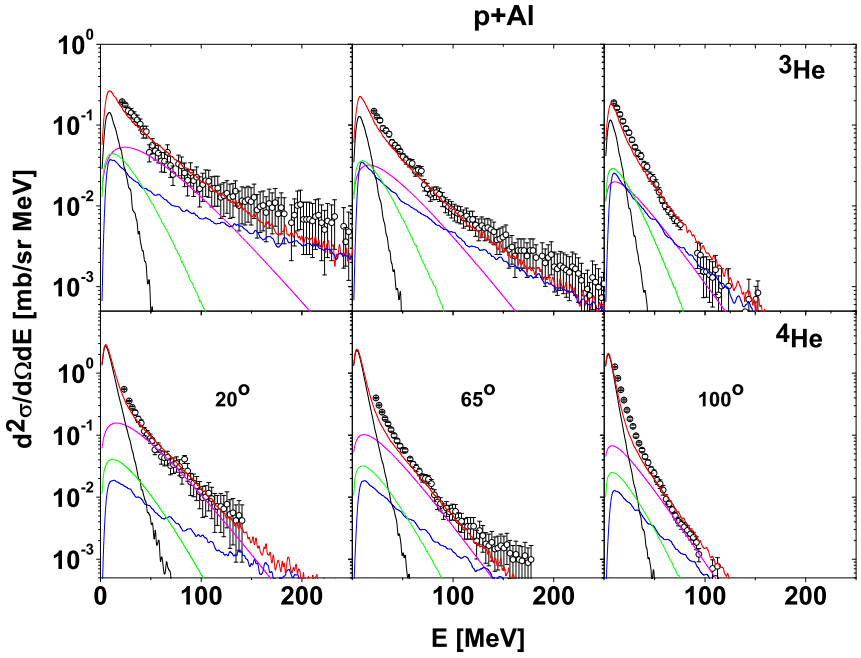

Figure 6.26: Same as on fig. 6.25 but for ^{3}He (upper row) and ^{4}He (lower row).

Table 6.3: The parameters of a fireball contributing to LCP emission in p+Al system (column 3 - 6), scaling factor f (for explanation see text), χ^2, and values of the cross sections from all considered reaction mechanisms. The parameters closed in square parentheses were fixed.

particle	energy [MeV]	k	β	T [MeV]	σ [mb]	f	χ^2	f*σ_{INCL} [mb]	σ_{GEM} [mb]	σ_{FBM} [mb]	$\sigma_{Tot.}$ [mb]
^1H	1.2	0.06	0.2089	44.20	642.8	[0.84]	59.11	449.09	351.39	24.61	1467.89
	1.9	0.14	0.2043	45.60	817.9	[0.75]	22.34	356.69	310.69	39.43	1524.71
	2.5	0.09	0.1968	48.32	1058.9	[0.55]	21.23	265.81	278.24	46.99	1649.94
^2H	1.2	0.24	0.1346	34.44	94.13	0.84	8.26	105.1	115.76	29.67	344.66
	1.9	0.02	0.1373	38.20	124.3	0.75	2.40	87.54	94.83	46.19	352.86
	2.5	0.03	0.1319	40.96	165.7	0.55	6.21	60.92	80.08	55.99	362.69
^3H	1.2	0.01	0.0893	26.56	18.12	[0.84]	12.55	17.71	22.92	13.25	72.00
	1.9	0.08	0.0894	30.68	22.81	[0.75]	11.95	15.07	18.49	20.72	77.09
	2.5	0.06	0.0930	35.19	29.98	[0.55]	13.20	10.59	15.19	26.23	81.99
^3He	1.2	0.01	0.0703	23.80	18.65	[0.84]	3.18	15.45	20.09	12.65	66.84
	1.9	[0.01]	0.0708	26.69	23.37	[0.75]	4.38	13.01	16.29	20.03	72.70
	2.5	0.07	0.0643	27.83	31.73	[0.55]	6.17	9.11	13.83	23.37	78.04
^4He	1.2	[0.01]	0.0451	17.29	42.31	[0.84]	71.72	6.69	256.56	10.88	316.44
	1.9	0.01	0.0305	15.37	76.61	[0.75]	45.90	5.60	224.34	18.03	324.60
	2.5	0.01	0.0358	17.30	65.37	[0.55]	73.78	3.98	195.71	24.31	289.37

6.3.2 Fireball in p+C system

The analysis of the data for the emission of light charged particles from p+C collisions has been performed along the same lines as that for the p+Al system. The only difference was searching for the scaling factor f not by fitting the spectra of deuterons but from the fit of the model cross sections to the proton data. Values of the scaling factors obtained in this way, separately for each beam energy, have been then applied for all other ejectiles without the attempt to fit them again.

Results of the fit are shown in Fig. 6.27 for Hydrogen isotopes and in Fig. 6.28 for ^{3}He and ^{4}He. The theoretical description of the data is very good what can be seen in the above Figures and can be stated from inspection of Table 6.4, where the parameters of the fireball are collected for all studied light charged particles. The chi-square values listed in this Table are close to unity what emphasizes the good quality of reproduction of the data by applied reaction models.

In the case of the Carbon target the cross sections of the fireball emission have less regular energy behaviour than that which was observed for Aluminium target, where they increased systematically with the energy for all ejectiles. For the p+C interaction the cross sections for LCP emission from the fireball do not increase with the energy but rather remain constant, however, with rather large energy fluctuations. A similar effect may be observed for the total production cross sections which are basically energy independent. Their energy fluctuations are significantly smaller than those visible for the cross section of LCP emission from the fireball. It means that there is some kind of compensation of the magnitude of the cross sections originating from different reaction models which leads to almost constant - energy independent total production cross sections. This constancy of the production cross sections for LCP production in p+C collisions agrees with the observation made in the literature (cf. section 2), that the limiting fragmentation region is observed at smaller beam energies for p+C than for p+Al collisions.

The interesting difference between p+C and p+Al collisions can be seen in behaviour of the fireball velocity, which for Carbon target seems to be larger than for Aluminium target, and decreases with the beam energy for proton and deuteron emission whereas for Aluminium target it is almost energy independent (cf. Table 6.3 and Table 6.4).

Furthermore, the α-particle emission seems to be qualitatively different for Carbon target than for Aluminium target. In the former case the velocity of the fireball and its apparent temperature is larger than these parameters for ^{3}He whereas for the Aluminium target the opposite situation is present.

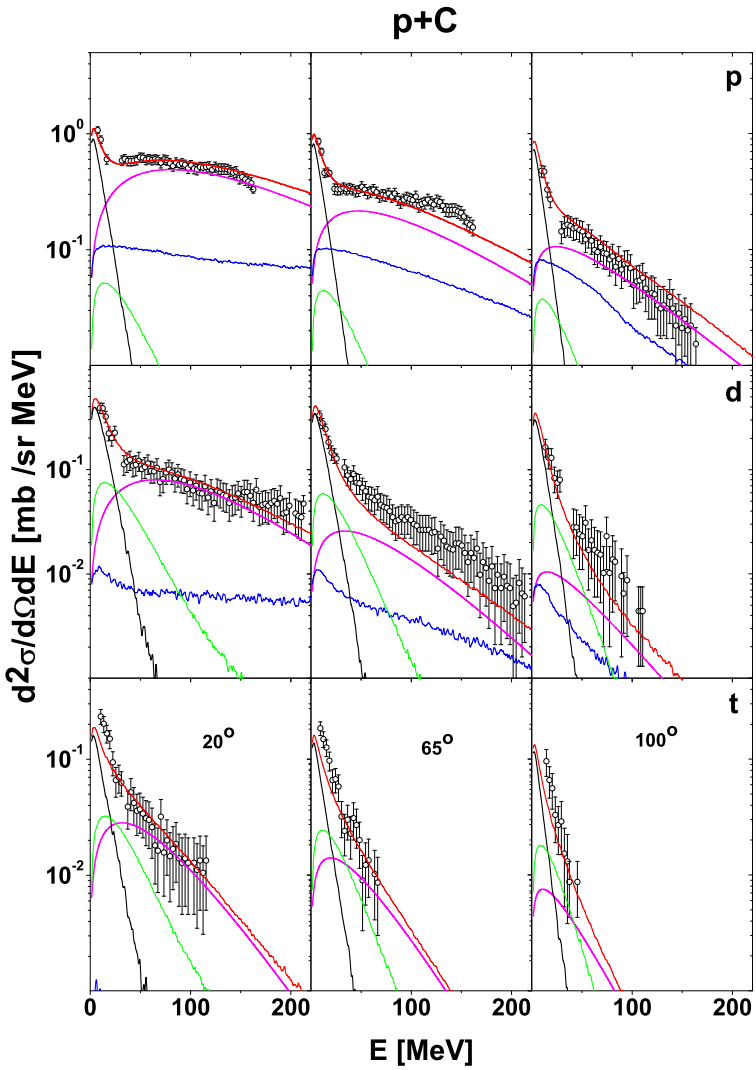

Figure 6.27: The experimental spectra (open circles) for production of ^{1}H (upper row), of ^{2}H, (middle row), and of ^{3}H (lowest row) in p+ ^{12}C collisions for three scattering angles: 20° (left column), 65° (middle column), and 100° (right column) at proton beam energy T_p=1.2 GeV. The black line represents the evaporation cross section, the blue line is attributed to INCL results (the nucleon-nucleon cascade for protons and the coalescence for deuterons and tritons), the green line depicts the contribution from multifragmentation, the magenta line shows the contribution from the fireball emission, and the red line presents the sum of all cross sections.

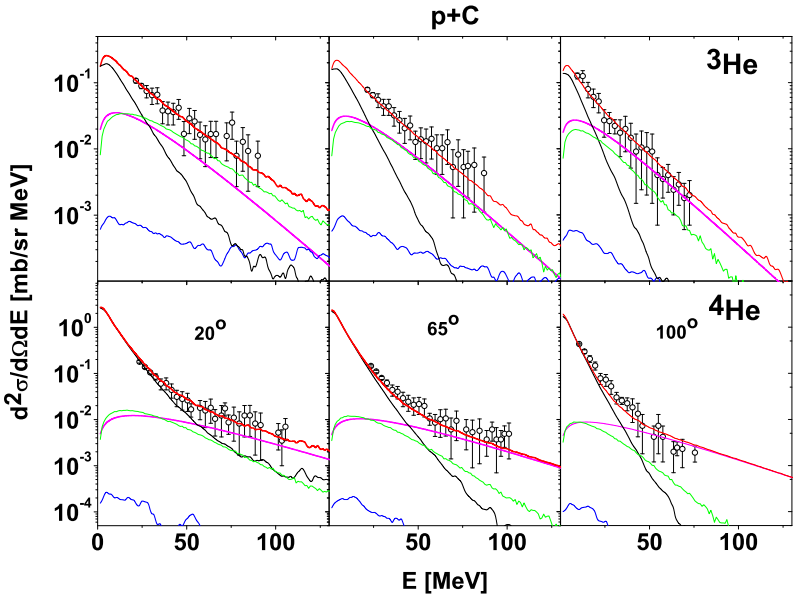

Figure 6.28: The same as in fig. 6.27 but for ^{3}He (upper row) and ^{4}He (lower row).

Table 6.4: The parameters of a fireball contributing to LCP emission in p+C system (column 3 - 6), scaling factor f (for explanation see text), χ^2, and values of the cross sections from all considered reaction mechanisms. The parameters listed in square parentheses were fixed.

particle	energy [MeV]	k	β	T [MeV]	σ [mb]	f	χ^2	f*σ_{INCL} [mb]	σ_{GEM} [mb]	σ_{FBM} [mb]	$\sigma_{Tot.}$ [mb]
	1.2	0.11	0.2789	59.35	360.4	0.51	1.33	181.48	100.46	18.97	661.31
^1H	1.9	0.12	0.2612	57.71	436.8	0.69	1.55	236.63	89.41	23.59	786.43
	2.5	0.07	0.2187	54.92	339.7	0.47	1.29	164.22	96.61	20.21	620.74
	1.2	0.04	0.1975	38.08	33.67	[0.51]	1.27	11.31	50.72	23.20	118.90
^2H	1.9	0.10	0.1282	47.54	77.75	[0.69]	0.97	12.31	42.89	28.77	161.72
	2.5	0.15	0.1010	45.18	64.82	[0.47]	0.95	7.48	46.92	24.35	143.57
	1.2	0.09	0.0816	25.95	9.64	[0.51]	2.32	0.45	16.03	8.98	35.10
^3H	1.9	0.03	0.1579	31.39	6.39	[0.69]	2.72	0.54	14.10	11.49	32.52
	2.5	0.06	0.0892	29.41	10.6	[0.47]	2.54	0.34	14.65	9.15	34.74
	1.2	0.06	0.0150	16.66	12.54	[0.51]	0.44	0.47	23.44	9.70	46.15
^3He	1.9	0.06	0.0175	17.39	16.28	[0.69]	0.37	0.55	20.41	12.38	49.62
	2.5	0.05	0.0115	15.38	18.92	[0.47]	0.37	0.34	22.36	9.79	51.41
	1.2	0.01	0.0254	30.63	7.62	[0.51]	2.55	0.06	203.26	4.44	217.87
^4He	1.9	0.16	0.0570	24.15	7.45	[0.69]	1.96	0.08	189.58	6.29	203.4
	2.5	0.04	0.0289	32.38	8.85	[0.47]	1.54	0.05	190.93	4.27	204.1

Chapter 7

Discussion

The analyses presented in the sections 6.2 and 6.3 showed that it is possible to describe well all data for light charged particles and intermediate mass fragments produced in proton-Carbon and proton-Aluminium collisions at three proton beam energies; 1.2, 1.9, and 2.5 GeV, using the following combinations of several competing reaction mechanisms:

- The angular and energy dependence of the double differential cross sections $\frac{d\sigma}{d\Omega dE}$ for production of ***the intermediate mass fragments*** can be reproduced assuming that the ejectiles ***are emitted from the remnants*** of the target nuclei produced by the intranuclear cascade of the nucleon-nucleon and nucleon-pion collisions. Two different mechanisms of this emission are necessary to describe quantitatively the measured data:

  1. ***the sequential evaporation*** of the particles from the nuclei which are excited to energies smaller than the critical energy per nucleon (cf. section 6.2), and
  2. ***the multifragmentation*** which appears for nuclei excited to the energies larger than the critical energy mentioned above.

  In modeling the decay process the choice for (1) sequential evaporation or (2) simultaneous multifragmentation *a sharp cut* has been applied as a first approximation. It may be expected that the transition from liquid to gas phase is in reality more smooth.

- The description of ***the light charged particle data*** requires besides these two mentioned above mechanisms also other processes which induce emission of particles during the first stage of the reaction:

  1. ***Emission of protons from intranuclear cascade***, i.e. from the series of nucleon-nucleon collisions and ***emission of complex LCPs due to the coalescence*** of the nucleons escaping from the target nucleus during the intranuclear cascade.
  2. The additional process, which corresponds to interaction of the impinging proton with a group of nucleons leading to appearing of a fast and hot group of nucleons -

the fireball, moving along the beam direction. ***Emission of protons and complex LCPs from the fireball*** gives very significant contribution to the observed cross sections.

As it was explained in the previous section, some scaling down of the intranuclear cascade cross sections must be introduced to allow for collision of the proton from the beam *with a group of nucleons* inside the target. In the present work the cross sections from the intranuclear cascade are simply multiplied by a factor f, the same for all ejectiles as well as for the full range of the ejectile energies. It should be pointed out that such a method must be treated as an approximation only, because for the fireball emission calculated on the same microscopic level as the intranuclear cascade, the competition between an intranuclear cascade mechanism and an emission of the fireball can be different for different ejectiles and even for different ranges of the ejectile energies. This might be caused, e.g., by the fact that the probability of collisions between proton from the beam and a group of the target nucleons is small for large impact parameters, where the nucleon density of the target is small, whereas this probability increases for smaller impact parameters where the nucleon density becomes larger.

Table 7.1: Relative contributions (in percent) of different mechanisms to the total production cross section of light charged particles in p+Al collisions. The presented contributions are averaged over the beam energies.

particle	$\sigma_{FIREBALL}/\sigma_{TOT}$	$f * \sigma_{INCL}/\sigma_{TOT}$	$\sigma_{GEM}/\sigma_{TOT}$	$\sigma_{FBM}/\sigma_{TOT}$
^{1}H	53.9	23.4	20.4	2.4
^{2}H	36.1	24.0	27.5	12.4
^{3}H	30.4	19.0	24.8	25.8
^{3}He	33.6	17.6	23.4	25.5
^{4}He	19.9	1.7	72.6	5.8
^{6}He			23.3	76.7
^{6}Li			53.0	47.0
^{7}Li			31.0	69.0
^{8}Li			11.3	88.7
^{9}Li			11.3	88.7
^{7}Be			24.0	76.0
^{9}Be			49.3	50.7
^{10}Be			36.7	63.3
^{10}B			64.0	36.0
^{11}B			68.0	32.0
^{12}B			54.0	46.0

Values of the scaling factors used in the present analysis vary in the range 0.55 – 0.84 for p+Al system, and 0.47 – 0.69 for p+C system suggesting, that the first step of the reaction proceeds mainly via intranuclear cascade mechanism. This, however, does not mean that the inclusive cross sections from the intranuclear cascade dominate because the inclusive cross sections are proportional to the multiplicity of emitted particles. Indeed, relative contributions of individual mechanisms which contribute to emission of light charged particles, listed in Tables 7.1 for p+A collisions, and 7.2 for p+C collisions are larger for the fireball emission than for the intranuclear cascade.

Table 7.2: The relative contributions (in percent) of different mechanisms to the total production cross section of light charged particles in p+C collisions. These contributions are averaged over the beam energies.

particle	$\sigma_{FIREBALL}/\sigma_{TOT}$	$f * \sigma_{INCL}/\sigma_{TOT}$	$\sigma_{GEM}/\sigma_{TOT}$	$\sigma_{FBM}/\sigma_{TOT}$
^{1}H	54.9	28.0	14.0	3.0
^{2}H	40.5	7.4	34.0	18.1
^{3}H	25.9	1.3	43.7	29.1
^{3}He	32.3	0.9	45.1	21.7
^{4}He	3.8	0.03	93.3	2.4
^{6}He			79.7	20.3
^{6}Li			93.0	7.0
^{7}Li			96.0	4.0
^{8}Li			92.3	7.7
^{7}Be			94.7	5.3

The content of Tables 7.1 and 7.2 can be used to derive several interesting conclusions concerning the reaction mechanism:

- ***The intermediate mass fragments*** originate only from the second step of the reaction, i.e., they are produced by decay of excited remnants of the first stage of the reaction. Good description of the data was achieved without introducing of the emission of intermediate mass fragments from the first step of the reaction.

- It should be pointed out, that ***the decay mechanism is different for intermediate mass fragments emitted from p+Al and from p+C collisions***. In the former nuclear system the multifragmentation as well as the sequential evaporation play comparable roles whereas in the latter system the evaporation exhausts approximately 90% of the reaction yield.

- Quite a different situation may be observed ***for light charged particles***. They are emitted from both, the first and the second step of the reactions.

- Emission of light charged particles from the intranuclear cascade exhausts approximately 20% of their total production cross sections ***for p+Al collisions***. This contribution is almost of the same magnitude as that originating from evaporation of these particles in the second stage of the reaction (with exception of the α-particles which are predominantly, i.e., $\sim$ 70%, produced through the evaporation). The emission of light charged particles from the fireball gives a very important contribution, which ranges from 20% to 54% of the total yield of the ejectiles. This contribution is the largest for protons and decreases with increasing of the mass of ejectiles. Multifragmentation of excited remnants of the first reaction stage gives also quite important contribution for deuterons, tritons, and ^{3}He (12 - 25%) but is almost negligible for protons and α-particles.

- ***In the case of p+C collisions*** the emission of protons exhausts a large part of the cross section (28%) in contradiction to the production of complex light charged particles via coalescence, which is negligibly small (with exception of deuterons where 7% of the cross section is due to the coalescence). The fireball emission of protons, deuterons, tritons and ^{3}He is very important (26% - 55%) but the emission of α-particles is very small ($\sim$ 4%). The evaporation contribution to the production cross sections is significant for all LCPs (14 - 45%) and is dominating for α-particles (93%). Multifragmentation participates considerably in production of deuterons, tritons and ^{3}He (18 - 29%) but is very small for protons and α-particles (3% and 2%, respectively).

- It is interesting to note, that the fireball contribution to the α-particle emission is significantly larger for the Aluminium target ($\sim$ 20%) than for the Carbon target ($\sim$ 4%).

- The fireball contribution to heavier ejectiles is not observed what may be expected because of limited size of the fireball.

The fireball properties obtained from the present analysis are similar to those found in previous investigations of proton induced reactions on Au [3] and Ni [5] targets for the same proton beam energies; 1.2, 1.9, and 2.5 GeV. This is illustrated by Fig. 7.1 where the relative contribution of the emission of light charged particles from the fireball, the fireball temperature, and the fireball velocity, averaged over proton beam energies are shown in the upper, the middle and the lower panel of the figure, respectively. Different colours represent the results obtained for four different targets. Results for C and Al targets are taken from the present analysis and those for Ni and Au targets from references cited above. As can be seen, the values of all presented fireball parameters, i.e., the yield, the temperature parameter and the velocity decrease with the mass of emitted ejectiles. The same qualitative and quantitative behaviour of these parameters is visible for all targets under consideration. It should be emphasized, that the values of the parameters do not differ more than $\sim$ 20% for different target nuclei in spite of the fact that the targets cover a very broad range of mass number (from 12 to 197).

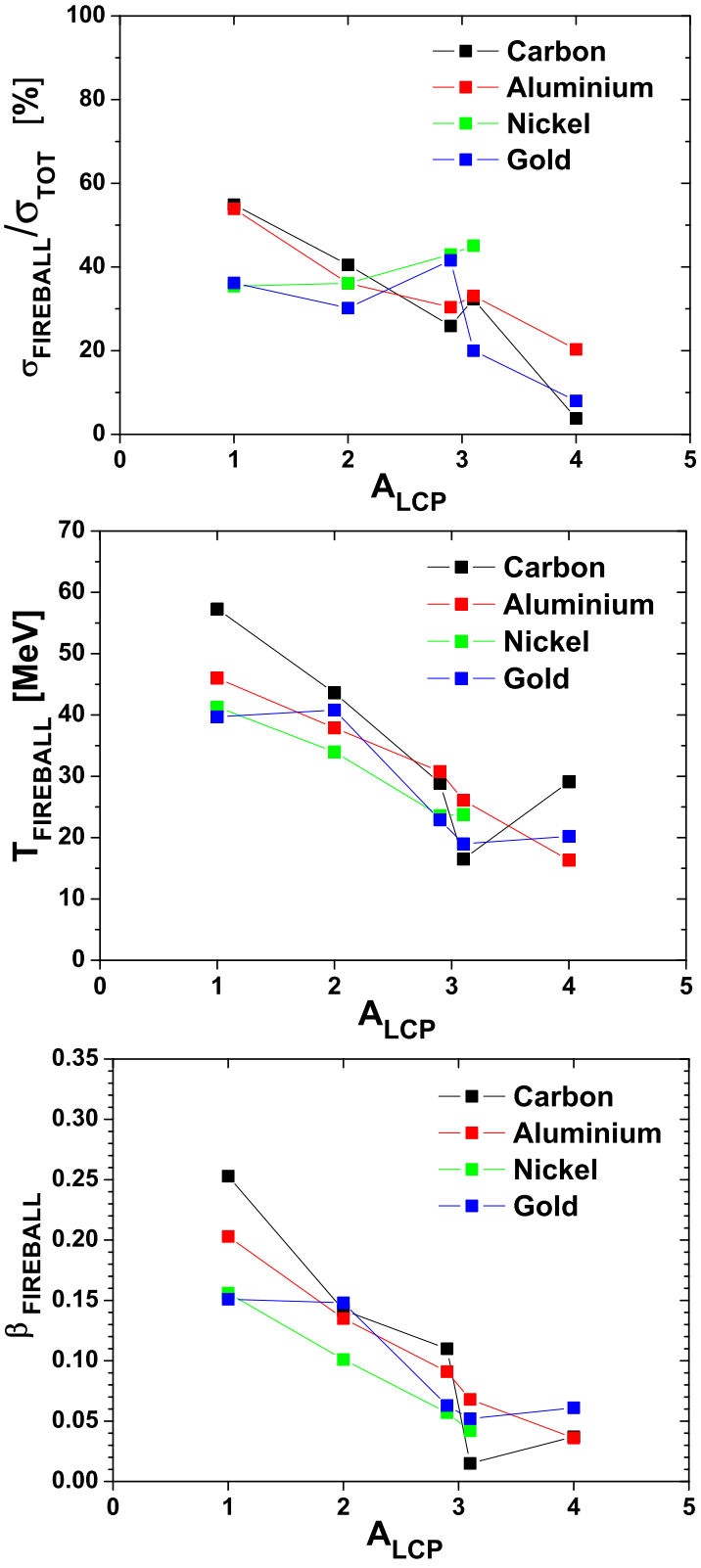

Figure 7.1: Upper panel - averaged over beam energy (1.2, 1.9, and 2.5 GeV) the ejectile mass number dependence of the relative contribution of emission of light charged particles from the fireball for C, Al, Ni, and Au targets. Middle panel - the same dependence of the fireball temperature. Lower panel - the same dependence of the fireball velocity. The triton results are shown for A_{LCP}=2.9, and ^{3}He results for A_{LCP}=3.1 to allow for easy distinction between tritons and ^{3}He.

Chapter 8

Summary

Double differential cross sections $\frac{d\sigma}{d\Omega dE}$ of proton induced reactions on ^{12}C and ^{27}Al targets have been measured for three proton beam energies: 1.2, 1.9, and 2.5 GeV. Isotopically identified hydrogen, helium, lithium, beryllium and boron ejectiles have been detected at seven scattering angles: 15.6° , 20° , 35° , 50° , 65° , 80° , and 100° . The present results agree well with scarce data from the literature measured at similar proton beam energies.

The data were analyzed assuming a presence of several competing reaction mechanisms. A fast proton impinging on a target nucleus may initiate an intranuclear cascade of nucleon-nucleon and pion-nucleon collisions. This cascade results in the emission of fast nucleons, which are ejected independently or together with several nucleons of the target – forming a composite particle due to a coalescence mechanism. The coalescence appears when the momentum and position coordinates of the target nucleons are close to the momentum and the position coordinates of the escaping nucleon. The probability of this process decreases quickly with increasing number of nucleons which coalesce. Thus only the emission of deuterons, tritons, ^{3}He, and ^{4}He from the cascade stage of the reaction has been evaluated in the coalescence model whereas it was assumed that the probability of the emission of heavier products due to such a mechanism is negligible.

Since the remnant nucleus from the intranuclear cascade is usually excited, its decay was taken into account. Two different mechanisms of the decay were applied; (1) the remnant nuclei which are only slightly excited evaporate neutrons, light charged particles, and intermediate mass fragments, whereas (2) highly excited remnant nuclei are subject of a multifragmentation. The first mechanism was described using the GEM2 computer program of Furihata [70,71], which treats evaporation according to the statistical formalism of Weisskopf and Ewing [75] and the simultaneous decay was calculated with the computer program ROZPAD of Magiera [83] which applies the formalism of the Fermi break-up model [73]. The critical excitation energy per nucleon at which multifragmentation sets in was treated as a free parameter and was searched for by comparing double differential $\frac{d\sigma}{d\Omega dE}$ experimental data with the model cross sections.

This critical excitation energy was found to be of the order of 7 – 9 MeV/A for proton induced reactions on Al and C, respectively. It depends only slightly on proton incident energy.

The above described combination of reaction models was able to reproduce perfectly energy spectra and angular distributions of *intermediate mass fragments* from p + ^{27}Al and p+^{12}C collisions measured in the present experiment at all three beam energies. It was found that the contribution of multifragmentation is significant for the description of the IMF spectra measured with both, Al and C targets, but the absolute value of this contribution to the total production cross sections is important only for the Al target. Moreover, it was observed that this contribution increases monotonically with the beam energy thus leading to its dominance at the highest beam energy (2.5 GeV) in the case of Al target, but it is almost energy independent for the C target.

It is interesting to point out that these results were obtained using the standard value (1.4 fm) for the reduced radius characterizing the freeze-out volume of the decaying nuclei and with the critical energy per nucleon values which agree very well with the compilation of critical energy values published in the literature [49].

The spectra of *light charged particles*, i.e., protons, deuterons, tritons, and ^{3,4}He, measured at small scattering angles are underestimated strongly by the above reaction model. They can be, however, well reproduced introducing an additional process, which was parameterized by the emission of LCPs from a hot source ("fireball") moving fast in the forward direction, i.e., along the beam.

The following findings form the most important results of the thesis:

- *Behaviour of the double differential cross sections* $\frac{d\sigma}{d\Omega dE}$ *measured in the present work for light targets;* ^{12}C *and* ^{27}Al *for three proton beam energies 1.2, 1.9, and 2.5 GeV is qualitatively analogous to that observed previously for heavier targets - Ni [4, 5] and Au [2, 3] at the same energies.*

    1. The spectra of *intermediate mass fragments* consists of two components which correspond to the second stage of the reaction, i.e, to the emission of particles from the excited remnants of the first stage of the reaction: (1) A low energy component - the evaporation, which is isotropic and has steep energy decrease equivalent to low temperature of the emitting nucleus, and (2) a high energy component - the multifragmentation, which is forward peaked and has the energy dependence indicating high temperature of the emitting nucleus.
    2. The spectra of *light charged particles* contain three or more different contributions. Additional processes take place besides the mechanisms, which are responsible for emission of intermediate mass fragments. These additional processes correspond to the emission of light charged particles from the first stage of the reaction. There

are: (1) the emission of high energy protons from the intranuclear cascade, (2) the emission of high energy composite particles emerging due to coalescence, and (3) the emission of particles from a "fireball" - fast and hot group of several nucleons moving in the forward direction. This third contribution is very distinct for proton and deuteron spectra, it is smaller for tritons and ^{3}He, and almost absent for ^{4}He.

- *In the present thesis another explanation of the existence of two components in IMF spectra for Al and C target was proposed than that considered in refs [2, 3] for Au target and [4, 5] for Ni target.*

  It was assumed in these latter studies that the proton impinging on to the target knocks out the fireball and thus induces break-up of the heavy remnant of the target into two pieces with significantly different masses. This asymmetry is caused by the fact that the distribution of impact parameters favours peripheral collisions. These two excited prefragments move with different velocities (proportional to the reciprocal of mass of fragments) and with different excitation energies per nucleon (this excitation energy is higher for the lighter prefragment). Therefore, such an asymmetric break-up leads to the appearing of two moving sources with distinctly different properties and consequently to two different contributions to the spectra of the same ejectiles.

  Such a picture is improbable for Al target and impossible for C target, where the "fireball" has dimensions comparable to dimensions of the target, thus the remnant cannot break into two significantly different prefragments emitting intermediate mass fragments. However, the existence of the phase transition between liquid (usual nuclear matter) and gas (IMFs, LCPs and free nucleons) leads to a distinct, critical excitation energy per nucleon at which the deexcitation of the nucleus changes its character. At excitation energies smaller than the critical energy the nuclei evaporate particles, whereas at higher excitation energies a multifragmentation takes place. In the present thesis a simple treatment of the phase transition has been performed which consisted in the assumption of a sharp cut on the critical excitation energy.

  This resulted in appearing of two distinctly different components in the experimental spectra, which were interpreted for heavier targets as originating from the asymmetric two-body break-up of the excited nucleus - remnant after the fireball emission.

- *It is important to point out that the above discussed picture of the reaction allows to find the critical excitation energy at which a phase transition of the nuclear matter proceeds by the investigation of differential cross sections* $\frac{d\sigma}{d\Omega dE}$ *without the need of studying the caloric curves as it is usually done in the literature. Results obtained due to the method presented in the current thesis agree with findings of the caloric curve studies.*

- *The properties of the "fireball", i.e., fast and hot source of light charged particles, necessary to reproduce the present data for C and Al targets are very similar to those found in studies of Ni [4, 5] and Au [2, 3] targets.*

The new results obtained in the present investigation are not able to answer all the questions concerning the reaction mechanism of proton - nucleus interaction at GeV energies. Moreover, they lead to new questions and problems. There are the most important among them:

- The present *inclusive* experiment does not give an unambiguous experimental proof of the existence of a "fireball", which was postulated in the analysis of double differential cross sections $\frac{d\sigma}{d\Omega dE}$ of light charged particles measured in the present work for C and Al targets as well as investigated in refs. [2] and [3] for the Gold target , and in refs. [4] and [5] for the Nickel target. The *coincidence measurements*, dedicated to experimental study of this problem would be desirable.

- It would be very interesting to study properties of the fireball emission in the frame of a microscopic model, which could treat on the same footing the cascade of the nucleon-nucleon collisions and the fireball creation by collisions of the projectile with a group of nucleons from the target. Such a model would avoid an arbitrary scaling down of the intranuclear cascade cross sections by a constant factor and introduce a competition of both reaction mechanisms which could quantitatively modify the shape and magnitude of the spectra and angular distributions.

- The question arises whether the explanation of the presence of two different components in the energy spectra of the intermediate mass fragments, which was successfully applied in the present work for light target nuclei - Carbon and Aluminium, can be extrapolated to heavy target nuclei as, e.g. Gold nucleus. The present investigations were based on the comparison of the experimental data with the (almost) parameter-free calculations of the multifragmentation cross sections in the model of the Fermi break-up. Such calculations are tedious even for light nuclei and become almost impossible for heavier targets. Thus, the invention of an efficient numerical scheme is necessary to apply the analogous calculations for heavy target nuclei.

Appendix A

Previous experiments on p+C and p+Al collisions

Table A.1 Publications in which experimental investigations of p+Al collisions were discussed

beam energy $[GeV]$	**beam**	**target**	**measured particles**	**measured observables**	**comments**	**ref.**
0.01 - 1.6	p	Al,Mg,Si	He,Ne	total cross section excitation function	data from [6] [87] [32] [88] [89] [90]	[12]
0.02-0.05	p p	^{12}C ^{27}Al	^{11}C ^{22,24}Na	total cross section		[43]
0.03-0.1	p	C,Al,^{11}B ^{34}S	^{11}C,^{22,24}Na, ^{34}Cl,^{18}F	excitation function total cross section		[91]
0.5-2.6	p	O,Mg,Al, Si,Mn,Fe, Ni	^{10}Be, ^{26}Al	total cross section		[25]
0.07-2.6 1	p p	Al Pb	^{22,24}Na,^{7}Be, ^{27}Mg	total cross section	Al target as a monitor add. data [6] [92] [93] [32] [95] [7] [96] [97]	[94]
0.082,0.15	p	C,Al,Fe, Nb,Sn,Au, Th	^{3}H	total cross section		[98]
0.09,0.12 0.16, 0.2	p	^{27}Al, ^{58}Ni, ^{90}Zr	p,n	$\frac{d^2\sigma}{d\Omega dE}$	QMD, FKK calculation data from [100] [101] [102]	[99]
0.1-3.17	p	Al,Fe,Pb	p,n,π^-	$\frac{d\sigma}{d\Omega dE}$ $7.5° \leq \theta \leq 150°$	theoretical paper QMD+SDM add. data [103] [104] [105]	[62]
0.1-6.2	p	^{27}Al	^{24}Na	total cross section		[44]
0.1, 0.164	p	^{27}Al,^{58}Ni, ^{62}Ni,^{208}Pb	p -^{4}he	$\frac{d^2\sigma}{d\Omega dE}$ $25° \leq \theta \leq 150°$	2-step model theor. calc. VEGAS [107]	[106]
0.18	p	^{27}Al		total cross section $\frac{d^2\sigma}{d\Omega dA}$ $\frac{d^3\sigma}{d\Omega dAdE}$ $10° \leq \theta \leq 90°$	add. exp. data [108] calc.: casc.+evap. [110] [107] [111] preequilibrium excitation model: [112] semiempirical calculation: [113]	[109]
0.335	p,α	C,Al,Cu Ag,Au	^{7}Be,	excitation function total cross section		[34]
0.36 - 1.8	p	Al	^{24}Na			[114]

Continued on next page

Table A.1 – continued from previous page

beam energy $[GeV]$	**beam**	**target**	**measured particles**	**measured observables**	**comments**	**ref.**
0.4	p	^{6}Li,Be,C Al,Cu,Ta	d,t,^{3,4}He	70° -160° E$\frac{d^3\sigma}{dp^3}$		[115]
0.4-3	p	Al	^{7}Be,^{11}C, ^{13}N,^{15}O, ^{18}F,^{22,24}Na	excitation functions total cross sections	data from [35]	[28]
0.42	p	O,F,Al,Cl Cu,Ag,Au	^{7}Be,^{11}C,, ^{13}N,^{18}F, ^{22,24}Na	total cross section excitation function	data from [116], [117] [118]	[35]
0.42,0.45	p,n	Al,Cu	C,F,N, Na,Mg,Ti, Cr,Mn,Fe, Co,Ni,Cu,	total cross section		[119]
0.45	p	Be,C,Al, Cu,Co,Pb, Bi	p,n	$0^o \leq \theta \leq 60^o$, $\frac{d^2\sigma}{d\Omega dE}$		[120]
0.45, 2.05	p	C,N,O, Mg,Al,Fe Ni,Ag,Pb	^{3}H	total cross section		[21]
0.585	p	Al, C, Nb In, Ta, Pb, U	n	$\frac{d^2\sigma}{d\Omega dE}$ $\theta = 30°, 90°, 150°$		[121], [122]
0.6	p	Be,C,Na, Al,Ca,Fe, Ag,Au,U	H,He	$\frac{d^2\sigma}{d\Omega dE}$ $30° \leq \theta \leq 105°$ total cross section	2-step model themodynamical model data from [124] [30]	[123]
0.6	p	O-Au	^{7}Be-^{196}Au	total cross section		[32]
0.73-3.86	p π	C,Al,Sn, Cu,Pb	p	$E\frac{d^3\sigma}{dp^3}$ multiplicity distribution $\sigma_{stopped}$, 30° -120°		[52]
0.8, 1.6 1.2	p p	Fe,Pb Al,Fe,Zr W,Pb,Th	n	$\frac{d^2\sigma}{d\Omega dE}$ $0° \leq \theta \leq 160°$	comparision with exp. [105] [125] [126] [128] and wiht calc. LAHET (Bertini, Isabel) TIERCE [129](INCL) excitation energy, multiplicity	[127]
0.8,1.2, 1.6,2.6	p	O,Mg,Al, Si,Ca,Ti, V,Mn,Fe, Co,Ni,Cu, Zr,Rh,Nb, Ba,Au	^{3}He - ^{65}Zn	total cross section excitation function	review paper	[6]
1.6	p	C,N,Rb, Sr,Y			theoretical calculation HET	
1	p	Al,Ni Ag,Au	IMF $Z_F \geq 3$	energy spectra total cross section	velocity residuum excitation energy	[130]
1.0, 1.9, 2.85	p	C,Al,Cu, Ag,Pb	^{6}He	total cross section		[26]
1.0, 2.8	p	B,C,N,O, F,Na,Mg, Al,Si,S, Ca,Ti,Ni, Cu,Nb,Ag, La,Pr,Nd, Ta,W,Pb,U	^{9}Li,^{16}C, ^{17}N	total cross section		[27]
1.0, 3.0	p	C,Al,Cu Ag,Au	^{7}Be	total cross section		[29]

Continued on next page

Table A.1 – continued from previous page

beam energy $[GeV]$	**beam**	**target**	**measured particles**	**measured observables**	**comments**	**ref.**
1-11.5	p	Al	^{7}Be, ^{11}C, ^{18}F	F/B	two-velocity model, excitation function to 400GeV, data from [69]	[131]
1.5, 2.6	p	^{56}Fe ^{27}Al	^{4}He, ^{18}F, ^{24,22}Na, ^{38}Ar, ^{54}Mn ^{7}Be	total cross section	theoretical paper QMD+SDM impact parameter dependence, data from [6]	[132]
2.1-4.9	p	C,Al,Ag, U	He-Ar	$\frac{d^2\sigma}{d\Omega dE}$ $\theta = 20°, 90°, 160°$	parametrisation add data [124] [133]	[69]
2.0, 3.0	p	^{12}C, ^{27}Al	^{11}C,^{24}Na	total cross section		[41]
2.2	p	Al,C,Cu, Ag,Au,U	^{8}Li	not normalized energy spectra $29° \leq \theta \leq 152°$	nuclear emulsion	[134]
3-300	p	Al	^{22,24}Na	2W(F+B), F/B	add. data [114]	[135]
5.7	p	Be,C,N,O F,Na,Al	^{3}H, ^{7}Be, ^{11}C, ^{13}N, ^{14,15}O,^{18}F, ^{22}Na, ^{24}Ne, ^{27}Mg	total cross section		[23]
6	p	C,N,O,Mg, Al,Fe,Ni, Ag,Sn,Pb	^{3}H	total cross section		[22]
12	p	Al,Fe,Co, Ni,Cu,Zn, Ag,Au	^{10}Be,^{26}Al, ^{24}Na	excitation function energy spectra total cross section	add. data [25] [33] [136] [137] [138] [139] [140] [141] [143] [144] [145] [146]; parametrisation of total cross section [147]	[142]
28	p	C,Al	^{7}Be,^{11}C, ^{13}N,^{15}O, ^{18}F, ^{22,24}Na, ^{24}Ne, ^{27}Mg	total cross section		[36]
30	p	C,Be,Al	p,$\bar{p}$, κ, π,d,t	momentum spectra $30°$	TOF	[148]
30-33	p	Al, Be	H,π, κ $\bar{p}$	momentum spectra $\theta = 13\frac{1}{4}°, 45°, 90°$	magnetic deflection TOF	[149]
30,50,70	p	Al	^{7}Be,^{11}C, ^{18}F,^{22,24}Na,	yield ratios		[39]
300	p	Al	^{7}Be,^{11}C, ^{13}N,^{18}F, ^{22,24}Na,	total cross section		[37]

Table A.2 Publications in which experimental investigations of p+C collisions were discussed.

beam energy $[GeV]$	**beam**	**target**	**measured particles**	**measured observables**	**comments**	**ref.**
0.02-0.05	p p	^{12}C ^{27}Al	^{11}C ^{22,24}Na	total cross section		[43]
0.02,0.03, 0.06	n	C	^{1,2,3}H, ^{3,4}He	$15°$ -$150°$ $\frac{d\sigma}{d\Omega dE}$	data from [151]	[150]
0.03-0.1	p	^{11}B,C, Al, ^{34}S	^{11}C,^{22,24}Na, ^{34}Cl,^{18}F	excitation function total cross section		[91]

Continued on next page

Table A.2 – continued from previous page

beam energy [GeV]	beam	target	measured particles	measured observables	comments	ref.
0.044-25	p	^{12}C	^{6,7}Li	total cross section		[152]
0.05-28	p	^{12}C, ^{27}Al	^{7}Be,^{11}C, ^{24}Na,^{18}F	total cross section		[38]
0.082,0.15	p	C,Al,Fe, Nb,Sn, Au,Th	^{3}H	total cross section		[98]
0.096	n	C	^{1,2,3}H, ^{3,4}He	20° - 160°	data from [153]	[154]
0.15, 0.60 0.88	p α	^{12}C	^{6,7}Li	total cross section		[155]
0.25-6.2	p	^{12}C	^{12}C(p,pn)^{11}C	F/B ratio, range impact velocity		[156]
0.39-2.95	p	C	^{11}C	$\frac{\sigma_{^{11}C}}{\sigma_{^{24}Na}}$		[157]
0.4	p	^{6}Li,Be, C, Al,Cu, Ta	d,t,^{3,4}He	70° -160° E$\frac{d^3\sigma}{dp^3}$		[115]
0.4-0.65	Be,B, C,N, O,Ne, Fe,Ni	H	Be-Co	$\frac{d\sigma}{dZ}$, $\frac{d\sigma}{dA}$		[158] [159]
0.45	p	Be,C, Al,Cu, Co,Pb, Bi	p,n	$0^o \leq \theta \leq 60^o$, $\frac{d^2\sigma}{d\Omega dE}$		[120]
0.45, 2.05	p	C,N,O, Mg,Al, Fe,Ni, Ag,Pb	^{3}H	total cross section		[21]
0.5-2.9	p	O,C,Mg Si,Ni,Fe	^{7}Be,^{22,24}Na ^{32}P,^{44m,47}Sc ^{48}V,^{48,51}Cr ^{52,54}Mn,^{56}Co	total cross section		[160]
0.585	p	Al, C, Nb In, Ta, Pb, U	n	$\frac{d^2\sigma}{d\Omega dE}$ $\theta = 30°, 90°, 150°$		[121], [122]
0.6 0.8	p p	Be,C, Cu,Ta Ag,Ta, Pt	p,d,t	$\frac{d\sigma}{d^3p}$ 180°		[161]
0.6	p	Be,C,Na, Al,Ca,Fe, Ag,Au,U	H,He	$\frac{d^2\sigma}{d\Omega dE}$ $30° \leq \theta \leq 105°$ total cross section	2-step model themodynamical model data from [124] [30]	[123]
0.6, 3 33	p	C,Si,O	^{3}H, ^{3,4}He ^{3}H:^{3}He:^{4}He	total cross section		[162]
0.73-3.86	p π	C,Al,Sn, Cu,Pb	p	$E\frac{d^3\sigma}{dp^3}$ multiplicity distribution $\sigma_{stopped}$, 30° -120°		[52]
0.8	p	C,Ti,Pb	^{3,4}He	$\frac{d\sigma}{d\Omega dE}$ 5° -15°		[163]
0.8	p	^{12}C	^{11}C	total cross section		[164]
0.8,1.2, 1.6,2.6	p	O,Mg,Al, Si,Ca,Ti, V,Mn,Fe, Co,Ni,Cu, Zr,Rh,Nb,	^{3}He - ^{65}Zn	total cross section excitation function	review paper theoretical	[6]

Continued on next page

Table A.2 – continued from previous page

beam energy $[GeV]$	beam	target	measured particles	measured observables	comments	ref.
1.6	p	Ba,Au C,N,Rb, Sr,Y			calculation HET	
1	p	C	He,Li, Be,B	$\frac{d^2\sigma}{d\Omega dE}$, total cross section $\theta = 30^o, 126^o$	TOF, Bragg spectroscopy moving source parametrization	[85]
1.0, 1.9, 2.85	p	C,Al,Cu, Ag,Pb	^{6}He	total cross section		[26]
1.0, 2.8	p	B,C,N,O, F,Na,Mg, Al,Si,S, Ca,Ti,Ni, Cu,Nb,Ag, La,Pr,Nd, Ta,W,Pb,U	^{9}Li,^{16}C,^{17}N	total cross section		[27]
1.0, 3.0	p	C,Al,Cu Ag,Au	^{7}Be	total cross section		[29]
1.05,2.1	^{12}C, ^{16,18}O ^{56}Fe	H,Be,C, Al,Cu,Ag Pb	^{1}H-^{15}O	total cross section		[45]
2.0, 3.0	p	^{12}C, ^{27}Al	^{11}C,^{24}Na	total cross section		[41]
2.1-4.9	p	C,Al,Ag, U	He-Ar	$\frac{d^2\sigma}{d\Omega dE}$, $\theta = 20^\circ, 90^\circ, 160^\circ$	parametrisation add data [124] [133]	[69]
2.2	p	Al,C,Cu, Ag,Au,U	^{8}Li	not normalized energy spectra $29^\circ \leq \theta \leq 152^\circ$	nuclear emulsion	[134]
3.0, 4.5, 6.0	p	^{12}C	^{11}C	total cross section		[165]
3.66	^{12}C	p	^{1}H-^{11}C	total cross section		[166]
5.7	p	Be,C,N,O F,Na,Al	^{3}H, ^{7}Be, ^{11}C, ^{13}N, ^{14,15}O,^{18}F, ^{22}Na, ^{24}Ne, ^{27}Mg	total cross section		[23]
6	p	C,N,O,Mg, Al,Fe,Ni, Ag,Sn,Pb	^{3}H	total cross section		[22]
7.6	p	^{12}C	^{11}C	total cross section	add. data from [167], [41], [165],	[168]
28	p	C,Al	^{7}Be,^{11}C, ^{13}N,^{15}O, ^{18}F, ^{22,24}Na, ^{24}Ne, ^{27}Mg	total cross section		[36]
30	p	C,Be,Al	p,$\bar{p}$, κ, π,d,t	momentum spectra 30°	TOF	[148]

Appendix B

The model of emitting moving sources

This model was originally described by Westfall et al. in Ref. [69]. In the present thesis a slightly different realization of the model, introduced in Ref. [2] is applied.

According to model assumptions the ejectiles are emitted isotropically from the sources moving in the forward direction, i.e. along the beam. The energy of emitted particles is distributed according to the Maxwellian function, characterized by *the apparent temperature parameter* T.

This parameter is different from the temperature τ characterizing a probability distribution $f(E^*)$ of the excitation energy E^* of the emitting nucleus

$$f(E^*) = \frac{1}{2\left(\pi\tau\right)^{3/2}}\sqrt{E^*}\exp\left[-\frac{E^*}{\tau}\right] \tag{B.1}$$

because the energy and momentum conservation put constraints on this part of the excitation energy which can be transformed into kinetic energy of the ejectile. The kinetic energy $E^{'}$ of the ejectile of mass A_F emitted from the source of the mass A_S is related to the excitation energy E^* of the source by the following formula:

$$E^* = \nu E^{'}_A \tag{B.2}$$

where

$$\nu \equiv \frac{A_S}{A_S - A_F} \tag{B.3}$$

The kinetic energy distribution of the emitted fragment in the rest frame of the source is equal to:

$$\frac{d^2\sigma}{dE^{'}d\Omega^{'}} = \frac{\nu\sigma}{2\left(\pi\tau\right)^{3/2}}\sqrt{\nu E^{'}}\exp\left[-\frac{\nu E^{'}}{\tau}\right]. \tag{B.4}$$

This distribution is normalized to *the total production cross section* σ in contrast to normalization of the probability distribution (B.1) of the excitation energy E^*, which is normalized to unity, i.e., integral from the function $f(E^*)$ is equal one.

The formula for kinetic energy distribution (B.3) is usually presented without explicit writing the recoil correction, i.e. by introducing *the apparent temperature parameter* T

$$T \equiv \tau/\nu \tag{B.5}$$

what leads to the following form of this distribution:

$$\frac{d^2\sigma}{dE'd\Omega'} = \frac{\sigma}{2\left(\pi T\right)^{3/2}}\sqrt{E'}\exp\left[-\frac{E'}{T}\right]. \tag{B.6}$$

Such a form of this formula is used also in the present thesis.

The kinetic energy distribution (B.6) does not take into account a presence of the Coulomb barrier which must be overcame by charged ejectiles. The simplest method of inclusion of the barrier would be shifting the argument in the Maxwell formula by the height of the barrier, as it was originally proposed in Ref. [69]. Such a prescription is equivalent to the sharp cut-off applied to the energy of charged particles. It is obvious that this method gives not realistic results because various excited nuclei, produced in the proton-nucleus collisions, can serve as a source of these particles thus instead a single height of the barrier a distribution of heights should be taken into consideration. Furthermore, the tunneling effect of the particles through the barrier should also lead to smooth cut-off the ejectile energies instead the sharp cut-off postulated by the shifting of the energy by some value. In the present work, the probability to overcome the Coulomb barrier was parameterized in the following form:

$$P = \frac{1}{1+\exp\left[-\left(\frac{E-k\cdot B}{d}\right)\right]} \tag{B.7}$$

where B is the Coulomb barrier of two touching spheres corresponding to the emitted fragment of mass number A_F and charge number Z_F and to the remaining part of the source with the mass number of $A_S - A_F$ and charge number $Z_S - Z_F$:

$$B = \frac{Z_F(Z_S - Z_F)e^2}{1.44\left({A_F}^{1/3} + (A_S - A_F)^{1/3}\right)}. \tag{B.8}$$

The quantities k and d are the parameters. The first parameter (k) was searched looking for best fit of model spectra to the experimental data whereas the second parameter (d) was fixed in the present analysis by keeping constant the ratio of the height of the barrier kB to its diffuseness parameter d: $kB/d = 5.5$.

$$\begin{aligned} \frac{d\sigma}{dE'd\Omega'} &= \frac{\sigma}{4\pi T^{3/2} I(kB,d,T)} \cdot \frac{\sqrt{E'}\exp\left(-\frac{E'}{T}\right)}{1+\exp\left(\frac{kB-E'}{d}\right)} \\ I(B,d,T) &= \int_0^\infty \frac{dx\cdot\sqrt{x}\cdot\exp\left(-x\right)}{1+\exp\left(\frac{kB-T\cdot x}{d}\right)} \end{aligned} \tag{B.9}$$

The integral $I(B, d, T)$ used for normalization of the distribution (preserving previous interpretation of σ parameter) has been evaluated numerically by Gauss-Laguerre method.

For comparison of the experimental cross sections, given in the laboratory system, with theoretical cross sections it is necessary to transform the model double differential cross sections calculated in the rest system of the emitting source to the laboratory system. It can be shown that the transformation may be performed by following formula:

$$\frac{d\sigma}{dEd\Omega} = \frac{p}{p'} \cdot \frac{d\sigma}{dE'd\Omega'} \approx \sqrt{\frac{E}{E'}} \cdot \frac{d\sigma}{dE'd\Omega'} \tag{B.10}$$

where the first equality is exact and the second is valid in nonrelativistic limit, normally realized in the motion of observed ejectiles. The nonrelativistic relationship between kinetic energy E of the particle emitted at the angle θ_{LAB} in the laboratory system and the energy $E^{'}$ of emitted particle in the rest frame of the source is as follows:

$$E^{'} = E + \frac{m\beta^2}{2} - \sqrt{2mE} \cdot \beta \cdot \cos\theta_{LAB} \tag{B.11}$$

where m ($\equiv A_F$) is mass of emitted particle and β - velocity of the source in the laboratory system.

Acknowledgements

I would like to thank all the people, who helped me during the years of PhD. studies, and who helped me to create this dissertation.

I wish to express my deep gratitude to my supervisor Prof. Dr hab. Bogusław Kamys for teaching and guiding me through all the years of my PhD. study, for devoted time, patience, many ideas, which helped me to create this work and finally for his invaluable help in completion and detailed correction of this thesis.

I am grateful to Prof. Dr hab. Lucjan Jarczyk for constructive discussion and for many important questions, which showed me a proper way of understanding the physical phenomena.

I would like to express my appreciation to Prof. Dr hab. Andrzej Magiera for making the computer program ROZPAD available and for enlightenment of the Fermi Break-up Model.

I wish to thank Dr hab. Frank Goldenbaum for invitation to Forschungszentrum Jülich, for discussions concerning results of my work, and for many suggestions how to improve this thesis.

I am grateful to all Colleagues from PISA Collaboration, especially to Dr Borys Piskor-Ignatowicz for his help connected with preparation of experimental data, and INCL4.3 and GEM2 program,

I would like to acknowledge gratefully financial support of Polish Ministry of Science and Higher Education (Grant No N N202 174735, contract number 1747/B/H03/2008/35).

I would like to thank to my Colleagues from "the room 03a" for a nice atmosphere during work and especially to Dr Izabela Ciepał, M. Sc. Beata Michalska-Trębacz, M. Sc. Radosław Trębacz, and M. Sc. Damian Gil for their help and support.

At the end I wish to express gratitude to my Mom, my dearest husband Łukasz, our little son Julian and to all family for their love, support and strong belief in me. Without your help and support this dissertation probably would not come to existence at all.

Bibliography

[1] Y. E. Titarenko, V. F. Batyaev, A. Y. Titarenko, M. A. Butko, K. V. Pavlov, S. N. Florya, R. S. Tikhonov, S. G. Mashnik, A. V. Ignatyuk, N. N. Titarenko, W. Gudowski, M. Těšínský, C.-M. L. Persson, H. A. Abderrahim, H. Kumawat, H. Duarte, Cross sections for nuclide production in a ^{56}Fe target irradiated by 300, 500, 750, 1000, 1500, and 2600 MeV protons compared with data on a hydrogen target irradiated by 300, 500, 750, 1000, and 1500 MeV/nucleon ^{56}Fe ions, Physical Review C 78 (2008) 034615.

[2] A. Bubak, A. Budzanowski, D. Filges, F. Goldenbaum, A. Heczko, H. Hodde, L. Jarczyk, B. Kamys, M. Kistryn, S. Kistryn, S. Kliczewski, A. Kowalczyk, E. Kozik, P. Kulessa, H. Machner, A. Magiera, W. Migdał, N. Paul, B. Piskor-Ignatowicz, M. P. a, K. Pysz, Z. Rudy, R. Siudak, M. Wojciechowski, P. Wüstner, Non-equilibrium emission of complex fragments from Au+p collisions at 2.5 GeV proton beam energy, Physical Review C 76 (2007) 014618.

[3] A. Budzanowski, M. Fidelus, D. Filges, F. Goldenbaum, A. Heczko, H. Hodde, L. Jarczyk, B. Kamys, M. Kistryn, S. Kistryn, S. Kliczewski, A. Kowalczyk, E. Kozik, P. Kulessa, H. Machner, A. Magiera, B. Piskor-Ignatowicz, K. Pysz, Z. Rudy, R. Siudak, M. Wojciechowski, Competition of coalescence and fireball processes in non-equilibrium emission of light charged particles from p+Au collisions, Physical Review C 78 (2008) 024603.

[4] A. Budzanowski, M. Fidelus, D. Filges, F. Goldenbaum, A. Heczko, H. Hodde, L. Jarczyk, B. Kamys, M. Kistryn, S. Kistryn, S. Kliczewski, A. Kowalczyk, E. Kozik, P. Kulessa, H. Machner, A. Magiera, B. Piskor-Ignatowicz, K. Pysz, Z. Rudy, R. Siudak, M. Wojciechowski, Variation of nonequilibrium processes in the p + Ni system with beam energy, Physical Review C 80 (2009) 054604.

[5] A. Budzanowski, M. Fidelus, D. Filges, F. Goldenbaum, A. Heczko, H. Hodde, L. Jarczyk, B. Kamys, M. Kistryn, S. Kistryn, S. Kliczewski, A. Kowalczyk, E. Kozik, P. Kulessa, H. Machner, A. Magiera, B. Piskor-Ignatowicz, K. Pysz, Z. Rudy, R. Siudak, M. Wojciechowski, Comparison of nonequilibrium processes in p+Ni and p+Au collisions at GeV energies, Physical Review C 82 (2010) 034605.

[6] R. Michel, M. Gloris, H.-J. Lange, I. Leya, M. Lüpke, U. Herpers, B. Dittrich-Hannen, R. Rösel, T. Schiekel, D. Filges, P. Dragovitsch, M. Suter, H.-J. Hofmann, W. Wölfli, P. W. Kubik, H. Baur, R. Wieler, Nuclide production on proton-induced reaction on elements ($6 \leq Z \leq 29$) in the energy range from 800 to 2600 MeV, Nuclear Instruments and Methods in Physics Research B 103 (1995) 182–222.

[7] R. Michel, R. Bodemann, H. Busemann, R. Daunke, M. Gloris, H.-J. Lange, B. Klug, A. Frins, I. Leya, M. Lüpke, S. Neumann, H. Reinhardt, M. Schanatz-Büttgen, U. Herpers, T. Schiekel, F. Sudbrock, B. Holmqvist, H. Condé, Cross sections for the production of residual nuclides by low- and medium-energy protons from the target elements C, N, O, Mg, Al, Si, Ca, Ti, V, Mn, Fe, Co, Ni, Cu, Sr, Y, Zr, Nb, Ba and Au, Nuclear Instruments and Methods in Physics Research B 129 (1997) 153.

[8] B. D. Wilkins, S. B. Kaufman, E. P. Steinberg, J. A. Urbon, D. J. Henderson, Evidence for a new reaction mechanism in the bombardment of ^{238}U with 11.5-GeV protons, Phys. Rev. Lett. 43 (15) (1979) 1080–1083.

[9] K. Nakai, Study of energy deposition of GeV particles in nuclei, Nuclear Physics A 418 (1984) 163c.

[10] R. G. Korteling, R. E. L. Green, J. M. D'Auria, R. L. Helmer, K. P. Jackson, S. B. Kaufman, B. D. Wilkins, Light fragment emission as studied by the (p,pHe) reactions on Be and Ag with 300 MeV protons, Physical Review C 41 (6) (1990) 2571.

[11] V. E. Viola, K. Kwiatkowski, L. Beaulieu, D. S. Bracken, H. Breuer, J. Brzychczyk, R. T. de Souza, D. Ginger, W.-C. Hsi, R. G. Korteling, T. Lefort, W. G. Lynch, K. Morley, R. Legrain, L. Pienkowski, E. C. Pollacco, E. Renshaw, A. Ruangma, M. B. Tsang, C. Volant, G. Wang, S. J.Yennello, N.R.Yoder, Light-ion-induced multifragmentation: The ISiS project, Physics Reports 434 (2006) 1–46.

[12] I. Leya, H. Busemann, H. Baur, R. Wieler, M. Gloris, S. Neumann, R. Michel, F. Sudbrock, U. Herpers, Cross sections for the proton-induced production of He and Ne isotopes from Magnesium, Aluminum, and Silicon, Nuclear Instruments and Methods in Physics Research B 145 (1998) 449 – 458.

[13] A. Bubak, B. Kamys, M. Kistryn, B. Piskor-Ignatowicz, Parameterization of the total cross-section for (p,^{7}Be) reaction, Nuclear Instruments and Methods in Physics Research B 226 (2004) 507–516.

[14] N. T. Porile, A. J. Bujak, D. D. Carmony, Y. H. Chung, L. J. Gutay, A. S. Hirsch, M. Mahi, G. L. Paderewski, T. C. Sanger, R. P. Scharenberg, B. C. Stringfellow, Approach to criticality in the fragmentation of Xenon by 1- 19 GeV protons, Physical Review C 39 (5) (1989) 1914.

[15] G. D. Westfall, J. Gosset, P. J. Johansen, A. M. Poskanzer, W. G. Meyer, H. H. Gutbrod, A. Sandoval, R. Stock, Nuclear fireball model for proton inclusive spectra from relativistic heavy-ion collisions, Physical Review Letters 37 (18) (1976) 1202–1205.

[16] J. Aichelin, J. Hüfner, R. Ibarra, Cold breakup of spectator residues in nucleus-nucleus collisions at high energy, Physical Review C 30 (1984) 107–118.

[17] J. Benecke, T. T. Chou, C. N. Yang, E. Yen, Hypothesis of limiting fragmentation in high-energy collision, Physical Review 188 (1969) 2159.

[18] J. B. Cumming, P. E. Haustein, R. W. Stoenner, L. Mausner, R. A. Naumann, Spallation of Cu by 3.9-GeV ^{14}N ions and 3.9-GeV protons, Physical Review C 10 (1974) 739.

[19] J. B. Cumming, P. E. Haustein, R. W. Stoenner, Spallation of Copper by 25-GeV ^{l2}C ions and 28-GeV protons, Physical Review C 14 (1976) 1554.

[20] J. B. Cumming, P. E. Haustein, H.-C. Hseuh, Momentum transfer in the reactions of 25-GeV ^{12}C and 28-GeV ^{1}H with Cu, Physical Review C 18 (1978) 1372.

[21] L. A. Currie, W. F. Libby, R. L. Wolfgang, Tritium production by high energy protons, Physical Review 101 (5) (1956) 1557.

[22] L. A. Currie, Tritium production by 6-BeV protons, Physical Review 114 (3) (1959) 878.

[23] P. A. Benioff, Nuclear reactions of low-Z elements with 5.7-BeV protons, Physical Review 119 (1) (1960) 316.

[24] K. Goebel, H. Schultes, J. Zähringer, Production cross-section of tritium and rare gases in various target elements, Tech. rep., CERN European Organisation for Nuclear Research (1964).

[25] B. Dittrich, U. Herpers, M. Lüpke, R. Michel, H. J. Hofmann, W. Wölfli, Radiochim. Acta 50 (1990) 11.

[26] F. S. Rowland, R. L. Wolfgang, Production of ^{6}He by high-energy protons, Physical Review 110 (1958) 175.

[27] I. Dostrovsky, J. R. Davis, A. M. Poskanzer, P. L. Reeder, Cross sections for the production of Li^{9}, C^{16}, and N^{17} in irradiations with GeV-energy protons, Physical Review 139 (6B) (1965) B1513.

[28] G. Friedlander, J. Hudis, R. L. Woflgang, Disintegration of Aluminum by protons in the energy range 0.4 to 3.0 Bev, Physical Review 99 (1955) 263.

[29] E. Baker, G. Friedlander, J. Hudis, Formation of Be^{7} in interaction of various nuclei with high-energy protons, Physical Review 112 (4) (1958) 1319.

[30] A. M. Poskanzer, G. W. Butler, E. K. Hyde, Fragment production in the interaction of 5.5-GeV protons with Uranium, Physical Review C 3 (2) (1971) 882.

[31] J. Hudis, R. Wolfgang, N. Sugarman, G. Friedlander, Physical Review 94 (1954) 775.

[32] R. Michel, B. Dittrich, U. Herpers, T. Schiffmann, P. Cloth, P. Dragovitsch, D. Filges, Proton-induced spallation at 600 MeV, Analyst (Cambridge U.K.) 114 (1989) 289.

[33] B. Dittrich, U. Herpers, H. J. Hofmann, W. Wölfli, R. Bodemann, M. Lüpke, R. Michel, P. Dragovitsch, D. Filges, AMS measurements of thin-target cross sections for the production of ^{10}Be and ^{26}Al by high-energy protons, Nuclear Instruments and Methods B 52 (1990) 588.

[34] L. Marquez, I. Perlman, Observations on Lithium and Beryllium nuclei ejected from heavy nuclei by high energy particles, Physical Review 81 (6) (1951) 953.

[35] L. Marquez, The yield of ^{18}F from medium and heavy elements with 420-MeV protons, Physical Review 86 (1982) 405.

[36] J. B. Cumming, G. Friedlander, J. Hudis, M. Poskanzer, Spallation of Aluminum by 28-GeV protons, Physical Review 127 (3) (1962) 950.

[37] S. B. Kaufman, M. W. Weisfield, E. P. Steinberg, B. D. Wilkins, D. Henderson, Spallation of Aluminum by 300 GeV protons, Physical Review C 19 (3) (1979) 926.

[38] J. B. Cumming, Monitor reactions for high energy proton beams, Annual Review Nuclear Particle Science 13 (1963) 261.

[39] L. P. Moskaleva, G. A. Fedoseev, A. N. Khalemsky, Yield of the isotopes $Be^7, C^{11}, F^{18}, Na^{22,24}$ in bombardment of Aluminum by 30-, 50-, and 70-BeV protons, Yadernaya Fizika 12 (1970) 871.

[40] J. Tobailem, C. H. de Lassus, S. Genies, Report CEA-N-1466 3.

[41] J. B. Cumming, G. Friedlander, C. E. Swartz, C^{12}(p,pn)C^{11} cross section at 2 and 3 BeV, Physical Review 111 (5) (1958) 1386.

[42] M. A. Tabers, G. Delibrias, Comptes Rendus B 253 (1961) 1202.

[43] J. B. Cumming, Absolute cross section for the C^{12}(p,pn)C^{11} reaction at 50 MeV, Nuclear Physics 49 (1963) 417.

[44] G. Friedlander, L. Friedman, B. Gordon, L. Yaffe, Excitation functions and nuclear charge dispersion in the fission of Uranium by 0.1- to 6.2-GeV protons, Physical Review 129 (4) (1963) 1809.

[45] D. L. Olson, B. L. Berman, D. E. Greiner, H. H. Heckman, P. J. Lindstrom, H. J. Crawford, Factorization of fragment production cross sections in relativistic haevy-ion collisions, Physical Review C 28 (1983) 1602.

[46] R. K. Tripathi, F. A. Cucinotta, J. W. Wilson, Accurate universal parametrization of absorption cross section, Nuclear Instruments and Methods in Physics Research B 117 (1996) 347–349.

[47] J. Hüfner, Heavy fragments produced in proton-nucleus and nucleus-nucleus collisions at relativistic energies, Physics Reports 125 (4) (1985) 129–185.

[48] J. Richert, P. Wagner, Microscopic model approaches to fragmentation of nuclei and phase transition in nuclear matter, Physics Reports 350 (2001) 1–92.

[49] J. B. Natowitz, R. Wada, K. Hagel, T. Keutgen, M. Murray, A. Makeev, L. Qin, P. Smith, C. Hamilton, Caloric curves and critical behavior in nuclei, Physical Review C 65 (2002) 034618.

[50] B. Borderie, M. Rivet, Nuclear multifragmentation and phase transition for hot nuclei, Progress in Particle and Nuclear Physics 61 (2008) 551.

[51] J. Aichelin, "Quantum" molecular dynamics - a dynamical microscopic n-body approach to investigate fragment formation and the nuclear equation of state in heavy ion collisions, Physics Reports 202 (1991) 233.

[52] K. Nakai, T.-A. Shibata, B. En'yo, S. S. abd M. Sekimoto, I. Arai, K. Nakayama, K. Ichimaru, H. Nakamura-Yokota, R. Chiba, Stopping and energy deposition of GeV particles in target nuclei, Physics Letters B 121 (6) (1983) 373.

[53] J. Cugnon, T. Mizutani, J. Vandermeulen, Equilibration in relativistic nuclear collisions. A Monte Carlo calculation, Nuclear Physics A 352 (1981) 505.

[54] J. Cugnon, Proton-nucleus interaction at high energy, Nuclear Physics A 462 (1987) 751.

[55] A. Boudard, J. Cugnon, S. Leray, C. Volant, Intranuclear cascade model for a comprehensive description of spallation reaction data, Physical Review C 66 (2002) 044615.

[56] A. Boudard, J. Cugnon, S. Leray, C. Volant, A new model for production of fast light clusters in spallation reactions, Nuclear Physics A 740 (2004) 195.

[57] E. Uehling, G. Uhlenbeck, Transport phenomena in Einstein-Bose and Fermi-Dirac gases., Physical Review 43 (1933) 552.

[58] G. F. Bertsch, H. Kruse, S. D. Gupta, Boltzmann equation for heavy ion collisions, Physical Review C 29 (1984) 673.

[59] G. F. Bertsch, S. D. Gupta, A guide to microscopic models for intermediate energy heavy ion collisions, Physics Reports 160 (4) (1988) 180–233.

[60] W. Cassing, V. Metag, U. Mosel, K. Niita, Production of energetic particles in heavy-ion collisions, Physics Reports 188 (1990) 363.

[61] K. Niita, W. Cassing, U. Mosel, Hard-photon production within a self-consistent transport approach to heavy-ion collisions, Nuclear Physics A 504 (1989) 391.

[62] K. Niita, S. Chiba, T. Maruyama, T. Maruyama, H. Takada, T. Fukahori, Y. Nakahara, A. Iwamoto, Analysis of the (n,xn') reactions by Quantum Molecular Dynamics plus Statistical Decay Model, Physical Review C 52 (5) (1995) 2620.

[63] J. B. Cumming, Effects of collectivity on target-fragmentation reactions, Physical Review Letters 44 (1980) 17.

[64] M. Ta-chung, Multiparticle production in high-energy hadron-nucleus collisions, Physical Review D 15 (1977) 197.

[65] J. Gosset, H. H. Gutbrod, W. G. Meyer, A. M. Poskanzer, A. Sandoval, R. Stock, G. D. Westfall, Center collisions of relativistic heavy ions, Physical Review C 16 (2) (1977) 629.

[66] W. D. Myers, A model for high-energy heavy-ion collisions, Nuclear Physics A 296 (1978) 177.

[67] J. Gosset, J. I. Kapusta, G. D. Westfall, Calculations with the nuclear firestreak model, Physical Review C 18 (2) (1978) 844.

[68] J. Hüfner, J. Knoll, Rows on rows - a theory for collisions between heavy ions at high energy, Nuclear Physics A 290 (1977) 460.

[69] G. D. Westfall, R. G. Sextro, A. M. Poskanzer, A. M. Zebelman, G. W. Butler, E. K. Hyde, Energy spectra of nuclear fragments produced by high energy protons, Physical Review C 17 (1978) 1368–1381.

[70] S. Furihata, Statistical analysis of light fragment production from medium energy proton-induced reactions, Nuclear Instruments and Methods in Physics Research B 171 (2000) 251.

[71] S. Furihata, T. Nakamura, Calculation of nuclide productions from proton induced reactions on heavy targets with INC/GEM, Journal of Nuclear Science and Technology, Supplement 2 (2002) 758.

[72] R. J. Charity, M. A. McMahan, G. J. Wozniak, R. J. McDonald, L. G. Moretto, D. G. Sarantites, L. G. Sobotka, G. Guarino, A. Pantaleo, L. Fiore, A. Gobbi, K. D. Hildenbrand, Systematics of complex fragment emission in Niobium - induced reactions, Nuclear Physics A 483 (1988) 371–405.

[73] E. Fermi, High energy nuclear events, Progress of Theoretical Physics 5 (1950) 570.

[74] J. P. Bondorf, A. S. Botvina, A. S. Iljinov, I. N. Mishustin, K. Sneppen, Statistical multifragmentation of nuclei, Physics Report 257 (1995) 133.

[75] V. F. Weisskopf, P. H. Ewing, On the yield of nuclear reactions with heavy elements, Physical Review 57 (1940) 472.

[76] A. Gilbert, A. G. W. Cameron, Can. J. Phys. 43 (1965) 1446.

[77] R. E. Prael, H. Lichtenstein, User guide to LCS: the LAHET code system, Tech. Rep. LA-UR-89-3014, Los Alamos National Laboratory (1989).

[78] W. Hauser, H. Feshbach, The inelastic scattering of neutrons, Physical Review 87 (2) (1952) 366–373.

[79] L. Vaz, J. M. Alexander, Empirical and theoretical fusion barriers for ^{1}H and ^{4}He: Connections to evaporation from hot nuclei, Zeitschrift für Physik A 318 (1984) 231.

[80] A. J. Sierk, Microscopic model of rotating nuclei, Physical Review C 33 (1986) 2039.

[81] L. G. Moretto, Statistical emission of large fragments: A general theoretical approach, Physical Review A 247 (1975) 211.

[82] E. Gradsztajn, F. Yiou, R. Klapisch, R. Bernas, Intranuclear cascade and Fermi-Model breakup calculations on the production of Li, Be, and B isotopes in C^{12} by 156-MeV protons, Physical Review Letters 14 (1965) 436.

[83] A. Magiera, Computer program ROZPAD, *Unpublished, private communication* (2010).

[84] B. Piskor-Ignatowicz, Energy dependence of proton induced fragmentation of atomic nuclei, Ph.D. thesis, Jagiellonian University (2009).

[85] L. N. Andronenko, M. N. Andronenko, A. A. Kotov, W. Neubert, G. E. Petrov, D. M. Seliverstov, L. A. Vaishnene, V. I. Yatsoura, Measurement of Fragment Production Cross Sections in 1 GeV Proton Interactions with Carbon, Preprint 2217, Russian Academy of Science, Petersburg Nuclear Physics Institute.

[86] Http://geant4.web.cern.ch/geant4/support/userdocuments.shtml.

[87] J. R. Walton, D. Heymann, A. Yaniv, D. Edgerley, M. W. Rowe, Production of He, Ne and Ar isotopes and U^{236} in lunar materials by solar cosmic ray protons – production rate calculation, Journal of Geophysical Research 81 (1976) 5701.

[88] P. Pulfer, Ph.D. thesis, University of Bern (1979).

[89] F. Baros, S. Regnier, J. Physique et le Radium 45 (1984) 855.

[90] J. M. Sisterson, M. W. Caffee, Proc. 28th LPSC 2 (1998) 1234.

[91] N. M. . Hintz, N. F. Ramsey, Excitation functions to 100 MeV, Physical Review 88 (1) (1952) 19.

[92] R. Michel, F. Peiffer, R. Stück, Measurement and hybrid model analysis of integral excitation functions for proton-induced reactions on Vanadium, Manganese and Cobalt up to 200 MeV, Nuclear Physics A 441 (1985) 617.

[93] R. Michel, P. Dragovitsch, P. Englert, F. Peiffer, R. Stück, S. Theis, F. Begemann, H. Weber, P. Singer, R. Wieler, D. Filges, P. Cloth, On the depth dependence of spallation reactions in a spherical thick diorite target homogeneously irradiated by 600 MeV protons : Simulation of production of cosmogenic nuclides in small meteorites, Nuclear Instruments and Methods in Physics Research B 16 (1986) 61.

[94] Y. E. Titarenko, O. V. Shvedov, V. F. Batyaev, E. I. Karpikhin, V. M. Zhivun, A. B. Koldobsky, R. D. Mulambetov, S. V. Kvasova, A. N. Sosnin, S. G. Mashnik, R. E. Prael, A. J. Sierk, T. A. Gabriel, M. Saito, H. Yasuda, Cross sections for nuclide production in 1 GeV proton-irradiated ^{208}Pb, Physical Review C 65 (2002) 064610.

[95] T. Schiekel, F. Sudbrock, U. Herpers, M. Gloris, H.-J. Lange, I. Leya, R. Michel, B. Dittrich-Hannen, H.-A. Syani, M. Suter, P. W. Kubik, M. Blann, D. Filges, Nuclide production by proton-induced reactions on elements ($6 \leqslant Z \leqslant 29$) in the energy range from 200 MeV to 400 MeV, Nuclear Instruments and Methods in Physics Research B 114 (1996) 91.

[96] W. Wlazlo, T. Enqvist, P. Armbruster, J. Benlliure, M. Bernas, A. Boudard, S. Czájkowski, R. Legrain, S. Leray, B. Mustapha, M. Pravikoff, F. Rejmund, K.-H. Schmidt, C. Stéphan, J. Taieb, L. Tassan-Got, C. Volant, Energy spectra of nuclear fragments produced by high energy protons, Physical Review Letters 84 (2000) 5736.

[97] T. Enqvist, W. Wlazlo, P. Armbruster, J. Benlliure, M. Bernas, A. Boudard, S. Czajkowski, R. Legrain, S. Leray, B. Mustapha, M. Pravikoff, F. Rejmund, K.-H. Schmidt, C. Stéphan, J. Taieb, L. Tassan-Got, C. Volant, Isotopic yields and kinetic energies of primary residues in 1 A GeV ^{208}Pb+p reactions, Nuclear Physics A 686 (2001) 481.

[98] P. C. Brun, M. Lefort, X. Tarrago, Contribution a l'étude du double pick-up indirect mesure de la production de tritum par des protons de 82 et 150 MeV dans diverses cibles, Le Journal de Physique et la Radium 28 (1962) 167.

[99] S. Chiba, M. B. Chadwick, K. Niita, T. Maruyama, T. Maruyama, A. Iwamoto, Nucleon-induced preequilibrium reactions in terms of the quantum molecular dynamics, Physical Review C 53 (1996) 1824–1832.

[100] S. V. Förtsch, A. A. Cowley, J. J. Lawrie, D. M. Whittal, J. V. Pilcher, F. D. Smit, Continuum protons from ^{58}Ni(p,p') at incident energies between 100 and 200 MeV, Physical Review C 43 (2) (1991) 691.

[101] W. A. Richter, A. A. Cowley, G. C. Hillhouse, J. A. Stander, J. W. Koen, S. W. Steyn, R. Lindsay, R. E. Julies, J. J. Lawrie, J. V. Pilcher, P. E. Hodgson, Preequilibrium (p,p') measurements and calculations for ^{90}Zr and neighboring nuclei for incident energies up to 200 MeV, Physical Review C 49 (2) (1994) 1001.

[102] W. Scobel, M. Tranbandt, M. Blann, B. A. Pohl, B. R. Remington, R. C. Byrd, C. C. Foster, R. Bonetti, C. Chiesa, S. M. Grimes, Preequilibrium (p,n) reaction as a probe for the effective nucleon-nucleon interaction in multistep direct processes, Physical Review C 41 (5) (1990) 2010.

[103] T. Nakamoto, K. Ishibashi, N. Matsufuji, N. Shigyo, K. Maehata, S. Meigo, H. Takada, S. Chiba, M. Numajiri, T. Nakamura, Y. Watanabe, Spallation neutron measurement by the time-of-flight method with a short flight path, Journal of Nuclear Science and Technology 32 (1995) 827.

[104] H. En'yo, S. Sasaki, T. Nagae, K. Tokushuku, M. Sano, M. Sekimoto, J. Chiba, K. Ichimaru, T. Mori, T. Katsumi, H. Yokota, R. Chiba, K. Nakai, Analyses of particle production in hadron-nucleus reactions at several GeV with a two-moving-source model, Physics Letters B 159 (1985) 1.

[105] W. B. Amian, B. C. Byrd, C. A. Goulding, M. M. Meier, G. L. Morgan, C. E. Moss, D. A. Clark, Differential neutron production cross sections for 800-MeV protons, Nuclear Science and Engineering 112 (1992) 78.

[106] R. E. Segel, T. Chen, L. L. R. Jr., J. V. Maher, J. Wiggins, P. P. Singh, P. T. Debevec, Inclusive proton reactions at 164 MeV, Physical Review C 26 (1982) 2424–2432.

[107] K. Chen, Z. Fraenkel, G. Friedlander, J. R. Grover, J. M. Miller, Y. Shimamoto, Vegas: A Monte Carlo simulation of intranuclear cascades, Physical Review 166 (4) (1968) 949.

[108] . Artun, Y. Cassagnou, R. Legrain, N. Lisbona, L. Roussel, J. P. Alard, A. Baldit, J. P. Costilhes, J. Fargeix, G. Roche, J. C. Tamain, Multinucleon removal induced by high-energy protons, Physical Review Letters 35 (12) (1975) 773.

[109] K. Kwiatkowski, S. H. Zhou, T. E. Ward, V. E. V. Jr., H. Breuer, J. Mathews, A. Gzkmen, A. C. Mignerey, Energy deposition in intermediate-energy nucleon-nucleus collisions, Physical Review Letters 50 (21) (1983) 1648 – 1651.

[110] V. S. Barashenkov, H. W. Bertini, K. Chen, G. Friedlander, G. D. Harp, A. S. Iljinov, J. M. Miller, V. D. Toneev, Medium energy intranuclear cascade calculations: a comparative study, Nuclear Physics A 187 (1972) 531.

[111] G. J. Mathews, B. G. Glagola, R. A. Moyle, V. E. V. Jr., Inclusion of deuteron and alpha-particle collisions in intranuclear cascade calculations, Physical Review C 25 (1982) 2181.

[112] M. B. et al., Annual Review Nuclear Science 25 (1975) 123.

[113] R. Silberberg, H. Tsao, Astrophysics Journal 2 (1973) 315.

[114] A. M. Poskanzer, J. B. Cumming, R. Wolfgang, Recoil study of the reaction ^{27}Al(p,3pn)^{24}Na, Physical Review 129 (1963) 374–384.

[115] S. Frankel, W. Frati, M. Gazzaly, Y. D. Bayukovm, V. Efremenko, A. Leksin, N. A. Nikiforov, V. I. Tchistilin, Y. M. Zaitsev, C. F. Perdrisat, Backward production of light ions in the interaction of 400 GeV protons with nuclei, Physical Review C 20 (6) (1979) 2257.

[116] R. E. Batzel, G. T. Seaborg, Fission of medium weight elements, Physical Review 82 (1951) 607.

[117] D. H. Greenberg, J. M. Miller, The production of light nuclei by high energy proton bombardment of medium weight elements, Physical Review 84 (1951) 845.

[118] Aamodt, Peterson, Philips, Unclassified Report 526, Univerity of California, Radiation Laboratory (November 1949).

[119] L. Marquez, Spallation of Cu with high energy neutrons, Physical Review 88 (1982) 225.

[120] J. W. Wachter, W. A. Gibson, W. R. Burrus, Neutron and proton spectra from targets bombarded by 450-MeV protons, Physical Review C 6 (5) (1972) 1496.

[121] S. Cierjacks, Y. Hino, F. Raupp, L. Buth, D. Filges, P. Cloth, T. W. Armstrong, Systematics of angular-dependent neutron production by 585 MeV protons on targets with $12 \leq A \leq 238$: Differential cross section measurements, Physical Review C 36 (1987) 1976–1987.

[122] D. Filges, P. Cloth, T. W. Armstrong, S. Cierjacks, Y. Hino, F. Raupp, L. Buth, Systematics of angular - dependence neutron production by 585 MeV protons on targets with $12 \leq A \leq 238$: validation of intranuclear cascade - evaporation model calculations, Physical Review C 36 (1987) 1988.

[123] J. P. Alard, A. Baldit, R. Brun, J. P. Costilhes, J. Dhermain, J. Fargeix, L. Fraysse, J. Pellet, G. Roche, J. C.Tamain, A. Cordaillat, A. Pasinetti, Light-fragment production in p-nucleus interction at 600 MeV. Astrophysical Application., Il Nuovo Cimento 30 A No. 2 (1975) 320–344.

[124] E. K. Hyde, G. W. Butler, A. M. Poskanzer, Characteristics of fragments produced in the interaction of 5.5-GeV protons with Silver, Physical Review C 4 (5) (1971) 1759.

[125] T. N. et al., Journal Nuclear Science Technology 32-9 (1992) 827.

[126] A. Letourneau, J. Galin, F. Goldenbaum, B. Lott, A. Péghaire, M. Enke, D. Hilscher, U. Jahnke, K. Nünighoff, D. Filges, R. D. Neef, N. Paul, H. Schaal, G. Sterzenbach, A. Tietze, Neutron production in bombardments of thin and thick W, Hg, Pb targets by 0.4, 0.8, 1.2, 1.8 and 2.5 GeV protons, Nuclear Instruments and Methods in Physics Research B 170 (2000) 299–322.

[127] S. Leray, F. Borne, S. Crespin, J. Fréhaut, E. M. X. Ledoux, Y. Patin, E. Petibon, P. Pras, A. Boudard, R. Legrain, Y. Terrien, F. Brochard, D. Drake, J. C. D. J. M. Durand, S. I. Meigo, G. Milleret, D. M. Whittal, W. Wlazlo, D. Durand, C. L. Brun, F. R. Lecolley, J. F. Lecolley, F. Lefebvres, M. Louvel, C. Varignon, F. Hanappe, S. Ménard, L. Stuttge, J. Thun, Spallation neutron production by 0.8, 1.2, and 1.6 GeV protons on various targets, Physical Review C 65 (2002) 044621.

[128] D. Filges, F. Goldenbaum, M. Enke, J. Galin, C.-M. Herbach, D. Hilscher, U. Jahnke, A. Letourneau, B. Lott, R.-D. Neef, K. Nünighoff, N. Paul, A. Péghaire, L. Pienkowski, H. Schaal, U. Schröder, G. Sterzenbach, A. Tietze, V. Tishchenko, J. Toke, M. Wohlmuther, Spallation neutron production and the current intra-nuclear cascade and transport codes, European Physical Journal A 11 (2001) 467–490.

[129] O. Bersillon, 2nd international conference on accelerator driven transmutation technologies, Kalmar, Sweden, 1996, p. 520.

[130] A. A. Kotov, L. N. Andronenko, M. N. Andronenko, Y. I. Gusev, K. V. Lukashin, W. Neubert, D. M. Seliverstov, I. I. Strakovsky, L. A. Vaishnene, Intermediate mass fragment production on Au, Ag, Ni and Al Targets Induced by 1 GeV protons, Nuclear Physics A 583 (1995) 575 – 580.

[131] L. Winsberg, E. P. Steinberg, D. Henderson, A. Chrapkowski, Recoil properties of nuclei produced in the interaction of protons with ^{27}Al, Physical Review C 22 (5) (1980) 2108.

[132] S. Chiba, O. Iwamoto, T. Fukahori, K. Niita, T. Maruyama, T. Maruyama, A. Iwamoto, Analysis of proton-induced fragment production cross sections by the quantum molecular dynamics plus statistical decay model, Physical Review C 54 (1996) 285–291.

[133] D. E. Greiner, P. J. . Lindstrom, H. H. Heckman, B. Cork, F. S. Bieser, Momentum distributions of isotopes produced by fragmentation of relativistic ^{12}C and ^{16}O projectiles, Physical Review Letters 35 (1975) 152.

[134] S. Katcoff, Energy distributions of ^{8}Li fragments emitted from C, Al, Cu, Ag, Au, and U bombarded by 2.2-Bev protons, Physical Review 114 (1959) 905–911.

[135] E. P. Steinberg, L. Winsberg, Recoil properties of ^{22}Na and ^{24}Na produced in the interaction of ^{27}Al with 3-to 300 GeV protons, Physical Review C 10 (5) (1974) 1925.

[136] M. Furukawa, K. Shizuri, K. Komura, K. Sakamoto, S. Tanaka, Production of ^{26}Al and ^{22}Na from proton bombardment of Si, Al and Mg, Nuclear Physics A 174 (1971) 539.

[137] R. J. Schneider, J. M. Sisterson, A. M. Koehler, R. Middleton, Measurement of cross sections for Aluminum-26 and Sodium-24 induced by protons in Aluminum, Nuclear Instruments and Methods in Physics Research B 29 (1987) 271.

[138] T. Asano, Y. Asano, Y. Iguchi, H. Kudo, S. Mori, M. Noguchi, Y. Takada, H. Hirabayashi, H. Ikeda, K. Katoh, K. Kondo, M. Takasaki, T. Tominaka, A. Yamamoto, Target dependence of charge distributions in spallation reactions of medium-mass nuclei with 12 GeV protons, Physical Review C 28 (1983) 1718.

[139] M. Honda, P. Lal, Spallation cross sections for long-lived radionucleides in Iron and light nuclei, Nuclear Physics 51 (1964) 363.

[140] C. Perron, Cross sections for production of stable and long-lived nuclides by high energy spallation of Iron; Cosmic ray implications, Physical Reviev C 14 (1976) 1108.

[141] J. Hudis, S. Tanaka, Production of ^{7}Be, ^{22}Na, and ^{24}Na fragments from heavy elements at 3, 10, and 30 GeV, Physical Review 171 (1968) 1297.

[142] S. Shibata, M. Imamura, H. Nagai, K. Kobayashi, K. Sakamoto, M. Furukawa, I. Fujiwara, Measurements of ^{10}Be and ^{26}Al production cross sections with 12GeV protons by accelerator mass spectrometry, Physical Review C 48 (6) (1993) 2617.

[143] G. M. Raisbeck, P. Boerstling, R. Klapisch, T. D. Thomas, Li, Be, and B production in the 3-GeV proton bombardment of Ni, Physical Review C 12 (1975) 527.

[144] G. English, N. T. Porile, E. P. Steinberg, Nuclear reactions of Silver with 11.5-GeV protons, Physical Review C 10 (1974) 2268.

[145] S. B. Kaufman, M. W. Weisfield, E. P. Steinberg, B. D. Wilkins, D. Henderson, Nuclear reactions of ^{197}Au with 11.5- and 300-GeV protons, Physical Review C 14 (1976) 1121.

[146] M. Honda, P. Lal, Some cross sections for the production of radio-nuclides in the bombardment of C, N, O, and Fe by medium energy protons, Physical Review 118 (1960) 1618.

[147] X. Campi, J. Desbois, E. Lipparini, Sum rules study and a scaling property of fragmentation mass yield curves, Physics Letters B 138 (1984) 353.

[148] A. Schwarzschild, Č. Zupančič, Production of tritons, deuterons, nucleons, and mesons by 30-GeV Protons on Al, Be, and Fe targets, Physical Review 129 (1963) 854–862.

[149] V. L. Fitch, S. L. Meyer, P. A. Piroué, Particle production at large angles by 30- and 33-BeV protons incident on Aluminum and Beryllium, Physical Review 126 (1962) 1849–1851.

[150] T. S. Subramanian, J. L. Romero, F. P. Brady, J. W. Watson, D. H. Fitzgerald, R. Garrett, G. A. Needham, J. L. Ullmann, C. I. Zanelli, D. J. Brenner, R. E. Prael, Double differential inclusive Hydrogen and Helium spectra from neutron-induced reaction on Carbon at 27.4, 39.7 and 60.7 MeV, Physical Review C 28 (2) (1983) 521.

[151] F. E. Bertrand, R. W. Peelle, Complete hydrogen and helium particle spectra from 30- to 60-MeV proton bombardment of nuclei with A=12 to 209 and comparison with the Intranuclear Cascade Model, Physical Review C 8 (3) (1973) 1045.

[152] R. Bernas, M. Epherre, E. Gradsztajn, R. Klapisch, F. Yiou, Mass-spectrometric determination of ^{6}Li and ^{7}7 production in ^{12}C and ^{16}O by high energy protons, Physics Letters 15 (2) (1965) 147.

[153] N. Olsson, H. Condé, E. Ramström, T. Rönnqvist, R. Zorro, J. Blomgren, A. Håkansson, G. Tibell, A. Brockstedt, P. Ekström, M. Österlund, S. van der Werf, D. Millener, G. Szeflinska, Z. Szeflinski, The ^{12}C(n, p) ^{12}B reaction at E = 98 MeV, Nuclear Physics A 559 (1993) 368–400.

[154] U. Tippawan, S. Pomp, J. Blomgren, S. Dangtip, C. Gustavsson, J. Klug, P. Nadel-Turonski, L. Nilsson, M. Österlund, N. Olsson, O. Jonsson, A. Prokofiev, P.-U. Renberg, V. Corcalciuc, Y. Watanabe, A. J. Koning, Light-ion production in the interaction of 96 MeV neutrons with Carbon.

[155] G. M. Raisbeck, J. Lestinguez, F. Yiou, Cross section of ^{6}Li and ^{7}Li production from the bombardment of ^{12}C by 150- and 600-MeV protons and 880-MeV alpha particles, Physical Review C 6 (1972) 685.

[156] S. Singh, J. M. Alexander, Recoil study of the reaction ^{12}C (p,pn)^{11}C, Physical Review 128 (2) (1962) 711.

[157] R. L. Wolfgang, G. Friedlander, Excitation function of the $^{12}C(p,pn)^{11}C$ raction in the BeV region, Physical Review 96 (1) (1954) 190.

[158] W. R. Webber, J. C. Kish, J. M. Rokstroh, Y. Cassagnou, R. Legrain, A. Soutoul, O. Testard, C. Tull, Production cross sections of fragments from beams of 400 - 650 MeV per nucleon ^{9}Be,^{11} B,^{12} C,^{14} N,^{15} N,^{16} O,^{20} Ne,^{22} Ne,^{56} Fe, and ^{58}Ni nuclei interacting in a liquid hydrogen target. I. Charge changing and total cross sections, The Astrophysical Journal 508 (1998) 940–948.

[159] W. R. Webber, J. C. Kish, J. M. Rokstroh, Y. Cassagnou, R. Legrain, A. Soutoul, O. Testard, C. Tull, Production cross sections of fragments from beams of 400 - 650 MeV per nucleon ^{9}Be,^{11} B,^{12} C,^{14} N,^{15} N,^{16} O,^{20} Ne,^{22} Ne,^{56} Fe, and^{58}Ni nuclei interacting in a liquid hydrogen target. II. Isotopic cross sections of fragments, The Astrophysical Journal 508 (1998) 949–958.

[160] G. V. S. Rayudu, Formation cross sections of various radionuclides from ni, fe, si, mg, o and c for protons of energies between 0.5 and 2.9 gev, Journal of Inorganic and Nuclear Chemistry 30 (1968) 2311.

[161] S. Frankel, W. Frati, O. V. Dyck, R. Werbeck, V. Highland, Inclusive cross sections for 180^o production of high-energy protons, deuterons, and tritons in p-nucleus collisions at 600 and 800 MeV, Physical Review Letters 36 (12) (1976) 642.

[162] S. T. Kruger, D. Heymann, High-energy proton production of ^{3}H, ^{3}He, and ^{4}He in light targets, Physical Review C 7 (1973) 2179.

[163] D. B. Barlow, B. M. K. Nefkens, C. Pillai, J. W. Price, I. Šlice, M. J. Wang, K. W. Jones, M. J. Leitch, C. S. Mishra, C. L. Morris, J.-C. Peng, P. K. Teng, J. M. Tinsley, ^{3}He and ^{4}He production by 800 MeV protons from ^{12}C, Ti, and Pb at forward angles, Physical Review C 45 (1) (1992) 293.

[164] K. R. Hogstrom, ^{12}C(p,pn)^{11}C cross section at 800 MeV, Physical Review C 14 (1976) 753.

[165] N. Horowitz, J. J. Murray, ^{12}C(p,pn)^{11}C cross section from 3 to 6 BeV, Physical Review 117 (1960) 1361.

[166] A. Korejwo, M. Giller, T. Dzikowski, J. Wdowczyk, V. V. Perelygin, A. V. Zarubin, Measurement of isotopic cross sections of ^{12}C beam fragmentation on hydrogen at 3.66 GeV/n, Journal of Physics G 26 (2000) 1171.

[167] A. M. Poskanzer, L. P. Remsberg, S. Katcoff, J. B. Cumming, ^{12}C(p,pn)^{11}C cross section at 1.0 GeV, Physical Review 133 (1964) B1507.

[168] G. W. Butler, S. B. Kaufman, E. P. Steinberg, B. D. Wilkins, ^{12}C(p,pn)^{11}C cross section at 7.6 GeV, Physical Review C 6 (1972) 1153.